

Springer Theses

Recognizing Outstanding Ph.D. Research

Nelson Enrique Barros Galvis

Geomechanics, Fluid Dynamics and Well Testing, Applied to Naturally Fractured Carbonate Reservoirs

Extreme Naturally Fractured
Reservoirs

 Springer

Springer Theses

Recognizing Outstanding Ph.D. Research

Aims and Scope

The series “Springer Theses” brings together a selection of the very best Ph.D. theses from around the world and across the physical sciences. Nominated and endorsed by two recognized specialists, each published volume has been selected for its scientific excellence and the high impact of its contents for the pertinent field of research. For greater accessibility to non-specialists, the published versions include an extended introduction, as well as a foreword by the student’s supervisor explaining the special relevance of the work for the field. As a whole, the series will provide a valuable resource both for newcomers to the research fields described, and for other scientists seeking detailed background information on special questions. Finally, it provides an accredited documentation of the valuable contributions made by today’s younger generation of scientists.

Theses are accepted into the series by invited nomination only and must fulfill all of the following criteria

- They must be written in good English.
- The topic should fall within the confines of Chemistry, Physics, Earth Sciences, Engineering and related interdisciplinary fields such as Materials, Nanoscience, Chemical Engineering, Complex Systems and Biophysics.
- The work reported in the thesis must represent a significant scientific advance.
- If the thesis includes previously published material, permission to reproduce this must be gained from the respective copyright holder.
- They must have been examined and passed during the 12 months prior to nomination.
- Each thesis should include a foreword by the supervisor outlining the significance of its content.
- The theses should have a clearly defined structure including an introduction accessible to scientists not expert in that particular field.

More information about this series at <http://www.springer.com/series/8790>

Nelson Enrique Barros Galvis

Geomechanics, Fluid Dynamics and Well Testing, Applied to Naturally Fractured Carbonate Reservoirs

Extreme Naturally Fractured Reservoirs

Doctoral Thesis accepted by
the Instituto Mexicano del Petróleo y the Universidad
Nacional Autónoma de México, Mexico City, Mexico

Author

Dr. Nelson Enrique Barros Galvis
Postgraduate Studies
Mexican Petroleum Institute (IMP)
and National Autonomous
University of Mexico, UNAM
Mexico City
Mexico

Supervisors

Prof. Héber Cinco Ley
National Autonomous University of Mexico
Mexico City
Mexico

Prof. Fernando Samaniego V.
National Autonomous University of Mexico
Mexico City
Mexico

Prof. Pedro Villaseñor Rojas
Mexican Petroleum Institute
Mexico City
Mexico

ISSN 2190-5053

Springer Theses

ISBN 978-3-319-77500-5

<https://doi.org/10.1007/978-3-319-77501-2>

ISSN 2190-5061 (electronic)

ISBN 978-3-319-77501-2 (eBook)

Library of Congress Control Number: 2018934948

© Springer International Publishing AG, part of Springer Nature 2018

This work is subject to copyright. All rights are reserved by the Publisher, whether the whole or part of the material is concerned, specifically the rights of translation, reprinting, reuse of illustrations, recitation, broadcasting, reproduction on microfilms or in any other physical way, and transmission or information storage and retrieval, electronic adaptation, computer software, or by similar or dissimilar methodology now known or hereafter developed.

The use of general descriptive names, registered names, trademarks, service marks, etc. in this publication does not imply, even in the absence of a specific statement, that such names are exempt from the relevant protective laws and regulations and therefore free for general use.

The publisher, the authors and the editors are safe to assume that the advice and information in this book are believed to be true and accurate at the date of publication. Neither the publisher nor the authors or the editors give a warranty, express or implied, with respect to the material contained herein or for any errors or omissions that may have been made. The publisher remains neutral with regard to jurisdictional claims in published maps and institutional affiliations.

Printed on acid-free paper

This Springer imprint is published by the registered company Springer International Publishing AG part of Springer Nature

The registered company address is: Gewerbestrasse 11, 6330 Cham, Switzerland

To my family (Angela, Enrique, Sauddy and Yelmis)

with love, gratitude, and regards.

*To my noble and great grandmother:
Dominga Benavides.*

*There in Barranquilla—Colombia to all
of them...*

To who said that this thesis was impossible...

To lost relationship...

Supervisor's Foreword

This thesis circumvents the traditional conventional modeling and the exploitation of Naturally Fractured Carbonated Reservoirs (NFCRs); based on the applications of tectonic fractures concepts or planar discontinuities, they have been simulated dynamically without considering nonplanar discontinuities such as sedimentary breccias, vugs, fault breccias, and impact breccias, assuming that these nonplanar discontinuities are tectonic fractures, causing confusion and contradictions in reservoirs characterization. A novelty of this work is the demonstration of different kinds of discontinuities using geological evidences, mathematical kinematics model, and computed tomography.

On the other hand, naturally fractured reservoirs must be classified on the basis to detect and to evaluate dominant discontinuities, integrating dynamic and static parameters; namely, discontinuities connectivity and fluid flow are fundamental conditions for the NFCRs classification. A new classification for NFCRs is proposed in this thesis. It is also previously listed that discontinuities can display flow patterns and geological features that may behave according to a variety of reservoir static–dynamic models.

Geomechanical models describe the rock deformation as a result of flow-induced pressure changes in stress-sensitive reservoirs. This work was developed and focused in an analytical coupled method using mathematical transformations to solve nonlinear terms of diffusivity equation. The effects of the nonlinear gradient term for radial flow, single phase (oil), for constant rate in an infinite reservoir, are analyzed using an exact solution of Navier–Stokes equation and Cole–Hopf transform.

Additionally, this study takes advantage of rock mechanics theory to demonstrate how natural fractures can collapse due to fluid flow and pressure changes in fractured media. This formulation captures all the physical variations involved with conductive fractures.

The explanations and mathematical modeling developed in this dissertation could be used as diagnostic tools to predict fluid velocity, fluid flow, tectonic fractures collapse, and pressure behavior during reservoir depleting, considering stress-sensitive and nonstress-sensitive in NFCRs. Another aspect that deserves

special attention is related to the description of this framework for real reservoirs with their field data because our principal goal is a mathematical description of the realistic phenomenology of NFCRs. All of the equations are solved in a coupled approach, which has been validated and presented.

The main novelties of this work are the analytical solutions presented, and the classification of NFCRs using static and dynamic parameters. These solutions demonstrate the presence of different types of discontinuities, the mechanical behavior of tectonic fractures, the stress-sensitive and nonstress-sensitive conditions of the reservoir through its pressure behavior, considering the nonlinear terms in the diffusivity equation.

Mexico City, Mexico
April 2017

Fernando Samaniego V.

Abstract

Conventional modeling and exploitation of Naturally Fractured Carbonate Reservoirs (NFCRs) are traditionally developed by applying tectonic fractures concepts or planar discontinuities, and they have been simulated dynamically without considering nonplanar discontinuities such as sedimentary breccias, vugs, fault breccias, and impact breccias, assuming that all these nonplanar discontinuities are tectonic fractures, causing confusion and contradictions in reservoirs characterization. A novelty of this work is the demonstration of different kinds of discontinuities using geological evidences, mathematical kinematics model, and computed tomography.

On the other hand, naturally fractured reservoirs must be classified on the basis to detect and to evaluate dominant discontinuities, integrating dynamic and static parameters; namely, discontinuities connectivity and fluid flow are elemental conditions for the NFCRs classification. A new classification for NFCRs was proposed in this thesis. Also, this doctoral dissertation demonstrated that diverse discontinuities can display flow patterns and geological features that may behave according to a variety of reservoir static–dynamic models.

Geomechanical models describe rock deformation as a result of flow-induced pressure changes in stress-sensitive reservoirs. There are several types of coupled methods in the literature, mainly iteratively coupled and fully coupled methods. This work was developed and focused in an analytical coupled method using mathematical transformations to solve nonlinear terms of diffusivity equation. The effects of the nonlinear gradient term for radial flow, single phase (oil), for constant rate in an infinite reservoir, are analyzed using an exact solution of Navier–Stokes equation and Cole–Hopf transform.

Additionally, this study takes advantage of rock mechanics theory to demonstrate how natural fractures can collapse due to fluid flow and pressure changes of the fractured media. The formulation developed here captures all the variations involved with conductive and open fractures.

The explanations and mathematical modeling developed in this dissertation could be used as diagnostic tools to predict fluid velocity, fluid flow, tectonic fractures collapse, and pressure behavior during reservoir depleting, considering

stress-sensitive and nonstress-sensitive in NFCRs. Another aspect that deserves special attention is related to describe this framework for real reservoirs with their field data because our principal goal is a mathematical description of the realistic phenomenology of NFCRs. All of the equations are solved in a coupled fashion, which have been validated and presented.

The main novelties of this work are the analytical solutions presented, and NFCRs are classified using static and dynamic parameters. These solutions demonstrate the different types of discontinuities, mechanical behavior of tectonic fractures, stress-sensitive and nonstress-sensitive in the reservoir, and pressure behavior, considering nonlinear terms in the diffusivity equation.

Acknowledgements

This thesis is the result of a lot of imagination. I would like to express my sincere gratitude to all those who gave me the chance to complete this research. My deepest appreciation goes to my supervisors, Prof. Fernando Samaniego, Dr. Pedro Villaseñor, and Prof. Héber Cinco Ley, for their support and guidance throughout the course of the research. It was a distinct privilege for me to work with them.

Specially, Prof. Samaniego has also become a good source for advice on all aspects of my work, for me he is my technical father. My other great mentor Dr. Héber Cinco Ley, simply a brilliant mind and a great person. In effect, I feel indeed grateful to Prof. Héber Cinco Ley, Agustín Ruíz Violante, Cristy Guevara, Prof. Nils Ackermann, F. Jerry Lucia, and Eduardo Joaquín Aguayo for sharing their visions that helped me to build a laboratory with infinite equipments, resources, and benefits only conceived in my mind and imagination.

I have greatly profited from the support, comments, free assistance, information, intensive discussions, and suggestions of many experts, colleagues, doctors, and friends, in particular: Gildardo Osorio Gallego, Daniel García Gavito, Juan José Valencia Islas, Gerardo de Alba, Recaredo Vilches, Prof. Gary Couples, Prof. Vamegh Rasouli, Prof. Alain Gringarten, Prof. Christine Ehlig-Economides, Prof. Roberto Aguilera, Prof. Maurice Dusseault, Juan Manuel Grajales Nishimura, Luis Velasquillo, Honorio Ramírez, Miguel Ángel Alarcón, Prof. Mario Garcia, Juan Manuel Alvarez, Prof. Edgar Rangel, Oscar Michel Salgado, Prof. Francisco Sanchez Sesma, Prof. Mario César Suárez, Prof. Erick Luna, Alfredo Carmona, Gregorio Inda, Roberto Montes, Andrés Moctezuma, Norma García, and all people that have helped me on this work. In addition, I want to express that “I strongly appreciate and respect ideas of people” thanks.

Also, I thank and dedicate this work to master of masters, mentor of mentors that only in dreams he showed me perfection and knowledge tree, who kept an eye on the progress of my work and was always available when I needed his advice. In life and death, I receive with humility your words and wisdom. To you, my great master, my old mentor, and friend. So, I am so thankful to you and God. Amen.

This research has been supported by CONACyT, Mexican Petroleum Institute (IMP), and National Autonomous University of Mexico (UNAM), which I thank, too.

Contents

1	Introduction	1
1.1	Problem Statement	2
1.2	Methodology	2
1.3	Scope	3
1.4	Outline of the Thesis	3
	References	4
2	Phenomenology and Contradictions in Carbonate Reservoirs	5
2.1	First Contradiction: Tectonic Fracture or Nonplanar Discontinuity?	6
2.2	Second Contradiction: How Do Different Discontinuities Impact?	8
2.3	Analogs Reservoirs and Outcrops for a Flow Analytical Model	9
2.4	Geological and Tomography Features of Tectonic Fractures	10
2.5	Analytical Model for the Profile Velocity of Tectonic Fractures	12
2.6	Kinematic Analytical Modeling for Tectonic Fractures	14
2.7	Third Contradiction: Darcy's Flow or Couette General Flow for Planar Discontinuity (Tectonic Fracture)	16
2.8	Geological and Tomography Features of Fault Breccias	16
2.9	Kinematic Analytical Modeling for Fault Breccias	19
2.10	Geological and Tomography Features of Chicxulub Impact Breccias and Cantarell Reservoir	23
2.11	Kinematic Analytical Modeling for Impact Breccias	26
2.12	Fourth Contradiction: Fluid Flow of the Cantarell Reservoir Modeled Without Considerer Chicxulub Impact	31
2.13	Geological and Tomography Features of Sedimentary Breccias	31
2.14	Kinematic Analytical Modeling for Sedimentary Breccia	34

2.15	Geological and Tomography Features of Vugs	36
2.16	Kinematic Analytical Modeling for Vugs	40
2.17	Fifth Contradiction: Liquids Retention Paradox for Vugs	41
2.18	Application Examples	42
2.18.1	Behavior of Fluid Velocities	42
2.18.2	Carbonate Reservoir Characteristics: Cardenas Field Application	44
2.19	Mathematical Models Summary	50
2.20	Nomenclature	50
	References	53
3	A Ternary, Static, and Dynamic Classification of NFCRs	59
3.1	Classification Proposal	60
3.2	Ternary Classification Proposal Considerations	60
3.3	Ternary Classification of NFCRs	61
3.4	Ternary Classification Parameters	62
3.5	Geological Discontinuities Lines	64
3.5.1	Line of Tectonic-Sedimentary Breccias	64
3.5.2	Line of Impact Breccias	64
3.5.3	Dissolution Line	65
3.5.4	Interception of Geological Discontinuities Lines	65
3.5.5	Classifying Fractured Carbonate Reservoirs	66
3.6	Generalized Ternary Classification	69
3.6.1	Classification of Naturally Fractured Reservoirs. Author: Ronald Nelson	70
3.6.2	Classification for Naturally Fractured Reservoir, by Gilman et al.	70
3.6.3	Types of Naturally Fractured Reservoirs. Author: Héber Cinco-Ley	71
3.6.4	Reservoirs Classification, by Soto et al.	71
3.6.5	Similarities Between Classifications Available in Literature and Ternary Classification	73
3.7	Examples of NFCRs	74
3.8	Nomenclature	74
	References	75
4	Analytical Model for Non Stress Sensitive Naturally Fractured Carbonate Reservoirs (NFCRs)	77
4.1	Overview	77
4.2	Analytical Considerations for Model	77
4.3	Couette and Darcy's Equation	78
4.4	Analytical Model	80
4.5	Mathematical Model and Solution for Constant Rate Radial Flow in an Infinite Reservoir	85

4.6 Solution of the Nonlinear Partial Differential Equation Without Stress-Sensitive 87

 4.6.1 Case Without Transfer Function 87

References 89

5 Analytical Model for Stress Sensitive Naturally Fractured Carbonate Reservoirs (NFCRs) 93

5.1 Analytical Considerations for Model 93

5.2 Analytical Model 94

5.3 Solution Nonlinear Partial Differential Equation 99

 5.3.1 Case 1: $\gamma = c_f$ 99

References 101

6 Westergaard’s Solution Applied to Carbonate Reservoirs 103

6.1 Westergaard’s Solution 103

 6.1.1 Airy Stress Function 104

 6.1.2 Displacement in the Horizontal Direction, u 107

 6.1.3 Displacement in the Vertical Direction, v 108

6.2 Westergaard’s Application for Tectonic Fractures 108

6.3 Westergaard’s Solution Applied to a Limestone Reservoir with Tectonic Fractures 111

 6.3.1 Field Geological Aspects 111

 6.3.2 Paleontological Description 116

 6.3.3 Petrography 116

 6.3.4 Permeability and Porosity 121

 6.3.5 X-Ray Diffraction for the Identification and Analysis of Carbonates Rocks 121

 6.3.6 Computed Tomography, CT 124

 6.3.7 Fluid Pore Pressure 124

6.4 Carbonate Rock Mechanical Properties 126

 6.4.1 Overburden Stress, S_v 127

 6.4.2 Maximum and Minimum Horizontal Stresses Magnitudes 128

 6.4.3 Elastic Parameters: Young’s Modulus and Poisson’s Ratio 132

6.5 Closed or Open Natural Horizontal Fractures 137

References 139

7 Applicability and Benefits of Doctoral Thesis for Hydrocarbons Industry 141

Reference 143

8 Conclusions and Recommendations 145

8.1 Conclusions 145

8.2 Recommendations 147

List of Figures

Fig. 1.1	Doctoral thesis general methodology	3
Fig. 2.1	Limestone core with planar tectonic fractures, Early Cretaceous, Samaria-Luna Region, TAB, Mexico	7
Fig. 2.2	Core slabs of Cladocoropsis. a Mud supported limestone. b Fragmented Cladocoropsis grainstone, Ghawar field, Saudi Arabia (After Voelker 2004, Fig. 6.7, p. 115)	8
Fig. 2.3	Tectonic fractures system outcrop, Canada	10
Fig. 2.4	Scan of limestone core, with dark shading associated with low density and white with high density regions with evident macroscopic fractures, Early Cretaceous, Samaria-Luna Region, Tabasco, Mexico	11
Fig. 2.5	Top and lateral views of fluid flow in a tectonic fracture. a Flow lines in an open fracture (top view). b Flow profile between two inclined parallel plates (lateral view) (Potter et al. 2012)	12
Fig. 2.6	Streamlines in uniform rectilinear flow in tectonic fractures with parallel walls, a horizontal direction, b inclined direction, and c vertical direction	15
Fig. 2.7	Fault breccia outcrop, Alberta, Canada	17
Fig. 2.8	Fault breccia core, Late Cretaceous, Campeche Sound, Marine Region, Mexico	17
Fig. 2.9	Representative appearance of fault breccia in computerized tomography (CT) images. a Slice of fault breccia cut perpendicular to core axis (interval 316-C0004D-28R-2, length: 45.13 cm). b Same as (a) with CT numbers of matrix and fragment. Note the small contrast in CT numbers between matrix and fragment (1162 vs. 1294) (Kinoshita et al. 2009)	18
Fig. 2.10	Streamlines through an angular fragment	19
Fig. 2.11	Flow kinematics through fault breccias, using Rankine half-body	22

Fig. 2.12 Core and outcrop of impact breccia embedded clasts. **a** Limestone core of the Campeche Sound with rip-up morphology clasts. Late Cretaceous, Campeche Sound, Marine Region, Cantarell Complex, Mexico (Ortuño 2012). **b** Analog limestone outcrop with rip-up morphology clasts, Guayal outcrop, TAB, Mexico (Grajales-Nishimura et al. 2000). 24

Fig. 2.13 Samples of CT slices through the Bosumtwi and Chicxulub impacts. **a** Breccia sequence in Yaxcopoil-1 borehole. Core images obtained with the Core Scan System for the breccias sections, illustrating the different textures (Urrutia-Fucugauchi et al. 2011). **b** Three-dimensional reconstruction of the clasts population of the Bosumtwi suevite. The image on the left shows the sample with color-coded clasts, with the matrix (groundmass) rendered partly transparent. The center image shows only the high-density clasts, with the low-density clasts (and the groundmass) rendered transparent, and the image on the right shows only the rock edges and the low-density clasts (Mees et al. 2003). 25

Fig. 2.14 Streamlines for the flow through in rip-up fragments in an impact breccia. 26

Fig. 2.15 Streamlines for a rip-up clast. Impact breccia. 27

Fig. 2.16 Sedimentary breccia outcrop with reworked clasts. La Popa basin, Nuevo León, Mexico 32

Fig. 2.17 Matrix-clast interface in sedimentary breccia core. Late Cretaceous, Cardenas Field, TAB, Mexico (Villaseñor-Rojas 2003). Note: W = clast width and L = clast length. 32

Fig. 2.18 Tomography (CT) image of sedimentary breccia. **a** Core. **b** Tomography. **c** Lithological description. Interval 316-C0004, 0–80 cm. (Kinoshita et al. 2009). 33

Fig. 2.19 Streamlines in sedimentary breccia with reworked clasts 34

Fig. 2.20 Source and sink angles in the Rankine body (Douglas et al. 2005) 35

Fig. 2.21 Streamlines for the Rankine solid with sink and source (Douglas et al. 2005) 35

Fig. 2.22 Limestone reservoir core with irregular vugs. Late Cretaceous, Campeche Sound, Marine Region, Mexico. 37

Fig. 2.23 Zoomed photo of vugs in a recycled outcrop. Guayal outcrop, Tabasco, Mexico (SENER-Conacyt 2013) 37

Fig. 2.24 Oil impregnated core of a vuggy limestone reservoir. Late Cretaceous, the Campeche Sound, Marine Region, Mexico 38

Fig. 2.25 CT images of an oil impregnated vuggy limestone core. Late Cretaceous, Campeche Sound core, Marine Region, Mexico . . . 39

Fig. 2.26	Lateral view of a composite porous medium with vugs, matrix, and a fluid flow field	40
Fig. 2.27	Proposed solution for a composite porous media with vugs, matrix, and a fluid flow field	40
Fig. 2.28	Section 1-1 producing levels correlation through breccias intervals longitudinal to the northeastern reservoir (Villaseñor-Rojas 2003)	45
Fig. 2.29	Matching pressure curve declination among wells is shown (After Villaseñor-Rojas 2003, Fig. 6.5, p. 161.)	46
Fig. 2.30	Oil cumulative production in wells of the Cardenas Field: wells C-109, C-129, and C-308 (Villaseñor-Rojas 2003)	48
Fig. 3.1	Ternary, static and dynamic classification of NFCRs	61
Fig. 3.2	Line of tectonic-sedimentary breccias	64
Fig. 3.3	Line of impact breccias.	65
Fig. 3.4	Dissolution line.	66
Fig. 3.5	A schematic cross plot of percent reservoir porosity versus percent reservoir permeability (percent due to matrix versus percent due to fractures) for the fractured reservoir classifications used by author (After Nelson 2001, Fig. 2-1, p. 102)	70
Fig. 3.6	Gilman Plot for conventional reservoirs, Cases 1 and 3. a Carbonate, light oil, pressure depletion via horizontal and vertical wells, moderate aquifer influx, b Sandstone, heavy oil, waterflood via vertical wells (After Gilman et al. 2011, Fig. 3, p. 16.)	71
Fig. 3.7	Types of NFRs. a Homogeneous model. b Fluids contained in the fractures system. c Multiple region or composite. d Anisotropic model. e Single fracture model. f Double porosity model. (After Cinco-Ley 1996, Fig. 2, p. 52)	72
Fig. 3.8	The five types of reservoirs based on the cementation factor variable, related to different kind of reservoirs (After Soto et al. 2011, Fig. 6, p. 8)	72
Fig. 3.9	A depiction of the NFCRs ternary classification of the investigated reservoirs.	74
Fig. 4.1	Applicability of Darcy's law (VICAIRE 2014).	78
Fig. 4.2	Stabilized zone of non Darcy flow (high velocity)	80
Fig. 4.3	Flow in two parallel surfaces (a tectonic fracture)	81
Fig. 5.1	Parallel surfaces	95
Fig. 6.1	Westergaard's model.	104
Fig. 6.2	Effect of overburden during reservoir depleting	109
Fig. 6.3	E. M. Anderson's classification. (Fossen 2010)	109
Fig. 6.4	Complejo Antonio J. Bermúdez geographic location (CNH 2013)	112
Fig. 6.5	CAJB structural contour map on top of Late Cretaceous	112

Fig. 6.6 3D structural contour of the Complejo J. Bermúdez on top of Late Cretaceous 113

Fig. 6.7 Thickness change in wells of CAJB 114

Fig. 6.8 Structure contour maps of representative active salt domes. Latitudes and longitudes of maps in this and the figures, except the Reitbrook dome, are derived from Lat-Long Services (2006). **a** Clay Creek dome, Texas, showing normal faults and contours on top of the Wilcox Formation (from McDowell 1951). **b** Reitbrook dome, Germany, showing normal faults and contours on the base of the Tertiary (from Schmitz and Flixeder 1993, with kind permission of Springer Science and Business Media). **c** Tiger Shoal dome, Louisiana, showing normal faults and contours on the top of T sand (from Smith et al. 1988; reprinted with permission from the New Orleans Geological Society). **d** West Clara dome, Mississippi, showing normal faults and contours on the base of the Ferry Lake anhydrite (from Davis and Lambert 1963; reprinted with permission from the Mississippi Geological Society) (After Yin and Groshong 2007, Fig. 1, p. 346.) This figure is taken from Yin and Groshong, McDowell, Schmitz and Flixeder, and Smith are authors and references than have included and modified. On the other hand, Lat-Long Services (2006) is a program and company 115

Fig. 6.9 Photomicrographs of radiolarian wackestone. **a** and **b** Discontinuous fractures without cement (dark color). Taken with parallel Nicols (2.5X). **c** Pseudostratification or interlayers of calcareous shale and oil (black color), and crystallized fracture. Taken with parallel Nicols (20X). **d** Photomosaic illustrating Algae recrystallized by calcite. Taken with parallel Nicols (2.5X). 117

Fig. 6.10 Photomosaic illustrating parallel continued fractures recrystallized by calcite. Taken with crossed Nicols (2.5X) 118

Fig. 6.11 Photomicrographs of radiolarian wackestone. **a** Micrit matrix with circular radiolarian. Taken with crossed Nicols (2.5X). **b** Radiolarian totally recrystallized. Taken with crossed Nicols (20X). **c** Alternation of brown hydrocarbon in micrit matrix and thin fractures partially cemented by calcite. Taken with crossed Nicols (2.5X). **d** Recrystallized radiolarian with impregnation of brown hydrocarbon. Taken with crossed Nicols (20X). 119

Fig. 6.12 Photomosaic. Micrit matrix with radiolarian, and cemented fractures. Taken with crossed Nicols (2.5X). 120

Fig. 6.13 X-ray diffraction 1 southern sample 123

Fig. 6.14 X-ray diffraction 1 north sample 123

Fig. 6.15	Scan of limestone core, with dark shading associated to low density and white to high density regions with evident macroscopic fractures. Early Cretaceous, Complejo A. J. Bermúdez, Samaria-Luna Region, Tabasco. Mexico.	125
Fig. 6.16	Pressure behavior of CAJB.	126
Fig. 6.17	Density log and overburden stress	127
Fig. 6.18	Leak off Test (LOT). Cambridge University Press Zoback, Reservoir Geomechanics (Fig. 7.2, p. 211).	129
Fig. 6.19	Leak off test of the Complex Antonio J. Bermúdez	130
Fig. 6.20	Pressure or Stress versus depth.	131
Fig. 6.21	Sonic log transit times, with pay zone respectively.	134
Fig. 6.22	Shear and compressional waves velocities, with pay zone respectively.	135
Fig. 6.23	Poisson's ratio determined using sonic log, with pay zone respectively.	135
Fig. 6.24	Young's modulus using sonic log, with pay zone respectively.	136
Fig. 7.1	Workflow of NFCR, for an advanced strategy and reservoirs production.	142

List of Tables

Table 2.1	Data and parameters of limestone reservoir A	43
Table 2.2	Additional data for the calculation of fluid velocities	43
Table 2.3	Calculated parameters values	43
Table 2.4	Data and parameters for the Cardenas Field, well Cardenas-109	46
Table 2.5	Data and parameters for the Cardenas Field, well Cardenas-129	47
Table 2.6	Data and parameters for the Cardenas Field, well Cardenas-308	47
Table 2.7	Calculated velocities and rates values for the Cardenas Field, wells C-109, C-129, and C-308	49
Table 2.8	Mathematical models summary for fractures, impact and fault breccias.	51
Table 2.9	Mathematical models summary for sedimentary breccia and vug	52
Table 3.1	Parameters and applications of flow models for NFRs (After Cinco-Ley 1996, Table 1, p. 52)	72
Table 3.2	Similarities between the literature available classifications and the ternary classification.	73
Table 6.1	Permeabilities and porosities under 800 psi confining pressure results	121
Table 6.2	Oxides quantification in carbonates rocks samples	122
Table 6.3	Content of calcite, quartz and others elements in samples	123
Table 6.4	Indirect test of tensile strength	130
Table 6.5	Triaxial test and elastic properties.	133
Table 6.6	Wave velocities	133
Table 6.7	Reservoir properties	137
Table 6.8	Mechanical properties.	137
Table 6.9	Wave velocities	137
Table 6.10	Single fracture width and length.	138
Table 6.11	Single fracture width and length with initial pressure.	138

Table 6.12 Single fracture width and length with initial pressure 139
Table 6.13 Fracture network width and length with initial pressure 139
Table 7.1 Applicability and benefits of the doctoral thesis 142

Chapter 1

Introduction



Despite the fact that the exploitation of carbonate reservoirs problem started more than 100 years ago, the remaining challenges regarding hydrocarbon production remain at all time high. These reservoirs that present discontinuities and inhomogeneities represent a strong challenge because they are complex systems with interdependent variables that require to be understood. Moreover, these carbonate reservoirs contain the largest and productive oil reserves in the world.

To achieve the optimum recovery the kind of naturally fractured reservoir is other great problem. In consequence our research questions will be: How could connected fractures describe and link up in a carbonate reservoir? geological and fluid dynamical point of view, do fractures represent all of discontinuities in a carbonate reservoirs? And finally, when would fractures close during carbonate reservoir depressurization? In the literature, there are many field reports about closed fractures during and after oil production, such as Ekofish, and Valhall field, generating trapped oil in this type of fractures and crude production reduction (Cook and Jewell 1995) and (Hermansen et al. 1997).

Our hypothesis is based on whether it is possible to develop an analytical coupled model integrating fluid dynamics and geomechanics, identifying stresses system and their impact in creation of open and closed fractures, as consequence of pressure change during reservoir oil production. To pursue this hypothesis, it is necessary to understand the rock, and to study fluid dynamics and geomechanics behavior of carbonate reservoirs considering their natural fractures as a dynamic system.

The main goal of this doctoral thesis is to propose and develop an analytical coupled model that considers in situ stress and fluid flow, focusing in natural fractures to plan the advanced development of carbonate reservoirs that would allow its production optimization. To achieve this essential objective is important to describe the fracture system dynamics during reservoir depletion and to establish a mathematical model with interaction between pore pressure, and local stress in carbonate reservoirs.

1.1 Problem Statement

A carbonate reservoir may contain various types of discontinuities such as impact, sedimentary, collapse, and fault breccias; tectonic fractures; vugs; and caverns. Discontinuities role in fluid flow in carbonate reservoirs is critical; these discontinuities act like as the main conduits for oil flow toward wells, and their small changes in “aperture” might cause a big change in permeability and in oil production rate. Discontinuities deformation could have a strong effect on reservoir compaction due to deformable rocks. Theses conductivity systems may be important in recovery carbonate reservoirs.

In this research, it was studied discontinuities with the principal objective of to prevent their collapse, to propose an advanced development strategy of reservoir, and to avoid negative impact in fluid flow. To reach this goal, it was used geomechanics, well testing and fluid dynamics as an interdisciplinary integrated work. This aspect, which has not been paid attention from simulation and modeling point of view, plays a role in management of Naturally Fractured Carbonate Reservoirs (NFCRs).

1.2 Methodology

Achieving the goals of this research requires diverse areas. Consequently, development of a coupled analytical model needs a multidisciplinary and interdisciplinary work. The integration of Geomechanics, Geology and Fluid dynamics, help the physics formulation of a coupled model (Fig. 1.1). In this way, the phenomenological description of problem can be developed with elegance and apparent easiness, that concludes in a coupled analytical model. Theoretically, pore pressure changes, open-closed fractures, in situ stresses and fluid flow in carbonate reservoirs can be included in a simple mathematical problem. However, in practice, it is very difficult to make a model that represent phenomenon without to use a geologic context and without understand the formation.

Understanding the rock implies reservoir anatomy, geological events juxtaposition, and static and dynamic variables quantification. Rock study begins by reviewing the results static model and identifying its characteristics, type of rock, petrography, and X-ray that has been analyzed. In addition to, the discontinuities description is obtained using logs, cores, and tomography.

Fluid dynamics involves fluid flow kinematics, and well testing. In spite of many restrictions, it describes reservoir physiology.¹ In the thesis, fluid kinematics problem is solved through the velocity potential. Production and well testing data are used to describe reservoir dynamic behavior and interaction with geological events.

Geomechanics is the action and reaction law in the reservoir, that always tends to find the equilibrium. Mechanical properties and in situ stresses are determined

¹Reservoirs anatomy and physiology are some learned words of my mentor, Dr. Héber Cinco Ley.

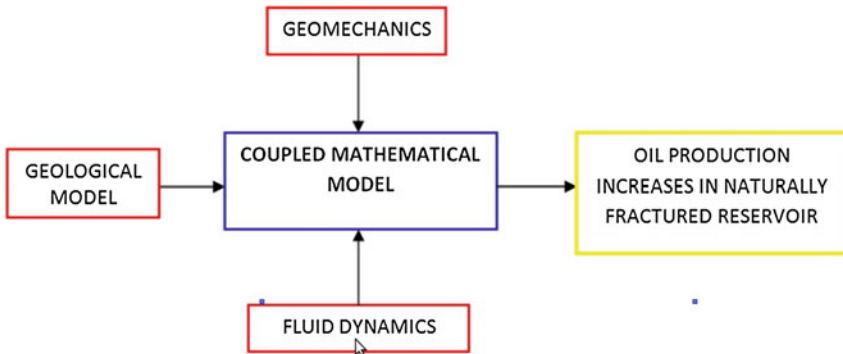


Fig. 1.1 Doctoral thesis general methodology

employing logs, laboratory test, and leak off test (LOT), focusing in the stress path during reservoir depressurization.

Our goal in the petroleum and gas industry is to increase oil production. Although, thesis may be visualized as a tool that helps to achieve the great objective of the hydrocarbons industry.

1.3 Scope

In this research, it is intended to model and to understand the open fractures behavior during reservoir depleting. Effects of stress and pressure on deformation of porous media is restricted to:

- Single phase oil flow.
- Analytical model.
- Validation with laboratory and well testing data.
- Related to Naturally Fractured Carbonate Reservoirs (NFCRs).

1.4 Outline of the Thesis

In the following chapters, we will discuss our research work in detail. Each chapter contains a literature review, a discussion, references, and applications, for the better understanding of the obtained developments and results. Nomenclature is (SI) Units; in some cases, Oilfield Units is specified. The organization of this thesis is as follows:

- Chapter 2. Phenomenology and Contradictions in Carbonate Reservoirs demonstrates different kind of discontinuities identified considering geological evidences, mathematical kinematics model and tomography are described.

- Chapter 3. Static and Dynamics Classification of Carbonate Reservoirs, includes a classification of carbonate reservoirs with field application and validation. This chapter discusses the diverse types of carbonate reservoirs and their relation with production and other dynamics variables.
- Chapter 4. Analytical model for Non Stress Sensitive Naturally Fractured Carbonate Reservoirs (NFCRs), includes the development a mathematical model for fluid flow in carbonate reservoirs with application and validation.
- Chapter 5. Analytical model for Stress Sensitive Naturally Fractured Carbonate Reservoirs (NFCRs), presents a mathematical model for stress sensitive naturally fractured carbonate reservoirs, with application and validation.
- Chapter 6. Westergaard's Solutions Applied to Naturally Fractured Reservoirs, evolves a fracture mechanics model for extensional and shear natural fracture in reservoirs. These solutions are used as predictive model during reservoir depleting.
- Chapter 7. Potential Applications and Impact in Petroleum Industry, presents the thesis as a tool that may contribute for petroleum industry and identify some problems that need to be considered in commercial simulators.
- Chapter 8. Conclusions and Recommendations, conclude this thesis and identifies several avenues for future research.
- Appendix. Figure 6.7 zoomed and included in this appendix to Chap. 6.

References

- Cook, C. C., & Jewell, S. (1995). *Reservoir simulation in a North Sea Reservoir experiencing significant compaction drive*. Paper SPE 29132 Presented at the 13th SPE Symposium on Reservoir Simulation held in San Antonio, TX, 12–15 February.
- Hermansen, H., Thomas, L. K., Sylte, J. E., & Aasboe, B. T. (1997). *Twenty five years of Ekofisk reservoir management*. Paper SPE 38927 Presented at the 1997 SPE Annual Technical Conference and Exhibition held in San Antonio, Texas, 5–8 October.

Chapter 2

Phenomenology and Contradictions in Carbonate Reservoirs



In 1972, Neale and Nader described the flow dynamics in a vuggy porous medium using the creeping Navier-Stokes and the Darcy equations in the surrounding homogeneous and isotropic medium. Koenraad and Bakker in (1981) proposed a theoretical study about fracture/vug, collapse breccias, and brecciated karst based on geological information. Wu et al. in (2011) proposed numerical models multiphase and single-phase flow for vuggy reservoirs using balance mass equations; Darcy and Forchheimer equations; and Hagen Poiseuille tube flow. In 1999, McKeown et al. developed a numerical groundwater flow model for Sellafeld, in which they modeled hydrogeological Brockram fault breccia using Darcy's equation applied to a limestone with porosity between 1 and 10%, obtaining a range of hydraulic conductivity. Gudmundsson studied fluid flow behavior using Darcy equation applied to breccias and faults.

These complex limestone reservoirs are associated with geological events (tectonic fractures, sedimentary breccias, impact breccias, vugs, and fault breccias) that require to be understood dynamically and geologically to properly derive an analytical model that would describe flow behavior. A significant portion of the world oil reservoirs is found in carbonates (Wenzhi et al. 2014) and (Manrique et al. 2004); early identification of the types of geological discontinuities that are dominant in limestone rock is one of the principal problems for advanced development and efficient exploitation of the reservoirs, because of impact in the reservoir oil flow.

The phenomenology of fluid flow in limestone carbonate reservoirs depends on type of discontinuities; connected discontinuities have a dependence on, at least, diagenesis, structural history, and lithology. A key concept is that planar or nonplanar discontinuities can lead to different flow response during oil production. Moreover, limestone carbonate reservoirs are modeled, confused, and associated with planar discontinuities named tectonic fracture networks causing contradictions. Processes that generate nonplanar discontinuities are usually excluded, and models do not represent the reservoir reality, when based on an equivalent flow medium. A case

well-known is Cantarell field, which is the eighth largest oil field in the world, with fractures, breccias, and vugs (Grajales et al. 1996; Murillo-Muñetón et al. 2002), and (Levresse et al. 2006) located in the Campeche Sound, Yucatán a Platform in Mexico. This reservoir is modeled using tectonic fracture networks without considering vugs, fault and impact breccias, and caverns (Rivas-Gómez et al. 2002; Manceau et al. 2001) and (Cruz et al. 2009); in effect, these tectonic fractures are used to represent all types of discontinuities.

The purpose of this paper is to demonstrate how qualitative and quantitative differences between tectonic fractures, fault breccias, sedimentary breccias, vugs, and impact breccias affect the exploitation strategy and advanced development of carbonate reservoirs. Our hypothesis considers that all the discontinuities in carbonate reservoirs are distinct and cannot be called or analyzed as tectonic fractures without knowing their genesis and discontinuity impact in the reservoir, or only focusing in fluid flow. To demonstrate this hypothesis, we understood the rocks nature and used sub-surface geological analogs (outcrops), cores, computerized tomography, and analytical modeling, making use of fluid flow kinematics.

Sedimentary breccias are related to debris flow. The physics of debris flow published by Iverson (1997) analyzed flows of dry, granular solids and solid-fluid mixtures and described the grains behavior through momentum, mass, and energy balances. Enos described debris reservoir and sedimentary breccias in Tamabra Limestone of the Poza Rica field in Mexico, with field ranges of porosity of 3.7–9.7% and permeability of 0.01–700 md with depth ranging between 1980 and 2700 m and cumulative production to July 1983 of 1.98 billion oil barrels. There are many impact breccias, but, associated with oil reservoir, the most known is KT limit in Cantarell located in Campeche Bay, Yucatan Platform in Mexico, related to the Chicxulub impact (Urrutia-Fucugauchi 2013). From the point of view of fluid flow, Mayr et al. in (2008) estimated rocks hydraulic permeability associated with the impact crater Chicxulub using Nuclear Magnetic Resonance, Kozeny-Carman equation, and the fractal PaRis-model obtaining low hydraulic permeability.

2.1 First Contradiction: Tectonic Fracture or Nonplanar Discontinuity?

Unfortunately, whatever the discontinuity (planar or nonplanar), it is considered as a natural fracture. Usually, oil reservoirs with discontinuities are “naturally fractured”, causing confusion in reservoirs simulation. Our discussion begins with the following: the word fracture derived from the Latin *fractus* means “broken” and its definitions are as follows.

“A natural fracture is a macroscopic planar discontinuity, which results from stresses that exceed the rupture strength of the rock” (Stearns and Friedman (1972); Stearns (1992)).

Fig. 2.1 Limestone core with planar tectonic fractures, Early Cretaceous, Samaria-Luna Region, TAB, Mexico



“A reservoir fracture is a naturally occurring macroscopic planar discontinuity in rock due to deformation or physical diagenesis” (Nelson 2001).

“A fracture is any planar or subplanar discontinuity that is very narrow in one dimension compared to the other two and forms as a result of external (e.g. tectonic) or internal (thermal or residual) stress” (Fossen 2010).

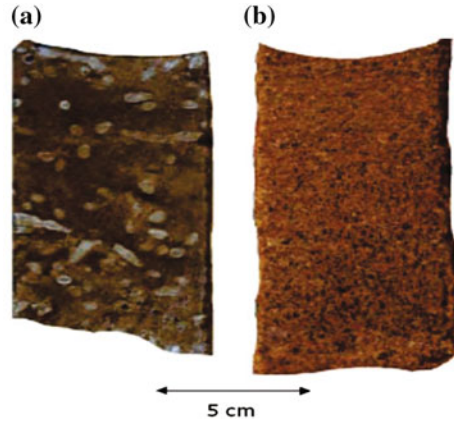
These definitions converge in that fractures result from stresses and deformation on the rock, mechanical diagenesis that generates volume reduction by compaction during burial. Whether natural tectonic fractures result as the effect of stresses and mechanical compaction, why are sedimentary breccia, impact breccia, fault breccia, and vug considered natural fractures regardless of the genesis of these geological events? This is the first contradiction.

The discontinuities observed in limestone reservoirs are planar or nonplanar. The observation of the core of limestone reservoirs in Fig. 2.1 shows a planar natural fracture with inclination; it is a preferential path for oil flow; its aperture has been developed on the plane of weakness (with low cohesion) as consequence of stresses on the rock. Although the core was badly preserved, its natural fracture presents an aperture increase, but it is natural.

However, many reservoirs normally contain nonplanar discontinuities caused by diagenesis. The dissolution processes (chemical diagenesis) as result of expelled water generate vugs, caverns, and clasts dissolution. This type of discontinuities affects the fluid flow and creates an interconnected system through pores. The Fig. 2.2a presents Cladocoropsis that could act as barrier because these fragments have not been fragmented or dissolved. Also, Fig. 2.2b shows a core with fragmented Cladocoropsis grainstone due to chemical diagenesis, creating a secondary porosity and permeability, connecting pores system (primary and secondary porosity).

Reservoir engineers have assumed discontinuities as a type of pores regardless of their origin or genesis, and tectonic fractures are considered as structural discontinuities impacting fluid flow (Alhuthali et al. 2011). So the discontinuities or heterogeneities such as vugs, tectonic fractures, and porosity associated with breccias can be interpreted with an equivalent medium (Lee et al. 2003). In this case, “all is tectonic fractures” regardless of their genesis creating confusion. When we compare and observe Fig. 2.1 with Fig. 2.2, it can be inferred that in dissimilar media oil flows have different velocities. From a modeling point of view, the discontinuities (planar or nonplanar) in the reservoirs should be related to their genesis and fluid characteristics flow to understand the phenomenology of limestone systems.

Fig. 2.2 Core slabs of *Cladocoropsis*. **a** Mud supported limestone. **b** Fragmented *Cladocoropsis* grainstone, Ghawar field, Saudi Arabia (After Voelker 2004, Fig. 6.7, p. 115)



2.2 Second Contradiction: How Do Different Discontinuities Impact?

Despite the fact that there exist different kinds of discontinuities, such as tectonic fractures, vugs, caves, collapse breccias, sedimentary breccias, fault breccias, and impact breccias, in transient pressure analysis and reservoir simulation all of them are considered as fractures or fissures. In consequence, they are represented as planes in the reservoir, with orientation, intensity, or fracturing frequency, with specific geometry, and with fluid dynamical properties. This study is based on open and connected discontinuities.

The discontinuities clearly affect fluid flow in the reservoir. However, each discontinuity creates a particular hydrocarbons flow behavior, specifically, in limestone reservoirs. It is essential to understand them to properly study its influence on the production behavior of the reservoirs.

The phenomenology of discontinuities begins with their geometry. In principle, a planar geometry describes a parabolic flow profile for conditions of laminar flow for tectonic fractures; the fluid velocity is associated with the aperture and roughness of the discontinuity, which is linked to the permeability. The pressure profile changes are due to friction, tortuosity, the complex interconnected system, and cross flow. This phenomenon is present in tectonic fractures.

A nonplanar discontinuity shows nonparabolic flow profile because of high oil velocity and heterogeneous media. The fluid high velocity is directly linked with geometry, shape, aperture, roughness, diameter, discontinuities distribution, irregular surfaces, and pressure. In the case of vugs and caverns, their diameters or apertures are large and generate zones of high permeability, or superhighway production.

Discontinuities (planar or nonplanar) can be described through visible geological features related to geometry; specifically, cross section flow area, which has a direct impact in fluid flow. This can be understood using the flow concept $q = Au$. A nonplanar discontinuity area is greater than planar discontinuity area; in effect,

flow increases because pores may be connected and their size are increased due dissolution. In addition, when the flow area is increased, oil velocity u increases too. This will be demonstrated using analytical models in this study. Moreover, it can be observed when vugs and caverns are compared with tectonic fractures that they have a greater permeability. In summary, fluid flow in a planar discontinuity (fracture) is different to flow in nonplanar discontinuity (vugs, breccias, and caverns). This is the second contradiction, considering that hydrodynamics intrinsic to geometry or flow area because there is a mass and momentum transfer process, oil flow in each discontinuity unique and cannot be traditionally considered as fractures. The understanding and comparison of these dynamic and geological differences in limestone reservoirs allow the accuracy of fluid flow characteristics and approach their optimum exploitation strategy.

Although discontinuities generate highly heterogeneous and anisotropic systems, a complex reservoir could evidence different types of geological characteristics; production and pressure behavior might identify dominant discontinuities, and, to achieve a reasonable modeling, it should be considered that they might in some cases perform as seal or flow barriers.

However, before carrying out pressure transient test and reservoir dynamic simulations, it is necessary to characterize these discontinuities and establish convergence between geology and fluid flow features, using cores, outcrops, seismic, well logs, tomography, pressures profiles, production, and mathematical modeling that describe the flow kinematic reservoir fluid flow.

It is becoming increasingly difficult to ignore the differences between types of discontinuities, in which all of them are called fractures by simplicity. Therefore, there is a need to be explicit about the phenomenology of discontinuities.

2.3 Analogs Reservoirs and Outcrops for a Flow Analytical Model

Reservoir analog based on outcrop studies provides definitions of geometry and heterogeneities at interwell scales and characterizes reservoirs (McMechan et al. 1997). A subsurface reservoir model using outcrop analog (Pringle et al. 2006) is employed for an understanding of geological parameters associated with reservoir and at outcrop rock (porosity, permeability, and heterogeneities) with the objective of characterizing it.

Outcrops were at geological conditions of subsurface; fortunately they are exposed, and we may describe a reservoir with similar features. In this paper, we used outcrops to understand physics of each discontinuity (vugs, breccias, and fractures) and tomography to know how is the fluid flow through the rock. As a result of understanding that rock, we developed an analytical model.

2.4 Geological and Tomography Features of Tectonic Fractures

Limestone reservoirs constitute a portion of the basin. Tectonic fractures are planar discontinuities in reservoirs. Generally, the genesis of fracturing is tectonism and it is related to local folds, faults, or a regional system (Stearns and Friedman 1972). There are different fractures types: shear fractures or slip surface, extension fractures such as joints, fissures, and veins, and contraction or closing fractures as stylolites (Fossen 2010). Open fractures can behave as hydraulic conductors and impact the productivity of the reservoir.

Tectonic fractures have been observed in carbonate cores, but it is difficult to obtain complete cores due to its brittle nature (Fig. 2.1). Tectonic fractures can be open, deformed, and mineral-filled. In spite of deformation, it is evident that tectonic fractures are planar discontinuities that could store and produce hydrocarbons. In outcrops, these fractures are studied because they explain paleostresses (Fig. 2.3). Also, these surface systems are used as an analogical model in reservoir characterization. Figure 2.3 shows different planar fractures systems as a result of paleostresses in the rock, and it is observed that each fracture has its aperture that may be interconnected, inclined, parallel, orthogonal, open, or closed. This outcrop was buried at subsurface conditions during a geological age; nowadays it is exposed. In Fig. 2.3, diverse types of natural fractures can be observed.

X-ray computerized tomography (CT) is a nondestructive technique that allows visualization of the internal structure of rocks, determined mainly by variations in density and atomic composition (Mees et al. 2003). One well-known advantage of tomography is fracture morphology description inside the rock. This implies that open fractures are observed as planar discontinuities with a specific physical behavior. In consequence, the dominant parameter in tectonic fractures is aperture. Aperture is associated with permeability, parabolic flow profile, maximum and mean velocity, and the flow rate.

A study illustrated how width or aperture impacts fracture permeability using an equation flow (Baker 1955). It was shown that a single fracture of 0.25 mm aperture

Fig. 2.3 Tectonic fractures system outcrop, Canada

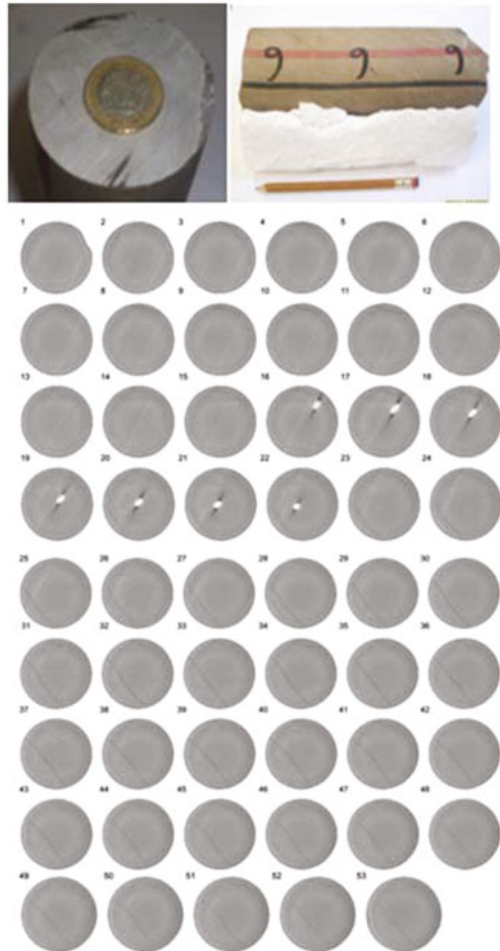


has the equivalent permeability of 188 m of unfractured rock, with a uniform permeability of 10 md, and a 1.27 mm aperture fracture is equivalent to 173 m of rock with a permeability of 1,000 md.

Tomography was used to show internal fractures and to verify their morphology. Useful, calcareous cores without dissolutions or visible discontinuities are considered as matrix rock without fractures. In many cases, narrow subplanar fractures can be observed using tomography or would be inferred if the density in the core internal structure shows changes.

A sample core in a limestone reservoir (15.9 cm in length and 10 cm in diameter) was obtained. The scan of a limestone core (Fig. 2.4) at 3 mm spacing showed that rock contains narrow subplanar fractures. They are open, deformed, and/or mineral-filled. In images 16–21 an open fracture with great aperture can be seen, and in images

Fig. 2.4 Scan of limestone core, with dark shading associated with low density and white with high density regions with evident macroscopic fractures, Early Cretaceous, Samaria-Luna Region, Tabasco, Mexico



30–42 other fractures can be observed, but with small aperture. Moreover, doing a visual inspection of core does not observe any fractures that may be connected (see slides 30–53 in Fig. 2.4). Approximately, these limited length fractures have 1–2 mm apertures and would allow hydrocarbons flow; in effect they also provide effective porosity because fracture connects spaces in this rock.

2.5 Analytical Model for the Profile Velocity of Tectonic Fractures

Fluid flow is defined by a velocity vector field and a pressure scalar field. In order to understand how permeability influences fluid flow in fractures, we analyze flow and fluid kinematics equations. Kinematic equations are applied to an isothermal, low viscosity, irrotational, and single-phase fluid flow and are referred to as potential flows and stream function. Applicability of kinematic equations is limited to Reynolds numbers, Re , more than unity because the inviscid fluid flow theory corresponds to high flow values and small fluid viscosity. Calcareous reservoirs heterogeneities may produce high velocity flow.

At larger Reynolds numbers, kinematic equations are suggested for Newtonian liquids of minimal viscosity and gases.

Fluid kinematics describes fluid motion using streamlines and potential function, with respect to a plane, and a flow equation describes a close relationship between fracture aperture, pressure, and velocity and flow rate, using classical methods in fluid mechanics. Kinematics of fluid flow would show a particular behavior of flow lines for each discontinuity, in this case for tectonic fractures (Fig. 2.5a). Classical methods in fluid mechanics are illustrated by an analytical model for velocity profile in parallel plates (Potter et al. 2012). Two symmetrically inclined parallel surfaces with respect to the x -axis are shown in Fig. 2.5b. Fluid motion is in the x direction and flow velocity distribution in the y direction, for steady state of an incompressible

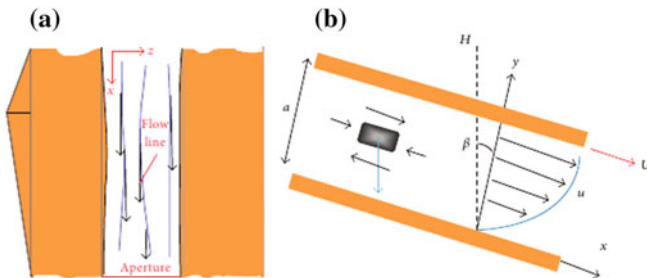


Fig. 2.5 Top and lateral views of fluid flow in a tectonic fracture. **a** Flow lines in an open fracture (top view). **b** Flow profile between two inclined parallel plates (lateral view) (Potter et al. 2012)

fluid of constant density is indicated in this figure; pressure variation is a function of x coordinate, and the surface longitudes are larger than the aperture.

Figure 2.5 shows top and lateral views in an open fracture simulated with two inclined plates that may be fixed. Figure 2.5a presents straight and parallel flow lines and Fig. 2.5b shows a parabolic velocity profile. Our contribution is the application of the Couette flow exact solution for natural fracture to obtain specific solution that describes flow profile for natural fissure. When a plate is moving; namely, system may be interpreted as a stress-sensitive system (use Couette flow). Fixed plates may be understood nonstress sensitive (use Poiseuille flow). So, Couette equation is a general case with respect to Poiseuille equation.

Newtonian fluid flow of a single phase through a fractured rock is governed by the Navier-Stokes equations (Witherspoon et al. 1980) and (Zimmerman and Yeo 2000). To simplify the discussion, we will consider a “one-dimensional” fracture and use the Navier-Stokes equations exact solution known as Couette flow, and this discussion about laminar flow between plates may be detailed in (Potter et al. 2012). Using Navier-Stokes equations,

$$\rho \left(\frac{\partial u}{\partial t} + u \frac{\partial u}{\partial x} + v \frac{\partial u}{\partial y} + w \frac{\partial u}{\partial z} \right) = -\frac{\partial p}{\partial x} + \mu \left(\frac{\partial^2 u}{\partial x^2} + \frac{\partial^2 u}{\partial y^2} + \frac{\partial^2 u}{\partial z^2} \right) + \gamma \sin \beta \quad (2.1)$$

Considering the previously stated fracture flow problem regarding Fig. 2.5a. Then, Eq. 2.1 can be simplified as follows:

$$0 = -\frac{\partial p}{\partial x} + \mu \left(\frac{\partial^2 u}{\partial y^2} \right) + \gamma \sin \beta \quad (2.2)$$

In Fig. 2.5b, $\sin \beta = dH/dx$ and applying in Eq. 2.2

$$\frac{\partial^2 u}{\partial y^2} = \frac{1}{\mu} + \left(\frac{\partial p}{\partial x} + \gamma H \right) \quad (2.3)$$

Boundary conditions are $u = 0$ for $y = 0$. In the limit, when y nearly reaches the fracture aperture a and fluid velocity (u) is close to the terminal upper plate velocity (U), then $u = U$ for $y = a$, and $\partial^2 u / \partial y^2 = \lambda$, where $\lambda = \text{constante}$.

To obtain the solution of Eq. 2.3, it is necessary to integrate and apply boundary conditions. This solution is $u(y) = (\lambda/2)y^2 + Ay + B$, which is a parabola. The constants A and B are obtained by integration and finally result in the following equation:

$$u(y) = \frac{1}{2\mu} (y^2 - ay) \frac{\partial(p + \gamma H)}{\partial x} + \frac{U}{a} y \quad (2.4)$$

Equation 2.4 describes the Couette flow because there is a linear plate movement and can be used for stress-sensitive tectonic fractures. However, Eq. 2.4 can be written as.

$$u(y) = \frac{1}{2\mu} (y^2 - ay) \frac{\partial(p + \gamma H)}{\partial x} \quad (2.5)$$

Equation 2.5 corresponds to the steady flow pressure distribution through two inclined parallel surfaces when $U = 0$ (Poiseuille flow); it can be used to derive an expression for the rate flow of nonstress-sensitive tectonic fractures using $q = \int u dA$, where $A = a \cdot 1$ gives

$$q = \int_0^a \frac{1}{2\mu} (y^2 - ay) \frac{\partial(p + \gamma H)}{\partial x} dy = -\frac{a^3}{12\mu} \frac{\partial(p + \gamma H)}{\partial x} \quad (2.6)$$

Equation 2.6 is known as The Cubic Law which has been used in fractured rocks (Witherspoon et al. 1980), and the mean velocity (\bar{u}) is obtained using $\bar{u} = q/A$; substituting Eq. 2.6 gives

$$\bar{u} = -\frac{a^2}{12\mu} \frac{\partial(p + \gamma H)}{\partial x} \quad (2.7)$$

Deriving with respect to y Eq. 2.5, substituting $y = a/2$, and applying the maximum and minimum criterion, the maximum velocity can be obtained:

$$u_{max} = -\frac{a^2}{8\mu} \frac{\partial(p + \gamma H)}{\partial x} \quad for \quad y = a/2 \quad (2.8)$$

Equations described based on the classical methods in fluid mechanics have been developed to calculate flow rate in tectonic fractures. The negative sign in Eqs. 2.6, 2.7, and 2.8 is related to flow in the direction of the negative pressure gradient. Although, the cubic equation was derived for tectonic fractures, it is used for diverse kinds of discontinuities (breccias, vugs, and channels) yet.

For natural fractures, our contribution is the application of the Couette flow general solution that describes flow profile in a natural fissure. But it will be compared with flow kinematics equations to know the range of velocity or when maximum and mean flow velocity can be used.

2.6 Kinematic Analytical Modeling for Tectonic Fractures

For flow visualization, three types of flow lines are used. Three types of fluid element trajectories are defined: streamlines, pathlines, and streaklines. They are all equivalent for steady flow but differ conceptually for unsteady flows.

Streamlines are lines tangents to the velocity vector and perpendicular at lines of constant potential, called equipotential lines, a pathline is a line traced out in time by a given fluid particle as it flows, and a streakline is a line traced out by a neutrally buoyant marker fluid which is continuously injected into a flow field at a fixed point in space (Currie 2003).

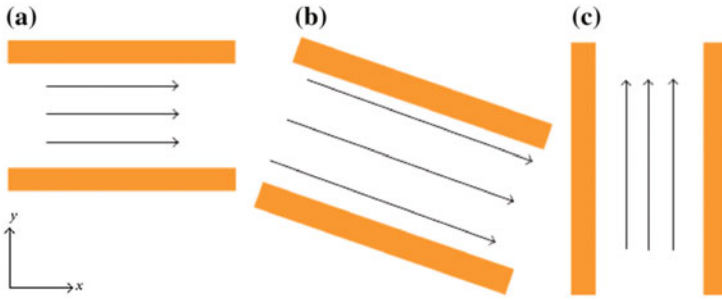


Fig. 2.6 Streamlines in uniform rectilinear flow in tectonic fractures with parallel walls, **a** horizontal direction, **b** inclined direction, and **c** vertical direction

To demonstrate the difference between the types of discontinuities, streamlines are used. These are associated with stream analytical function (Ψ) and potential analytical function (Φ). In tectonic fractures, their streamlines are parallel and would tend to be uniform (Fig. 2.6).

The theory of complex variable guarantees that Laplace’s equation for the velocity potential $\nabla^2\Phi = 0$ and for the stream function $\nabla^2\Psi = 0$ is satisfied and can be solved. Then,

$$\begin{aligned}
 u &= \frac{\partial\Phi}{\partial x} = \frac{\partial\Psi}{\partial y}, \\
 v &= \frac{\partial\Phi}{\partial y} = -\frac{\partial\Psi}{\partial x}.
 \end{aligned}
 \tag{2.9}$$

Equation 2.9 recognized as the Cauchy-Riemann equations for $\Phi(x, y)$ and $\Psi(x, y)$, and the analytical expressions used for uniform flow in Cartesian and polar coordinates are the following:

$$\Psi = uy, \quad \Phi = ux \tag{2.10}$$

$$u = U_\infty, \quad v = 0 \tag{2.11}$$

$$u_r = u\cos\beta, \quad u_\theta = u\sin\beta \tag{2.12}$$

Equations 2.10, 2.11, and 2.12 are Laplace’s equation solutions. Thus, they are satisfied to $\nabla^2\Phi = 0$ and $\nabla^2\Psi = 0$. For this demonstration in one-dimension is used the stream function $\Psi(x, y)$, as follows:

$$\begin{aligned}
\nabla^2\Psi &= 0, \\
\frac{\partial\Psi}{\partial x} &= 0, \\
\frac{\partial^2\Psi}{\partial x^2} &= 0.
\end{aligned}
\tag{2.13}$$

Following a similar procedure for velocity potential $\Phi(x, y)$,

$$\begin{aligned}
\nabla^2\Phi &= 0, \\
\frac{\partial\Phi}{\partial x} &= u, \\
\frac{\partial^2\Phi}{\partial x^2} &= 0
\end{aligned}
\tag{2.14}$$

Thus, Laplace's equations for the velocity potential $\nabla^2\Phi = 0$ and for the stream function $\nabla^2\Psi = 0$ have been satisfied.

2.7 Third Contradiction: Darcy's Flow or Couette General Flow for Planar Discontinuity (Tectonic Fracture)

For stress-sensitive system we recommend Couette flow, and for nonstress-sensitive system use Poiseuille flow. Initially, it has been referenced the use of Darcy's flow to describe behavior fluid flow in vugs (Neale and Nader 1974) and (Wu 2011), fault (McKeown et al. 1999), fault breccias (McKeown et al. 1999; Gudmundsson 2011), and fractures (Bogdanov et al. 2003).

The application of Darcy's flow is recommended when the range of value of Reynolds number (Re) is between zero and unity. Last information was reported by Muskat (1946) and is applied for low laminar velocity, namely, in porous media, although it is also applied for tectonic fractures or tectonic fractured media without considering value of Reynolds number. Our third contradiction is based on calculating Re, and if this number is greater than unity, then The Cubic Law for planar discontinuity (tectonic fracture) is necessary, in which it derived Couette flow. So, Darcy's Law should be used with caution.

2.8 Geological and Tomography Features of Fault Breccias

Fault breccias consist of planar discontinuities associated with faulting. These breccias are incohesive, characterized by predominant angular to subangular fragments and internal fractures of cataclastic rock present in a fault zone. Fragments are slickensided with variable slip directions, diverse sizes, and greater than 30% visibility.

Fig. 2.7 Fault breccia outcrop, Alberta, Canada



Fig. 2.8 Fault breccia core, Late Cretaceous, Campeche Sound, Marine Region, Mexico



Cataclastic rocks have internal planar structure, are incohesive when faulting occurs above depths of 1–4 km or upper crustal fault zones, where brittle deformation increases breccia formation processes because of stresses and tectonic activity.

Fault breccia zones enhance permeability (Woodcock and Mort 2008). In effect, fault breccias are a superhighway production in limestone reservoirs. High permeability is linked with unconsolidated faulted rock that can be a channel for the hydrocarbons flow.

A fault breccia is presented in Fig. 2.7, which shows an outcrop of limestone rock with subangular fragments, embedded in the matrix, with absence of primary cohesion and erosion; its fault breccia zone is approximately 7 m, which implies huge movement rock mass and stresses (Fig. 2.7). This outcrop is a point of comparison for fault breccia present in limestone reservoir, because it was clearly buried rock in the past geological time. In effect, fault breccias in limestone reservoirs are production paths with approximate 7–10 m (width).

Limestone reservoirs show fault breccias associated with faulting; these channels have been described as horizontal, inclined, and vertical flux surfaces, which can be regarded as planar discontinuities. A sample core (10 cm in diameter) was obtained in a limestone reservoir of the Campeche Sound. Figure 2.8 shows a limestone core with fault breccia; its geometry corresponds to successive flux planes between barriers. These planes are connected networks in the whole medium and generate interconductivity associated with permeability and effective porosity.

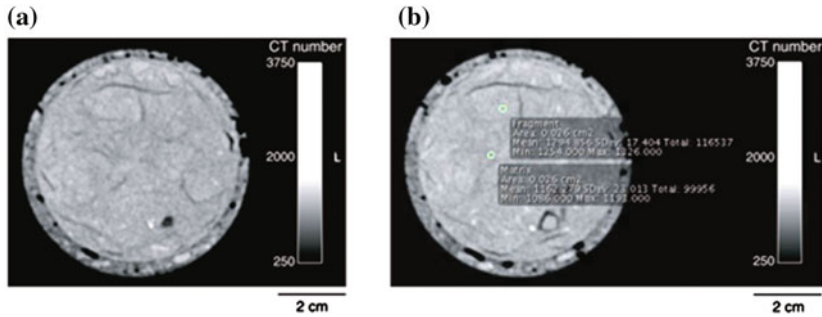


Fig. 2.9 Representative appearance of fault breccia in computerized tomography (CT) images. **a** Slice of fault breccia cut perpendicular to core axis (interval 316-C0004D-28R-2, length: 45.13 cm). **b** Same as (a) with CT numbers of matrix and fragment. Note the small contrast in CT numbers between matrix and fragment (1162 vs. 1294) (Kinoshita et al. 2009)

On the other hand, computerized tomography (CT) was used to study the internal morphology of fault breccias. Lime-stone cores with fault breccias present fragments embedded in the matrix. We used information of the Integrated Ocean Drilling Program (Kinoshita et al. 2009). Tomography images of limestone rock show the contrast between matrix and fragments that can be observed based on the different CT numbers.

Normally, fault breccia fragments are denser than the matrix, which indicates higher bulk density and low porosity, and are identified with high CT numbers. Moreover, fragments origin should be studied considering their age, lithology, CT numbers, total minerals, composition, and physical properties, to explain their density and porosity. Voids have minor CT numbers with respect to matrix and fragments.

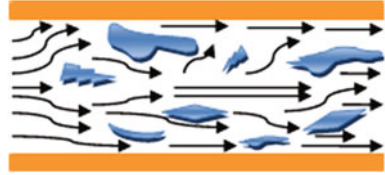
Fault and drilling-induced breccias show high contrast between fragments and matrix because of voids that CT has identified. Fault breccias present low contrast between fragments and matrix with voids, too. These empty spaces allow the oil flow through the rock; in effect, fragments act as barriers and fluid movement is linked to voids between matrix and fragments. This can be observed in Fig. 2.9.

Observing Figs. 2.7, 2.8, and 2.9, the following observations can be listed:

1. Embedded clasts in a fault breccia are subangular and angular, creating a huge flow area.
2. Fault breccias are consequence of stresses in the lime-stone rock, with planar and connected discontinuities that contain embedded clasts.
3. Fracturing and faulting intensity obeys stresses intensity.
4. In cores, the proportion of brecciated rock is greater than matrix.
5. In an outcrop, the brecciated rock has dimensions of meters.
6. Fault breccias can be described with multiple connected planes and embedded clasts.

These observations are useful for the development of an analytical model that will follow next.

Fig. 2.10 Streamlines through an angular fragment



2.9 Kinematic Analytical Modeling for Fault Breccias

In order to understand fluid flow in fault breccias, their kinematics should be studied. According to geological evidences and computerized tomography, these breccias show angular clasts with similar lithology, which act as barriers; they are poorly sorted and vary in size (1 mm–1 m). A representative scheme could be as shown in Fig. 2.10 in which clasts may be grain-supported or floating and have a matrix or cement to be responsible for close or open discontinuities.

Fractures contained in a fault breccia have a size aperture of millimeters, and zone influences of fault breccias are centimeters or meters. The unfilled spaces between clasts in a brecciated zone are preferential ways, or a complex network of discontinuities for fluid flow.

Flow modeling between unfilled spaces and clasts could be developed using the flow theory near a blunt nose, or Rankine half-body. This premise is based on geometrical similarity between the angular clasts and Rankine half-body, considering aerofoil shapes, particularly under flow conditions where the viscosity effects could be minimal (Faber et al. 1995). It is appropriate to use and to adapt the implications and equations of potential flow and streamlines to describe flow through fault breccias, considering the observations previously discussed regarding the physical phenomenon. This problem is solved in cylindrical and spherical coordinates. When cylindrical coordinates are used, physical condition is related to the radial geometry of clast and a radial function is used as a potential function. When spherical coordinates are used, the angular geometry of clast is considered and a potential function is represented using a cosine function to describe this flow problem. Then, using Laplace equation in cylindrical coordinates (r, x, θ) ,

$$\frac{\partial^2 \Phi}{\partial x^2} + \frac{\partial^2 \Phi}{\partial r^2} + \frac{1}{r} \frac{\partial \Phi}{\partial r} = 0 \tag{2.15}$$

The solution for Eq. 2.15 is a function as given by

$$\Phi = e^{cx} f(r) \tag{2.16}$$

For our physical phenomenon, $f(r)$ is a radial function due to clasts changing radially, and c is an integration constant that depends on the porous media (limestone). The velocities u_r and u_x are given as

$$u_r = \frac{\partial \Phi}{\partial r}, \quad u_x = \frac{\partial \Phi}{\partial x} \quad (2.17)$$

Equation 2.15 is a Partial Differential Equation (PDE) and substituting Eq. 2.16 into Eq. 2.15 gives an Ordinary Differential Equation (ODE):

$$\frac{d^2 f(r)}{dr^2} + \frac{1}{r} \frac{df(r)}{dr} + c^2 f(r) = 0 \quad (2.18)$$

Equation 2.18 is the Bessel differential equation of order zero, and its general solution is (Levi 1965)

$$f(r) = c_1 J_0(cr) + c_2 Y_0(cr) \quad (2.19)$$

where c_1 and c_2 are constants and J_0 and Y_0 are the Bessel function of order zero, of the first and second kinds, respectively. A series development for the first kind of Bessel function $J_0(cr)$ can be written as

$$J_0(cr) = 1 - \left(\frac{cr}{2}\right) + \frac{1}{(2!)^2} \left(\frac{cr}{2}\right)^4 + \frac{1}{(3!)^2} \left(\frac{cr}{2}\right)^6 + \dots \quad (2.20)$$

The particular solution of Laplace's equation given by Eq. 2.16 is

$$\Phi = e^{cx} J_0(cr) = e^{cx} \left[1 - \left(\frac{cr}{2}\right) + \frac{1}{(2!)^2} \left(\frac{cr}{2}\right)^4 + \frac{1}{(3!)^2} \left(\frac{cr}{2}\right)^6 \right] \quad (2.21)$$

Solution of analytical model has a constant (c) that is associated with material (limestone) and its roughness.

On the other hand, Laplace's equation can also be solved for a flow described in spherical coordinates (r, θ, \varnothing). If $\Phi = \Phi(r, \theta)$, then there is a solution $\Phi = r^n f(z)$, where $f(z)$ is function $z = \cos\theta$ and n is an integer (Levi 1965). Through the previous transformation, the following Laplace equation can be expressed as follows:

$$\sin\theta \frac{\partial}{\partial r} \left(r^2 \frac{\partial \Phi}{\partial r} \right) + \frac{\partial}{\partial \theta} \left(\sin\theta \frac{\partial \Phi}{\partial \theta} \right) = 0 \quad (2.22)$$

The velocities u_r and u_θ are given as $u_r = \partial \Phi / \partial r$ and $u_\theta = \partial \Phi / \partial \theta$. Deriving the solution Φ previously stated with respect to r and substituting it in Laplace's equation given by Eq. 2.22,

$$(1 - z^2) \frac{d^2 f(z)}{dz^2} - 2z \frac{1}{r} \frac{df(z)}{dz} + n(n + 1) f(z) = 0 \quad (2.23)$$

Equation 2.23 is the Legendre differential equation, which is a second-order ODE, and its solution for an integer n is given by the Legendre polynomials $P_n(z)$. Then, the solution for Eq. 2.23 is given by

$$\Phi(r, \theta) = r^n P_n(\cos\theta) \quad (2.24)$$

Legendre's polynomial of order n (0 and 1) is

$$\begin{aligned} P_0(x) &= 1, \\ P_1(x) &= x \end{aligned} \quad (2.25)$$

Equation 2.23 has a term $n(n+1)f(z)$, which indicates a linear combination (Levi 1965). A general solution has an additional term:

$$\Phi(r, \theta) = \left(A_n r^n + \frac{B_n}{r^{n+1}} \right) P_n(\cos\theta) \quad (2.26)$$

where A_n and B_n are constants.

The differential equation given by Eq. 2.22 is linear; then solutions can be superposed to produce more complex solutions:

$$\Phi(r, \theta) = \sum_{n=0}^{\infty} \left(A_n r^n + \frac{B_n}{r^{n+1}} \right) P_n(\cos\theta) \quad (2.27)$$

Equation 2.27 is a solution for Legendre's equation. According to Legendre's polynomial of order n with $P_n = 1$, this potential function can be used in stable steady, irrotational flow and spherical coordinates and can represent some fluid flow problems. This equation describes uniform flow, a source and a sink flow, a flow due to a doublet, a flow around a sphere, a line-distributed source, and a flow near a blunt nose. A_n and B_n play an important role in the solution because it is possible to superpose the geological events that influence the fault breccias. In addition, this solution does not depend on porous media (limestone) or experimental constant; namely, it considers fluid flow only. For example, for uniform flow (applied to planar discontinuities, whose conditions are parallel, irrotational flow), the A_n and B_n parameters in Eq. 2.27 simplify as

$$\begin{aligned} \text{If } B_n &= 0 & \forall n, \\ A_n &= 0 & \text{for } n \neq 1, \\ A_n &= u & \text{for } n = 1. \end{aligned} \quad (2.28)$$

Then, the potential, the stream function, and the radial and angular velocities can be expressed as

$$\begin{aligned} \Phi(r, \theta) &= ur(\cos\theta), \\ \Psi(r, \theta) &= \frac{1}{2}ur^2\sin^2\theta, \\ u_r &= \frac{\partial\Phi}{\partial r} = u\cos\theta, \\ u_\theta &= \frac{1}{r}\frac{\partial\Phi}{\partial\theta} = -u\sin\theta, \end{aligned} \quad (2.29)$$

For a source and sink flow (applied to discontinuity with embedded clasts, whose conditions are slow and irrotational flow),

$$\begin{aligned} \text{If } A_n &= 0 \quad \forall n, \\ B_n &= 0 \quad \text{for } n \neq 0, \\ B_n &\neq u \quad \text{for } n = 0. \end{aligned} \quad (2.30)$$

Then, the velocity potential, the stream function, and the radial and angular velocities can be expressed as

$$\begin{aligned} \Phi(r, \theta) &= -\frac{Q}{4\pi r}, \\ \Psi(r, \theta) &= -\frac{Q}{4\pi}(1 + \cos\theta), \\ u_r &= \frac{\partial\Phi}{\partial r} = \frac{Q}{4\pi r^2}, \\ u_\theta &= \frac{1}{r} \frac{\partial\Phi}{\partial\theta} = 0 \end{aligned} \quad (2.31)$$

Similarly, the last expressions can be deduced using Eq. 2.27 (the solution of Legendre's equation) and Cauchy equations.

For flow near a blunt nose or Rankine half-body, which can be modeled with the superposition of uniform flow and a source (applied to planar discontinuity with embedded clasts), as illustrated in Fig. 2.11,

$$\Psi(r, \theta) = \frac{1}{2}ur^2\sin^2\theta - \frac{Q}{4\pi}(1 + \cos\theta) \quad (2.32)$$

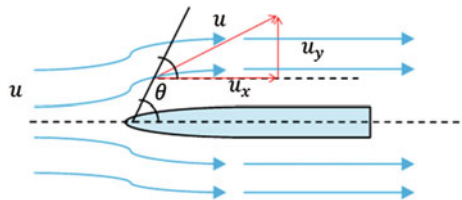
$$\Phi(r, \theta) = ur(\cos\theta) - \frac{Q}{4\pi r} \quad (2.33)$$

$$u_r = u\cos\theta + \frac{Q}{4\pi r^2} \quad (2.34)$$

$$u_\theta = -u\sin\theta \quad (2.35)$$

Equations (2.32), (2.33), (2.34), and (2.35) can be used to describe the flow kinematics in fault breccias. These analytical expressions apply to a steady,

Fig. 2.11 Flow kinematics through fault breccias, using Rankine half-body



irrotational, and axisymmetric flow. This problem can be considered as an irrotational flow because of the slow laminar movement of a viscous fluid on a planar surface (Levi 1965). Moreover, two classical methods have been proposed and adapted to describe fluid flow through fault breccias. The first method uses a solution of the Bessel equation with an experimental constant, and second method employs a solution of the Legendre equation.

2.10 Geological and Tomography Features of Chicxulub Impact Breccias and Cantarell Reservoir

Impact breccias are a consequence of the impact of asteroids, meteorites, and comets to the Earth. Meteorites are cosmic fragments rich in iron and nickel, which have generated craters on the earth surface. Impact melt breccias and suevite can contain material from the melting of target rocks. In impact breccias, brecciated target rocks, melt fragments, and allochthonous fallback breccia can be observed. Impact breccias have been observed in cores and out-crops, with embedded fragments in the ejected matrix due to the impact. A core sequence was recovered in the Yaxcopoil-1 (Yax-1) borehole located 40 km southwest of Merida and approximately 60 km from the center of the Chicxulub structure, between 794.65 and 894 m; a 100 m thick impact (suevite) breccia and impactites overlie a 617 m thick sequence of horizontally layered shallow-water lagoonal to subtidal Cretaceous limestone, dolomites, and anhydrites (Keller et al. 2004a, b). In contrast, Grajales-Nishimura et al. (2000, 2009), Rebollo-Vieyra and Urrutia-Fucugauchi (2004), Kring et al. (2004), Wittmann et al. (2004), Dressler et al. (2003), Tuchscherer et al. (2004), and Stöffler et al. (2004) used outcrops and core sequence from the Yax-1 borehole, but there are differences with respect to lithology, age, and stratigraphic column.

Representative core samples of Yaxcopoil-1 were analyzed for the estimation of hydraulic permeability. For Tertiary limestones and suevites, their bulk permeabilities range between 10–14 and 10–19 [m²] and their porosities are between 0.08 and 0.35. For Lowermost Suevite Unit, Cretaceous anhydrites, and dolomites (900–1350 m), their permeabilities range between 10–15 and 10–23 [m²] and their porosities are between 0.1 and 0.15. The previous permeability and porosity values do not include macroscopic events, such as faults and tectonic fractures (Mayr 2008).

Three decades ago, the impact crater discussion was begun. In 1975 and 1981, Lopez-Ramos (1975) and Penfield and Camargo in 1981 reported 210 km diameter circular structure with total magnetic-field data. In 1991, Hildebrand et al. (1991) suggested that a buried 180 km diameter circular structure (the Chicxulub impact crater)

was located on the Yucatán Peninsula, Mexico, which was formed 65 million years ago (Dressler et al. 2003), proposing it as candidate for the K/Pg boundary impact site.

In the offshore zone of the western margin of Yucatán Platform or Campeche Bay is located the largest oil field in Mexico and has produced more than 18000 million barrels of oil and 10000 billion of cubic feet of gas (PEMEX 2014). Outcrops analogs, petrographic analysis, well logs, and cores description indicate that Cantarell Oil Field is genetically related to the Chicxulub meteorite impact (Murillo-Muñetón et al. 2002). This genetic link is found for the Cretaceous-Tertiary (K/T) in Cantarell oil field that can also be seen in the Chiapas and Guayal outcrops located in Chiapas and Tabasco regions (Grajales-Nishimura et al. 2000).

Impact breccia clasts are impact melt fragments with rip-up morphology that are consolidated and embedded in the matrix and can be observed in Fig. 2.12, showing similar geometrical characteristics.

Figure 2.12a shows a Campeche Sound core with embedded clasts and rip-up morphology, and Fig. 2.12b shows an analog outcrop with rip-up morphology clasts, too. Considering Fig. 2.12, it can be inferred that embedded clasts act as nonflow barriers. Moreover, impact breccias contain ejected material, which generate nonplanar discontinuities, which can be observed in cores and in outcrop samples (Fig. 2.12).

The Cantarell reservoir includes the Upper Cretaceous (Upper Breccia) that is associated with the Chicxulub event, with total average porosity and permeabilities ranging from 8 to 10% and 800 to 5000 md, respectively, with average thickness of 11–105 m, thinning to the south-west, showing dissolution and dolomitization and the Upper Jurassic (Tithonian) with dolomitized limestone. The field oil production is associated with tectonic fractures that provide high permeability (Murillo-Muñetón et al. 2002; Cruz et al. 2009; Cervantes and Montes 2014) and (Barton et al. 2009).

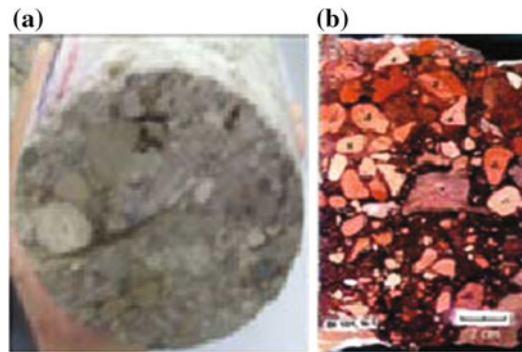
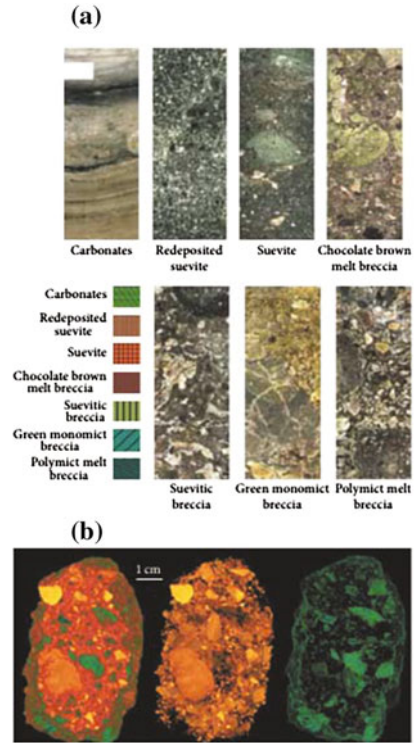


Fig. 2.12 Core and outcrop of impact breccia embedded clasts. **a** Limestone core of the Campeche Sound with rip-up morphology clasts. Late Cretaceous, Campeche Sound, Marine Region, Cantarell Complex, Mexico (Ortuño 2012). **b** Analog limestone outcrop with rip-up morphology clasts, Guayal outcrop, TAB, Mexico (Grajales-Nishimura et al. 2000)

Fig. 2.13 Samples of CT slices through the Bosumtwi and Chicxulub impacts. **a** Breccia sequence in Yaxcopoil-1 borehole. Core images obtained with the Core Scan System for the breccias sections, illustrating the different textures (Urrutia-Fucugauchi et al. 2011). **b**

Three-dimensional reconstruction of the clasts population of the Bosumtwi suevite. The image on the left shows the sample with color-coded clasts, with the matrix (groundmass) rendered partly transparent. The center image shows only the high-density clasts, with the low-density clasts (and the groundmass) rendered transparent, and the image on the right shows only the rock edges and the low-density clasts (Mees et al. 2003)



Computerized tomography is a tool to observe the differences between matrix and ejected clasts and describe internal texture of rock. Figure 2.13 indicates that clasts are nonflow barriers in impact breccias and generate nonplanar discontinuities.

Figure 2.13a shows different textures in breccia sequence of Yax-1 well; clasts or nonflow barriers are present; it indicates that there is a range of porosities and permeabilities in limestone rocks. Low porosity and permeability are related to fine ejected material. Figure 2.13b shows other impact breccias (Bosumtwi) in three dimensions; the nonflow barriers (high-density clasts) can be observed, with rip-up geometry, generating nonplanar discontinuities, and they are embedded in matrix rock (low-density).

Observing Figs. 2.12 and 2.13, the following can be inferred:

1. Embedded clasts in an impact breccia have rip-up geometry, creating a nonflow barrier in the porous media (matrix).
2. Impact breccias are a consequence of the impact of asteroids, meteorites, and comets in the Earth, generating nonplanar discontinuities that contain embedded clasts.
3. Porosity and permeability in an impact breccia are associated with ejected material (clasts), providing a type of primary porosity in the limestone.
4. In the core, the proportion of matrix rock is greater than embedded clasts.

5. In the outcrop and reservoirs, brecciated rock dimensions are related to impact size.
6. Impact breccias can be described with multiple embedded clasts (high-density) that act as nonflow barriers into connected matrix (low-density).

The previous inferences will be used in the present thesis for the development of an analytical model.

2.11 Kinematic Analytical Modeling for Impact Breccias

When an impact breccia is observed without the presence of other geological events as fault breccias, tectonic fractures, vugs, sedimentary breccias, dissolution, and dolomitization, its permeability would be ultralow (Mayr 2008) and can have a low to moderate porosity (1–8%) (Murillo-Muñetón et al. 2002). In consequence, impact breccia can act as seal and have fluid storage, but its oil production depends on tectonic fractures, fault breccias, dissolution, and vugs. It is very highly observed in the Cantarell field.

Because of its low permeability and porosity, fluid flow velocity in impact breccias is slow and can be considered as irrotational flow in a porous media with primary porosity. In addition to low permeability, rip-up geometry observed in tomography and geological evidences and clasts act as barriers for fluid flow in porous media. Figure 2.14 illustrates fluid flow with nonflow barriers and rip-up geometry for an impact breccia.

The impact breccia flow may be studied in terms of the streamlines, taking into consideration the axial flow symmetry. To solve this problem, we apply and adapt the flow through a sphere considered by Stokes; then, it is possible to use the Laplace Biharmonic equation to describe this flow (Bird et al. 2002) and (Warsi 1999):

$$\nabla^4 \Psi = \nabla^2 (\nabla^2 \Psi) = 0 \quad (2.36)$$

For spherical coordinates, Eq. 2.36 can be expressed by

$$\Psi(r, \theta) = 0 \quad (2.37)$$

Fig. 2.14 Streamlines for the flow through in rip-up fragments in an impact breccia

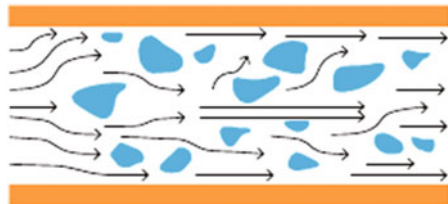
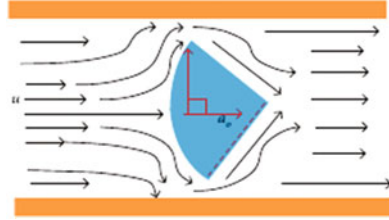


Fig. 2.15 Streamlines for a rip-up clast. Impact breccia



The boundary conditions for Eq. 2.37 are given by

$$u_r = \frac{1}{r^2 \sin \theta} \frac{\partial \Psi}{\partial \theta} = 0 \quad \text{for } r = a_o \quad (2.38)$$

$$u_\theta = -\frac{1}{r \sin \theta} \frac{\partial \Psi}{\partial r} = 0 \quad \text{for } r = a_o \quad (2.39)$$

$$\Psi = \frac{1}{2} u r^2 \sin^2 \theta = 0 \quad \text{for } r \rightarrow \infty \quad (2.40)$$

The boundary conditions given by Eqs. 2.38 and 2.39 describe fluid adherence on a clast with rip-up morphology in a porous media. Figure 2.15 represents this fluid adherence at a clast with similar rip-up morphology.

Boundary condition given by Eq. 2.40 describes the streamlines before-after a breccia clast, which implies a velocity change in fluid flow because the clast is a barrier; namely, for $r \rightarrow \infty$, the final clast velocity is obtained. In accordance with this boundary condition is a general solution for Laplace Biharmonic equation expressed as follows:

$$\Psi(r, \theta) = f(r) \sin^2 \theta \quad (2.41)$$

This solution proposes radius and angle change of clast. However, it is necessary to study the Stokes solution and test if it can be adapted to oil flow in an impact breccia. Equation 2.41 contains $f(r)$, which is a radial function related to the clast radius. Substituting Eq. 2.41 in Eq. 2.37,

$$\left[\sin^2 \theta \frac{\partial^2 f(r)}{\partial r^2} - \frac{2 \sin \theta f(r)}{r^2} \right]^2 = 0 \quad (2.42)$$

$$\left[\sin^2 \theta f(r) \left(\frac{\partial^2}{\partial r^2} - \frac{2}{r^2} \right) \right]^2 = 0$$

Considering streamlines with trajectory angle of 90° , then Eq. 2.42 can be expressed as

$$\left(\frac{\partial^2}{\partial r^2} - \frac{2}{r^2} \right) \left(\frac{\partial^2}{\partial r^2} - \frac{2}{r^2} \right) f(r) = 0 \quad (2.43)$$

Equation 2.43 is a fourth-order differential homogeneous linear equation, and its solution is of type $f(r) = cr^n$, where n can have values $(-1, 1, 2, 3)$ and c includes integration constants (A, B, C, D) , such that

$$f(r) = \frac{A}{r} + Br + Cr^2 + Dr^3 \quad (2.44)$$

Deriving Eq. 2.41 with respect to angle θ , $\partial\Psi/\partial\theta = 2f(r)\sin\theta\cos\theta$, and substituting it in Eq. 2.38,

$$u_r = \frac{1}{r^2\sin\theta} \frac{\partial\Psi}{\partial\theta} = f(r) \frac{2}{r^2} \cos\theta \quad (2.45)$$

Substituting Eq. 2.44 in Eq. 2.45

$$u_r = 2 \left(\frac{A}{r^3} + \frac{B}{r} + C + Dr \right) \cos\theta \quad (2.46)$$

u_θ can be expressed as

$$u_\theta = \frac{1}{r\sin\theta} \frac{\partial\Psi}{\partial\theta} \quad (2.47)$$

Substituting Eq. 2.44 in Eq. 2.41 and deriving the resulting equation,

$$\frac{\partial\Psi}{\partial r} = \sin^2\theta \left(-\frac{A}{r^2} + B + 2Cr + 3Dr^3 \right) \quad (2.48)$$

Then, substituting Eq. 2.48 in Eq. 2.47,

$$u_\theta = - \left(-\frac{A}{r^3} + \frac{B}{r} + 2C + 3Dr \right) \sin\theta \quad (2.49)$$

Applying boundary conditions given by Eqs. 2.38 and 2.39 to 2.46 and 2.49, an equations system is obtained

$$\begin{aligned} u_r &= 2 \left(\frac{A}{r^3} + \frac{B}{r} + C + Dr \right) \cos\theta = 0, \\ 2 \left(\frac{A}{a_o^3} + \frac{B}{a_o} + C + Da_o \right) \cos\theta &= 0, \\ u_\theta &= - \left(-\frac{A}{r^3} + \frac{B}{r} + 2C + 3Dr \right) \sin\theta = 0, \\ \left(-\frac{A}{a_o^3} + \frac{B}{a_o} + 2C + 3Da_o \right) \sin\theta &= 0 \end{aligned} \quad (2.50)$$

Now, applying the boundary condition described by Eq. 2.40 to velocity u_θ when $r \rightarrow \infty$,

$$\begin{aligned}
 u \sin \theta &= - \left(-\frac{A}{r^3} + \frac{B}{r} + 2C + 3Dr \right) \sin \theta \\
 u &= (2C + 3D * \infty) \sin \theta
 \end{aligned} \tag{2.51}$$

Considering in u_r that $r \rightarrow \infty$, then

$$\begin{aligned}
 u_r &= u \cos \theta = 2 \left(\frac{A}{r^3} + \frac{B}{r} + C + Dr \right) \cos \theta, \\
 u \cos \theta &= 2 \left(\frac{A}{r^3} + \frac{B}{r} + C + D * \infty \right) \cos \theta, \\
 u &= 2 (C + D * \infty)
 \end{aligned} \tag{2.52}$$

If $r \rightarrow \infty$, clasts should be smaller in layer thickness (two orders of magnitude). Moreover, initial fluid velocity changes when fluid impacts with clast (barrier), but fluid velocity must be different from zero to apply the mass and momentum conservation principles.

Thus $D = 0$ because $D \in \mathbb{R}$ and $u \in \mathbb{R}$. From Eq. 2.52,

$$C = \frac{u}{2}, \quad D = 0 \tag{2.53}$$

If $u_r = u_\theta = 0$ in Eqs. 2.38 and 2.39, then, the previously described procedure regarding velocity u_r indicates a stagnation point.

Following a similar solution for u_θ , the following equation can be derived:

$$- \left(-\frac{A}{r^3} + \frac{B}{r} + 2C + 3Dr \right) \sin \theta = 0, \tag{2.54}$$

Substituting $C = u/2$ and $D = 0$ and $\theta = -90$ (perpendicular streamline, that describe streamline around clast) in Eq. 2.54,

$$\left(-\frac{A}{r^3} + \frac{B}{r} + u \right) = 0, \tag{2.55}$$

For u_r from Eq. 2.46,

$$0 = u \cos \theta = 2 \left(\frac{A}{r^3} + \frac{B}{r} + C + Dr \right) \cos \theta \tag{2.56}$$

Substituting $C = u/2$ and $D = 0$ and $\theta = 0^\circ$ (radius localized at $\theta = 0^\circ$) in Eq. 2.56,

$$\left(\frac{2A}{r^3} + \frac{2B}{r} + u \right) = 0, \tag{2.57}$$

Solving the system of Eqs. 2.55 and 2.57, constants A and B are expressed as follows:

$$A = \frac{r^3}{4}, \quad B = \frac{-3ru}{4} \quad (2.58)$$

Then through the expressions (values) for the parameters A , B , C , and D , Eqs. 2.46, 2.49, and 2.39 can be written as

$$u_r = u \left(1 - \frac{3a_o}{2r} + \frac{a_o^3}{2r^3} \right) \cos\theta, \quad (2.59)$$

$$u_\theta = u \left(-1 + \frac{3a_o}{4r} + \frac{a_o^3}{4r^3} \right) \cos\theta = 0 \quad (2.60)$$

$$\Psi = \frac{r^2}{2} u \left(1 - \frac{3a_o}{2r} + \frac{a_o^3}{2r^3} \right) \sin^2\theta = 0 \quad (2.61)$$

The potential velocity is obtained using $u_\theta = 1/r \partial\Phi/\partial\theta$ and integration. Then, Φ can be derived as

$$\Phi = u \left(r + \frac{3a_o}{4} + \frac{a_o^3}{4r^3} \right) \cos\theta \quad (2.62)$$

As impact breccias clasts do not have spherical geometry and their rip-up morphology shows subrounded sides and other angular sides, in our analytical model we consider symmetry and an angle between 0 and 90° . Moreover, we propose that the range of θ may be $0^\circ < \theta < 180^\circ$ and rate change with respect to the angle can be expressed as

$$\frac{d\Psi}{d\theta} = r^2 u \left(1 - \frac{3a_o}{2r} + \frac{a_o^3}{2r^3} \right) \sin\theta \cos\theta, \quad (2.63)$$

$$\frac{du_\theta}{d\theta} = u \left(-1 + \frac{3a_o}{4r} + \frac{a_o^3}{2r^3} \right) \cos\theta, \quad (2.64)$$

$$\frac{du_r}{d\theta} = -u \left(1 - \frac{3a_o}{2r} + \frac{a_o^3}{2r^3} \right) \sin\theta, \quad (2.65)$$

Equations (2.63), (2.64) and (2.65) describe the changes in streamline velocities in impact breccias and could be used to study clasts with a variety of angles or subrounded side. In effect, as stated, the Stokes solution was adapted to impact breccias.

2.12 Fourth Contradiction: Fluid Flow of the Cantarell Reservoir Modeled Without Considerer Chicxulub Impact

Several authors document the influence of the Chicxulub impact in the Campeche Sound and discussed if the Chicxulub impact breccias are seal, hydrocarbon production and/or storage zones (Murillo-Muñetón et al. 2002; Grajales-Nishimura et al. 2000, 2009), or the impact is a geophysical survey reference as part of an oil exploration program (Urrutia-Fucugauchi 2013; Penfield and Camargo 1981; Ortuño 2012; Urrutia-Fucugauchi et al. 2011).

On the other hand, the Cantarell field is modeled as a tectonic fractures reservoir (Rivas-Gómez et al. 2002; Cruz et al. 2009; Manceau et al. 2001). As this paper is focused on oil flow in limestone reservoirs, then there is a question: why is the Cantarell reservoir modeled with tectonic fractures without considering the fluid flow through impact breccias? Or the impact breccia oil does not flow? A contribution of this paper is related to describing fluid flow through an impact breccia. In absence of vugs, fractures, and fault breccias, impact breccia has moderate porosity and low permeability, which indicates low flow velocity, unique in this type of breccia. Clearly, we modeled impact breccia without fractures or other geological events.

2.13 Geological and Tomography Features of Sedimentary Breccias

Sedimentary breccias are a type of clastic sedimentary rock with subangular to subrounded clasts. These rocks are deposited by transport and fast moving of a body of sediment particles by water and/or air. These breccias are observed in debris flows, mud flows, and mass flows, such as landslides and talus. According to type of clasts, sedimentary breccias can be monomict, oligomict, or polymict. Clasts may be extraformational or intraformational, matrix-supported or clast-supported.

The morphology of fragments clasts has been reworked by transport. Moreover, rocks with rounded clasts are known as conglomerates, and they are different from breccias. Sedimentary breccias contain clasts embedded in the matrix. These breccias do not have linear or internal planar structure resulting from lithification and consolidation of rocks, and they have been seen in outcrops (Fig. 2.16).

Figure 2.16 shows reworked clasts embedded in rock matrix with subrounded sides which indicates a short clasts transport. Long transport implies that clasts are rounded and can be modeled as ellipsoids. In principle, sedimentary breccias affect carbonate reservoirs and may enhance the total porosity. Fluid flow can be significant in the matrix-clast interface due to clast being impermeable and acting as flow barriers.

Figure 2.17 shows a sedimentary breccia core with embedded clasts in a limestone matrix, with subrounded and subangular side. Brecciation often results in enhanced porosity, but with poor interconnection of pores. A specific example is the Cretaceous Debris Reservoir, Poza Rica Field, Veracruz, Mexico (Enos 1985).

Fig. 2.16 Sedimentary breccia outcrop with reworked clasts. La Popa basin, Nuevo León, Mexico



Fig. 2.17 Matrix-clast interface in sedimentary breccia core. Late Cretaceous, Cardenas Field, TAB, Mexico (Villaseñor-Rojas 2003). Note: W = clast width and L = clast length

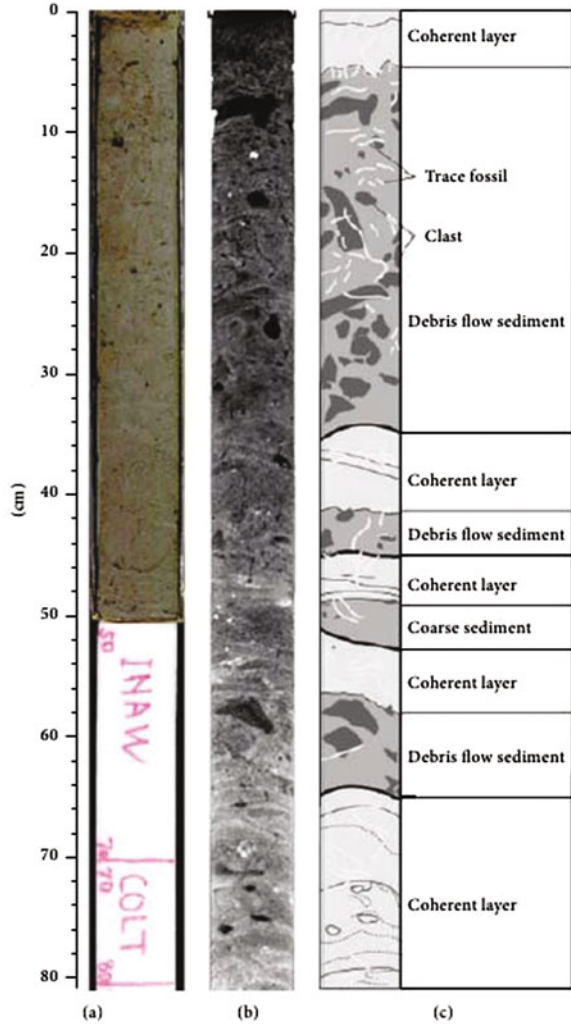


On the other hand, we used information of the Integrated Ocean Drilling Program that had sedimentary breccia tomography images (Kinoshita et al. 2009). Denser fragments embedded had a contrast with the matrix, indicating high bulk density and low porosity. In many cases, clasts can have high density and ultralow porosity. In Fig. 2.18, tomography shows dark shading that corresponds to low density and white to high density regions; this figure presents poorly sorted, elongated, and impermeable clasts with low porosity, in addition to Debris flow sediments in different layers. These events indicate that clasts are oligomict or polymict and extraformational that act as flow barriers in limestone reservoirs.

Observing Figs. 2.17 and 2.18, the following can be inferred:

1. Embedded clasts in a sedimentary breccia have sub-rounded, reworked, and elongated geometry, creating a nonflow barrier in porous media (matrix).
2. Clasts are poorly sorted and dispersed.
3. Sedimentary breccias are consequence of Debris flow, generating nonplanar discontinuities that contain embedded clasts.
4. Porosity and permeability in a sedimentary breccia are associated with matrix, embedded clast, and interface matrix-clast, producing a type of primary porosity in the limestone rock.

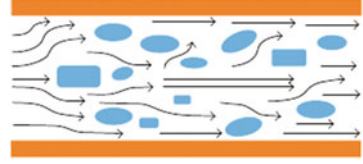
Fig. 2.18 Tomography (CT) image of sedimentary breccia. **a** Core. **b** Tomography. **c** Lithological description. Interval 316-C0004, 0–80 cm. (Kinoshita et al. 2009)



5. In the core, matrix rock portion is greater than embedded clasts.
6. The presence of Debris flow sediment in different layers indicates that there are diverse processes of sedimentation and that rock was exposed in the surface; namely, it was an outcrop in another geological age at subsurface conditions.
7. In outcrops and reservoirs, sedimentary breccia dimensions are related to Debris flow.

These observations are stated with the objective of the development of an analytical model.

Fig. 2.19 Streamlines in sedimentary breccia with reworked clasts



2.14 Kinematic Analytical Modeling for Sedimentary Breccia

Fluid kinematics could describe fluid flow in this type of rocks. A representative scheme is shown in Fig. 2.19, with streamlines for sedimentary breccia clasts, where reworked clasts may be grain-supported or matrix-supported.

Modeling between matrix-clast interfaces could be developed using flow around an elliptical body, like the Rankine solids, due to reworked clast. The Rankine methodology is similar to that previously applied to fault breccias to describe fluid kinematics; therefore, the flow around an elliptical body should satisfy Laplace's equation (Douglas et al. 2005).

Considering uniform flow, the Rankine solution is obtained using the superposition of a linear source and a linear sink of equal strength, combined with uniform flow (Fig. 2.19), given by

$$\Psi_{source}(r, \theta) = \frac{Q}{2\pi} \theta_1 \quad (2.66)$$

$$\Psi_{sink}(r, \theta) = -\frac{Q}{2\pi} \theta_2 \quad (2.67)$$

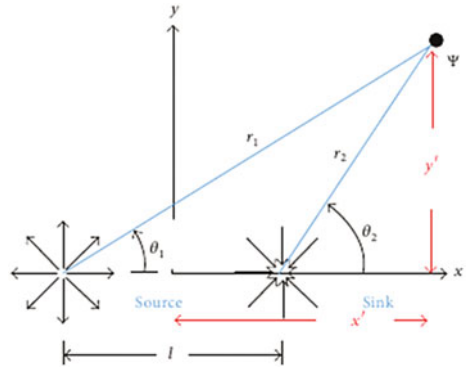
$$\Psi_{uniform}(r, \theta) = Uy \quad (2.68)$$

Conceptually, Eqs. 2.66 and 2.67 express that a sink and a source are equivalent, but geometry shows differences: they have different angles with respect to streamlines Ψ and are separated from distance l . Distance between origin and source is $l/2$ due to their symmetry. This is observed in Fig. 2.20 that shows different angles and radius in a source and sink for Rankine's solid.

The combined flow (Ψ_T) is represented by the stream function. From geological point of view, clast geometry indicates angular rate, and oil flows around the impermeable clast, generating a nonplanar discontinuity:

$$\Psi_T(r, \theta) = \frac{Q}{2\pi} \theta_1 - \frac{Q}{2\pi} \theta_2 + Uy \quad (2.69)$$

Fig. 2.20 Source and sink angles in the Rankine body (Douglas et al. 2005)



where

$$\theta_1 = \tan^{-1} \left(\frac{y'}{x' - (l/2)} \right), \tag{2.70}$$

$$\theta_2 = \tan^{-1} \left(\frac{y'}{x' + (l/2)} \right)$$

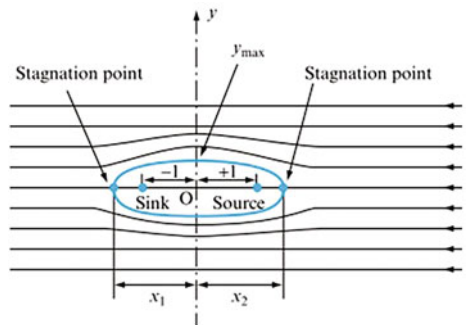
Considering Eqs. 2.69 and 2.70, the combined flow (Ψ_T) is given by

$$\Psi_T(r, \theta) = \frac{Q}{2\pi} \tan^{-1} \left(\frac{y'}{x' - (l/2)} \right) - \frac{Q}{2\pi} \tan^{-1} \left(\frac{y'}{x' + (l/2)} \right) + Uy \tag{2.71}$$

$$\Psi_T(r, \theta) = \frac{Q}{2\pi} \left[\tan^{-1} \left(\frac{y'}{x' - (l/2)} \right) - \tan^{-1} \left(\frac{y'}{x' + (l/2)} \right) \right] + Uy \tag{2.72}$$

Figure 2.21 shows two stagnation points associated with a source and sink; the length of the Rankine body is (x_T), $x_T = x_1 + x_2$, and the width of the Rankine body

Fig. 2.21 Streamlines for the Rankine solid with sink and source (Douglas et al. 2005)



(w) is related to the maximum value of y on the contour of the body in the y -axis direction.

Defining $u_x = \partial\Psi_T/\partial y$ and $u_y = -\partial\Psi_T/\partial x$ in rectangular coordinates, using Eq. 2.69, horizontal and vertical velocities are given by

$$\begin{aligned} u_y &= -\frac{Q}{2\pi} \left[\left(\frac{y'}{(x'-(l/2))^2+y'^2} \right) - \left(\frac{y'}{(x'+(l/2))^2+y'^2} \right) \right] \\ u_x &= \frac{Q}{2\pi} \left[\left(\frac{x'-(l/2)}{(x'-(l/2))^2+y'^2} \right) - \left(\frac{x'+(l/2)}{(x'+(l/2))^2+y'^2} \right) \right] + U \end{aligned} \quad (2.73)$$

The total velocity is given by $u = \sqrt{u_x^2 + u_y^2}$, and potential velocity is

$$\Phi_T = \frac{Q}{2\pi}\theta_1 - \frac{Q}{2\pi}\theta_2 + Uy \quad (2.74)$$

$$\Phi_T = \frac{Q}{2\pi}\tan^{-1} \left(\frac{y'}{x'-(l/2)} \right) - \frac{Q}{2\pi}\tan^{-1} \left(\frac{y'}{x'+(l/2)} \right) + Uy \quad (2.75)$$

To determine the width of the Rankine body, the maximum value of y (y_{max}) in Fig. 2.21 should be estimated at $x = 0$ ($v_{y_{max}} = 0$).

Geological information could provide the width and length of clasts embedded in cores of a sedimentary breccia, which would be assumed as length and width of the Rankine body.

2.15 Geological and Tomography Features of Vugs

Vugs are a type of pores in carbonate rocks. Choquette and Pray (1970) presented a classification based on the pore space genesis. Lucia (2007) proposed a classification focused on petrophysical properties and on distribution of pore sizes within the rock.

Vuggy pore space is classified into touching-vug pores and separate-vug pores. Touching-vug pores as tectonic fractures, breccias, and caverns are nonfabric-selective in their origin. Separate-vug pores are defined as pore space larger than the particle size and fabric-selective in their origin and are interconnected only through interparticle pore space, such as moldic, intrafossil, intragrain, and shelter pores (Lucia 2007). According to Lucia, vugs compared to separate-vug pores are secondary solution pores that are not fabric-selective in their origin, with irregular sizes and shapes, which could be interconnected.

In absence of tectonic fractures, vugs are not fabric-selective pore spaces or discontinuities from various sizes, with irregular shape, as a result of chemical dissolution, that could be interconnected or separated. Figure 2.22 shows a core with vugs created by chemical dissolution and irregular shapes. Normally, in a double porosity reservoir, vugs interact with the matrix.

Fig. 2.22 Limestone reservoir core with irregular vugs. Late Cretaceous, Campeche Sound, Marine Region, Mexico



Fig. 2.23 Zoomed photo of vugs in a recycled outcrop. Guayal outcrop, Tabasco, Mexico (SENER-Conacyt 2013)



Permeability of vugular porous media depends on its interconnection of the pore space. In this study, vugs are considered as nonplanar discontinuities that may be separated and nonfabric-selective and interact with the matrix of carbonate rocks.

Vuggy porosity can be produced by the interaction of meteoric waters with rock; by grains dissolution, fossils, and matrix pores; by deep-burial fluids; and by exposition of rock surfaces in humid climates.

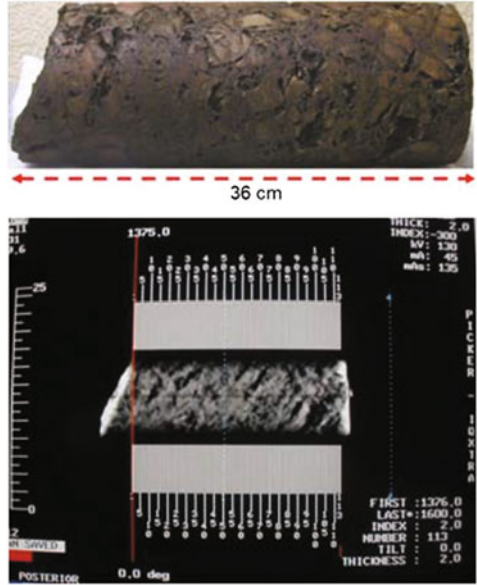
Vugs geometry is irregular. Moreover, spherical cavities have been used to describe them (Neale and Nader 1974; Moctezuma 2003; Rangel-German and Kovsky 2005) and (De Swaan 1976).

In limestone outcrops, vugs are interconnected only with matrix; vuggy pore space also can be regarded as interconnected with matrix and other vuggy systems (Fig. 2.23). Figure 2.23 shows a chemical dissolution process (diagenesis) with multiple size vugs similar to Fig. 2.22; then core and outcrops could be used as analogs.

Tomography images of an oil impregnated core obtained from a vuggy limestone reservoir were taken to determine the internal characteristics, geometry, and connectivity of the pore space.

The obtained one hundred and thirteen images describe the geometry and irregular shapes of the vugs. Figure 2.24 shows an oil saturated core, with a length of 36 cm,

Fig. 2.24 Oil impregnated core of a vuggy limestone reservoir. Late Cretaceous, the Campeche Sound, the Campeche Region, Mexico



with visible and irregular vugs as result of a chemical diagenesis, and CT slices were taken every 3 mm of distance through the sample (Fig. 2.25).

CT slices for the vuggy core of Fig. 2.24 are presented in Fig. 2.25. Figure 2.25 shows slices with vugs (black color), matrix (yellow color), filled or recrystallized cavities (green color), and embedded clasts (orange color). Cavities with black color are big pore spaces, or void spaces saturated with oil. When the slices are compared, vugs connectivity changes are observed. If we see a vug with black color in an image, it disappears in subsequent images. In contrast, connected vugs can be observed through different slices.

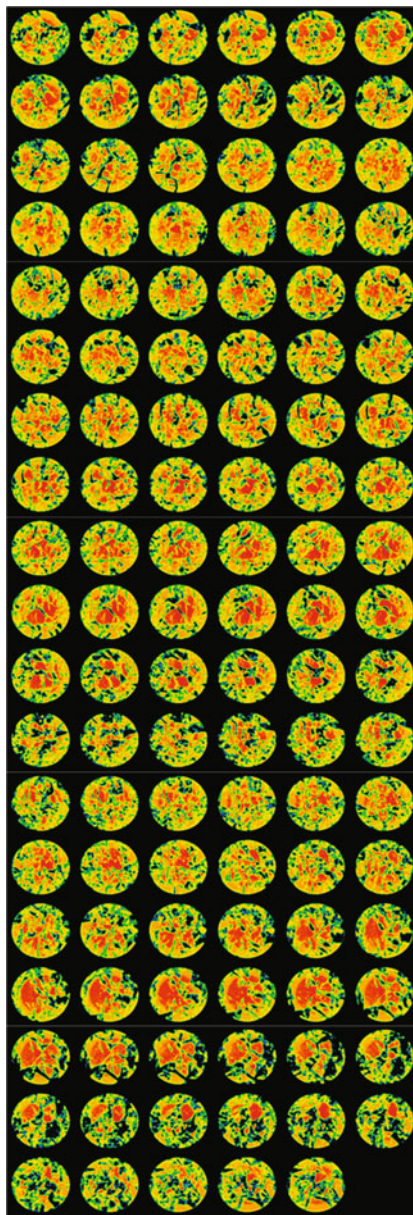
Considering core axisymmetry, there are permeable zones with isolated porosity and others with interconnected porosity. Isolated zones interchange fluid with matrix, but connected region presents matrix-vug and vugs system flow. Moreover, dissolution is the dominant process that enhances connection vugs.

Observing Figs. 2.22, 2.23, 2.24, and 2.25, the following can be inferred:

1. Limestone vugs geometry is irregular and spherical for outcrop as for core.
2. In the core, the vugs proportion is equivalent to the matrix proportion.
3. The vugs distribution is approximately uniform.
4. Vugs may be connected or isolated, depending on interface vug-matrix.
5. The presence of vugs indicates chemical diagenesis, specially dissolution due to meteoric water.

Considering these observations, the analytical model proposed by Neale and Nader may be used, although we will propose expressions for angular, radial, and potential velocities using Neale and Nader’s analytical model.

Fig. 2.25 CT images of an oil impregnated vuggy limestone core. Late Cretaceous, Campeche Sound core, Marine Region, Mexico



2.16 Kinematic Analytical Modeling for Vugs

Vugs are irregular spaces, like spheroids and ellipsoids, that interact with the matrix. To predict the flow field within a vug, we consider the mathematical solution developed by Neale and Nader, which was used to describe the pressure distribution within an isotropic and homogeneous porous medium, with a spherical cavity. Considerations employed to derive the mathematical solution were as follows: (1) uniformly vuggy medium with monosized cavities, (2) spherical cavity geometry, (3) surrounding homogeneous and isotropic porous media, (4) steady-state flow, and (5) incompressible fluid.

The problem and solution described by Neale and Nader are represented as shown in Figs. 2.26 and 2.27.

To develop the analytical solution for the flow problem described, a composite porous medium (matrix and vugs) was considered, and the creeping Navier-Stokes and the Darcy equations were used. Combining these two equations, the Laplace Biharmonic equation in spherical coordinate can be obtained and solved with its boundary conditions; the solution is given by

$$\Psi(\aleph, \theta) = \frac{ku^*}{2} [A\aleph^2 + B\aleph^4] \sin^2\theta \quad 0 < \aleph < X, \tag{2.76}$$

$$\Psi^*(\aleph, \theta) = \frac{ku^*}{2} [C\aleph^{-1} + D\aleph^2] \sin^2\theta \quad 0 < \aleph < \infty, \tag{2.77}$$

using the normalized radial coordinate and the normalized radius of the cavity, where

Fig. 2.26 Lateral view of a composite porous medium with vugs, matrix, and a fluid flow field

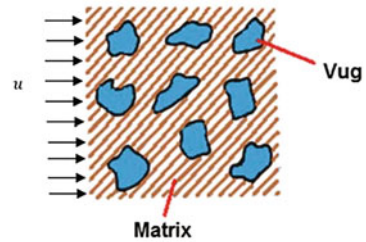
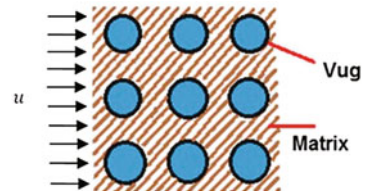


Fig. 2.27 Proposed solution for a composite porous media with vugs, matrix, and a fluid flow field



$$\begin{aligned}
A &= \frac{6(\aleph^2+5\sigma)}{X^2+10\sigma+20}, \\
B &= \frac{3}{X^2+10\sigma+20}, \\
C &= \frac{2X^3(X^2+10\sigma-10)}{X^2+10\sigma+20}, \\
D &= 1, \\
\aleph &= \frac{r}{\sqrt{k}}, \\
X &= \frac{R}{\sqrt{k}}, \\
\sigma &= \sigma(\phi), \quad 0 < \phi < 1
\end{aligned} \tag{2.78}$$

Equations 2.76 and 2.77 with their constants ($A, B, C, D, X, \sigma, \aleph$) predict the streamlines behavior in vugs and porous media. However, the authors Neale and Nadar did not describe angular, radial velocities or potential function. Considering Eqs. 2.76 and 2.77 with their constants, we developed the angular, radial velocities and potential function, which are given by

$$\begin{aligned}
u_r &= \frac{1}{r} \frac{\partial \Psi}{\partial \theta} = \left(\frac{9r^3+30\sigma rk}{R^2+10\sigma k+20k} \right) u^* \sin\theta \cos\theta, \\
u_\theta &= - \left(\frac{36r^3+60\sigma rk}{R^2+10\sigma k+20k} \right) u^* \sin^2\theta
\end{aligned} \tag{2.79}$$

Defining potential flow as $\Phi = \int_0^r u_r dr$, then

$$\Phi = \left(\frac{\mu \sin\theta \cos\theta}{R^2 + 10\sigma k + 20k} \right) \left(\frac{9r^3}{4} + 15r^3 k^3 \right) \tag{2.80}$$

Equations 2.79 and 2.80 provide a description of the fluid flow in a composite porous media.

2.17 Fifth Contradiction: Liquids Retention Paradox for Vugs

Regarding vugs, there is a physical phenomenon related to oil flow and their geometry, because they are concave and convex cavities with irregular shapes, which creates oil entrapping. This phenomenon has been called “dead zone” (Perez-Rosales 1969) or “the stagnation porosity” (Martinez-Angeles et al. 2002); however this problem is well-known in fluidized bed reactors and their design in the chemical engineering area (Bird et al. 2002).

During the production, oil entrapping is a result of two fluid dynamic processes. Initially, oil can be saturating the cavities, and its flow obeys a pressure gradient and a balance between viscous and inertial forces; thus, this is a dynamic flow process. When the first process concludes, oil flow follows a diffusion process, with slower velocities, generating a second process with static characteristics and fluid entrapping. The described phenomenon is related to the cavity geometry and vuggy pore space; this problem is associated with static-dynamic liquid retention in vugs and should be called liquids retention paradox.

It is a paradox because liquid in the cavities may be trapped in stagnation or dead zones; however, fluid flow will always occur in the vuggy porosity (secondary) producing a change in fluid velocity. In consequence, stagnation zones do not exist because there is always movement of fluid.

2.18 Application Examples

In this section, examples are presented to illustrate the proposed kinematics models in the analysis of limestone reservoirs with different discontinuities.

2.18.1 *Behavior of Fluid Velocities*

To examine the differences between the types of discontinuities, we used analytical kinematics models to calculate and compare fluid velocities. Key data and parameter values employed are presented in Table 2.1. Note that quantitative models should be implemented with geological characterization for a better prediction.

Additionally, to quantify fluid velocities in this study, we took in to consideration a pressure drop, a discontinuity angle with respect to streamline, aperture, clasts angle, and sink and source for sedimentary breccia which are included in Table 2.2.

Table 2.3 shows obtained velocities and flow rates values for diverse kinds of discontinuities. The goal is to compare these parameters. These models and their results would be applicable to oil limestone reservoirs. In this example, the calculated values of Table 2.3 illustrate that discontinuities related to fluid flow are dissimilar and that flow velocities and volumetric flow can be different. The results suggest that discontinuities in a limestone reservoir may not yield the same level of oil production. This implies that it is necessary to identify and verify the dominant discontinuity using static and dynamic characterization.

Note that the calculated values of Table 2.3 were obtained using Eqs. 2.5, 2.6, 2.12, 2.34, 2.35, 2.59, 2.60, and 2.73, which imply the described constants for all of the discontinuities presented in this paper. For sedimentary breccias, it is necessary to convert Cartesian coordinates to radial coordinates using trigonometrical functions.

Table 2.1 Data and parameters of limestone reservoir A

Parameters	Symbol	Values
Initial reservoir pressure	p_i	3.450×10^7 Pa
Bubble-point pressure	p_b	1.717×10^7 Pa
Reservoir depth	D	2726 m
Formation thickness	h	2.5 m
Primary porosity	ϕ_1	0.015 (fraction)
Primary permeability	k_1	395×10^{-17} m ²
Secondary porosity	ϕ_2	0.15 (fraction)
Secondary permeability	k_2	158×10^{-10} m ²
Oil viscosity	μ_o	0.00038 Pa·s
Reservoir temperature	T	121.85 °C
Oil specific gravity (15.6 °C)	γ_o	0.8156 (dimensionless)
Oil specific gravity ^a	γ_o	0.745 (dimensionless)

^aOil specific gravity at 121.85 °C was determined by $\gamma_o = \gamma_o(15.6^\circ\text{C})/1 + \delta(T - 60)$, where $\delta = \exp(0.0106 \times API \times 8.05)$ (Streeter 1961). Oil API gravity was 42° API

Table 2.2 Additional data for the calculation of fluid velocities

Simulation properties	Values
Pressure drop	2 Pa
Discontinuity angle	45°
Clast angle	45°
Aperture (fracture)	0.005 m
Vug radius	0.02 m
Distance (vug-matrix)	0.04 m
Clast radius	0.02 m
Sink and source	1 m ² /s
Initial velocity	0.00639

Table 2.3 Calculated parameters values

Discontinuities	Parameters			
	u (m/s)	u_r (m/s)	u_θ (m/s)	q (m ³ /s)
Fracture	0.0064	0.0045	0.0045	0.0399
Fault Breccia	0.0066	0.0048	0.0045	0.0413
Impact Breccia	0.0013	0.0003	0.0012	0.0078
Vug	0.0190	0.0046	0.0184	0.1186
Sedimentary Breccia	0.0046	0.0033	0.0033	0.0290

The positive sign in fluid velocities represents its direction from of origin in x -axis or y -axis direction

The total velocity and volumetric flow are given by $u = \sqrt{u_x^2 + u_y^2}$ and $q = uA$, respectively. Equation 2.12 (The Cubic Law) is used for tectonic fracture.

Calculated values show the differences for each type of discontinuity. Horizontal tectonic fracture presents equivalent velocities (radial and angular) because streamlines are parallel and volumetric flow depends on fracture aperture. Fault breccia has high velocity and flow because it depends on elongated and subangular clast. Also, vugs have superhigh velocity and flow because they are connected cavities without flow barriers.

In contrast, impact and sedimentary breccias have low velocity and volumetric flow due to clast geometry (rip-up and ellipsoidal), creating low radial velocity. In addition, clasts are flow barriers and fluid flow is related to interaction matrix-clast and their permeabilities that are normally very low because they behave as primary permeability and porosity. This implies that proportion matrix is greater than the proportion clast.

2.18.2 Carbonate Reservoir Characteristics: Cardenas Field Application

According to the proposed geological model for the Cardenas Field, which is an anticline with a fault system, controlled by stratigraphic traps rather than structural traps. In accordance with the characteristics of primary porosity (1.5–1.7%), secondary porosity (5–11%), primary permeability ($395 \times 10^{-17} - 329 \times 10^{-17} \text{ m}^2$), and secondary permeability ($196 \times 10^{-10} - 89 \times 10^{-10} \text{ m}^2$), production layers are subdivided into different breccias intervals in the reservoir. Figure 2.28 shows correlation through longitudinal breccias intervals for the Cardenas Field wells; moreover, breccias sequence with a chemical diagenesis (dolomites and vugs) and limestone layers were a criterion for the selection of wells. It is shown in the cross section (Fig. 2.28). Oil production in the Cardenas reservoir comes from lateral interconnected sedimentary breccias and vugs (Villaseñor-Rojas 2003).

Application of the flow kinematic models (vugs, sedimentary breccia models) to the Cardenas Field may be used as a diagnosis tool for the fluid velocities prediction and in the discontinuity characterization. In this case, there are wells with a similar pressure behavior Fig. 2.29 that produce from breccia intervals with vugs and microfractures.

In Figs. 2.28 and 2.29, we observe a cross section 1-1 with eight wells and their similar pressure history. In Fig. 2.29, 3D seismic section shows wells layers correlation and confirms their lateral continuity. Also, the section correlation shows clearly a connected thickness of Debris flow. As an application, we have chosen three wells: Cardenas-109, Cardenas-129, and Cardenas-308, with geologic heterogeneities related to sedimentary breccias and vugs. The goal is to compare fluid velocities and characteristics flow in sedimentary breccias and vugs and validate

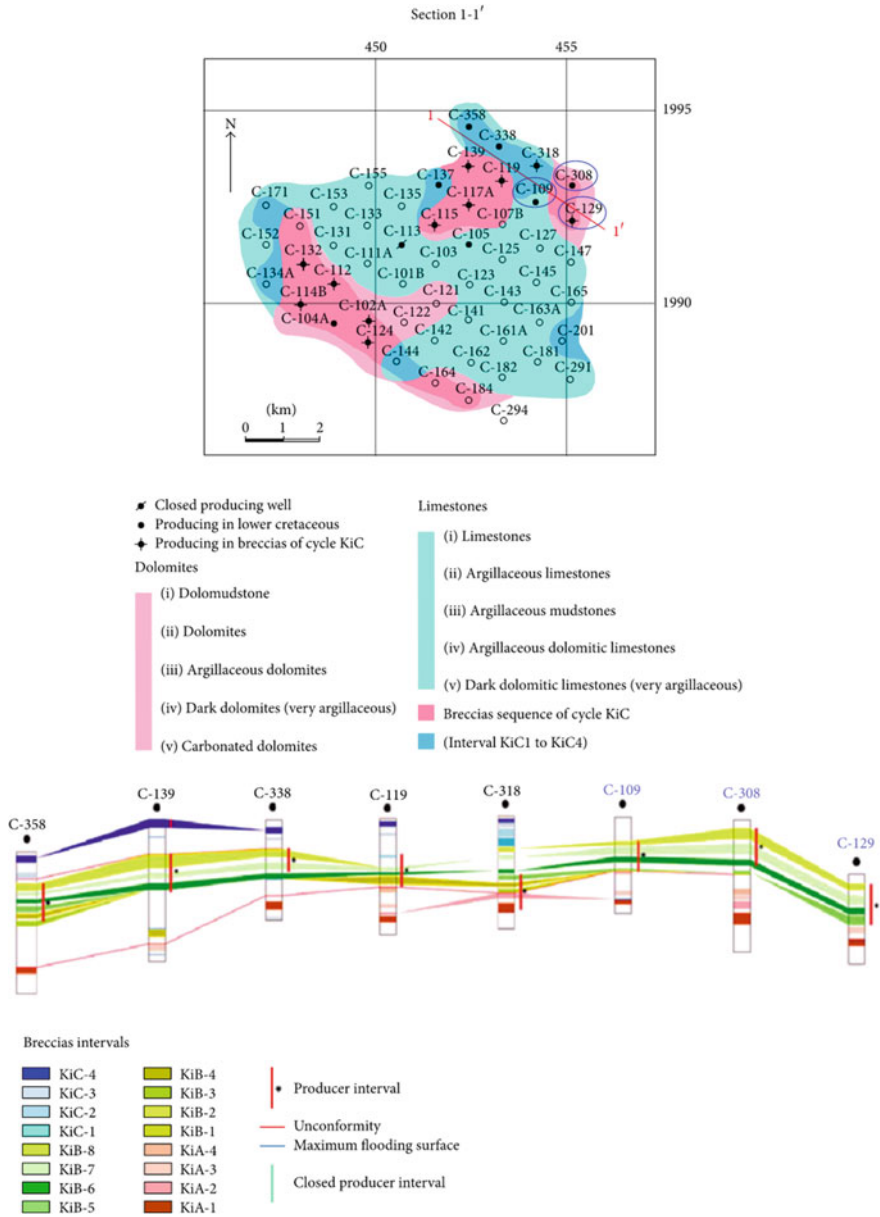


Fig. 2.28 Section 1-1 producing levels correlation through breccias intervals longitudinal to the northeastern reservoir (Villaseñor-Rojas 2003)

them with production data. Wells data and parameters are given in Tables 2.4, 2.5, and 2.6.

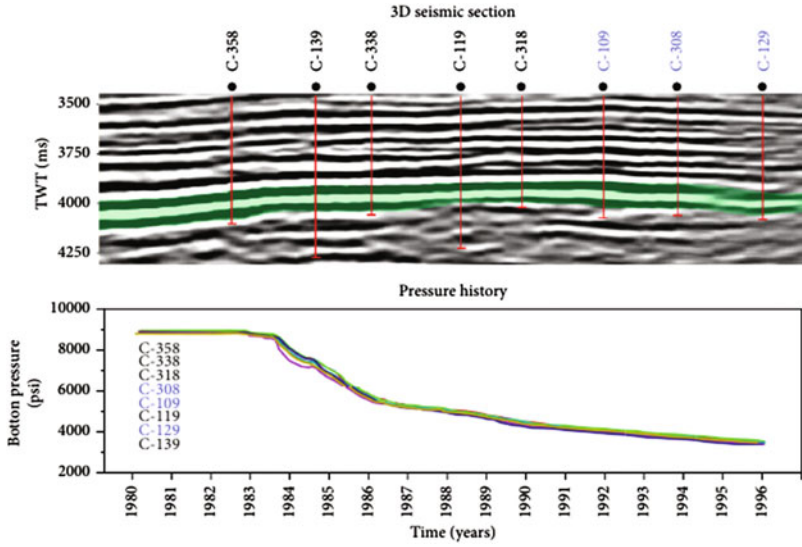


Fig. 2.29 Matching pressure curve declination among wells is shown (After Villaseñor-Rojas 2003, Fig. 6.5, p. 161.)

Table 2.4 Data and parameters for the Cardenas Field, well Cardenas-109

Parameters	Symbol	Values
Initial reservoir pressure	p_i	61.54×10^6 Pa
Pressure drop	Δp	20 Pa
Reservoir depth	D	3969 m
Formation thickness	h	270 m
Primary porosity	ϕ_1	0.015 (fraction)
Primary permeability	k_1	395×10^{-17} m ²
Secondary porosity	ϕ_2	0.11 (fraction)
Secondary permeability	k_2	196×10^{-10} m ²
Oil viscosity	μ_o	0.00066 Pa·s
Reservoir temperature	T	124 °C
Clast radius	r	0.08 m
Vug radius	R	0.03 m
Sink and source	Q	1 m ² /s
Oil specific gravity (15.6 °C)	γ_o	0.720 (dimensionless)

Table 2.5 Data and parameters for the Cardenas Field, well Cardenas-129

Parameters	Symbol	Values
Initial reservoir pressure	p_i	61.54×10^6 Pa
Pressure drop	Δp	20 Pa
Reservoir depth	D	4002 m
Formation thickness	h	382 m
Primary porosity	ϕ_1	0.017 (fraction)
Primary permeability	k_1	329×10^{-17} m ²
Secondary porosity	ϕ_2	0.06 (fraction)
Secondary permeability	k_2	92×10^{-10} m ²
Oil viscosity	μ_o	0.00066 Pa·s
Reservoir temperature	T	124.5 °C
Clast radius	r	0.08 m
Vug radius	R	0.01 m
Sink and source	Q	1 m ² /s
Oil specific gravity (15.6 °C)	γ_o	0.720 (dimensionless)

Table 2.6 Data and parameters for the Cardenas Field, well Cardenas-308

Parameters	Symbol	Values
Initial reservoir pressure	p_i	61.54×10^6 Pa
Pressure drop	Δp	20 Pa
Reservoir depth	D	3948 m
Formation thickness	h	293 m
Primary porosity	ϕ_1	0.015 (fraction)
Primary permeability	k_1	358×10^{-17} m ²
Secondary porosity	ϕ_2	0.05 (fraction)
Secondary permeability	k_2	89×10^{-10} m ²
Oil viscosity	μ_o	0.00066 Pa·s
Reservoir temperature	T	124.1 °C
Clast radius	r	0.08 m
Vug radius	R	0.01 m
Sink and source	Q	1 m ² /s
Oil specific gravity (15.6 °C)	γ_o	0.720 (dimensionless)

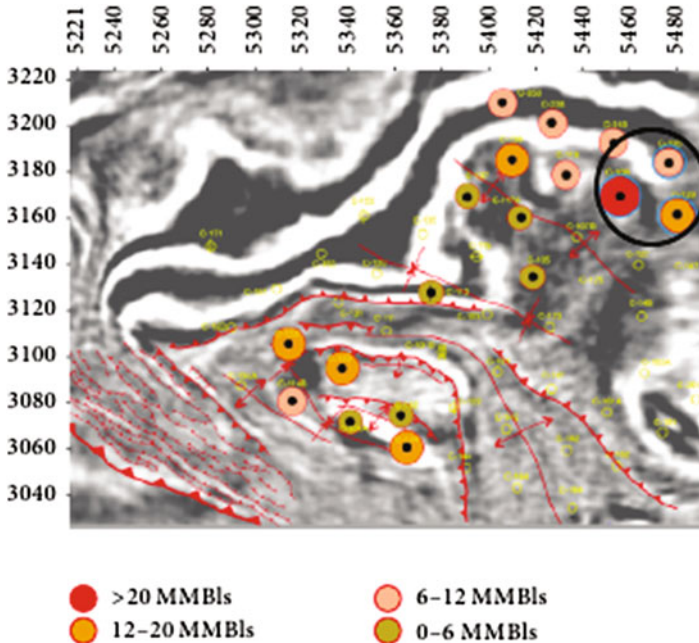


Fig. 2.30 Oil cumulative production in wells of the Cardenas Field: wells C-109, C-129, and C-308 (Villaseñor-Rojas 2003)

Figure 2.30 shows wells Cardenas-109, Cardenas-129, and Cardenas 308. In accordance with this figure, well Cardenas-109 has a high oil cumulative production (>20 MMBls) due to geological events juxtaposition, of sedimentary breccias and vugs. Vugular porosity was created by dissolution processes associated with pressure and temperature drop, and circulation of high corrosive hydrothermal fluids, and its breccias deposits were exposed to subaerial erosion, after they affected by dissolution and dolomitization. In addition, oil cumulative production for well Cardenas-129 is associated with vugular porosity, although its described production (12–20 MMBls) in Fig. 2.30 is smaller than for Cardenas-109. Well Cardenas-308 geological description is related to sedimentary breccia intervals. Its production (6–12 MMBls) is low with respect to the other two wells (Fig. 2.30), but it can be considered that there is a high oil storage in the breccia intervals; namely, oil storage is localized in its primary porosity.

According to Figs. 2.28, 2.29, and 2.30, diverse volumetric flow and velocities should be calculated because geological events for the Cardenas Field are different and juxtaposed. Juxtaposed geological events imply a high volumetric flow and fluid velocity.

We applied the kinematic equations as a semiquantitative diagnosis tool to determine fluid velocities and fluid flow for the three study wells. Used equations for sedimentary breccia, vugs, and superposed flow (sedimentary breccia and vugs) are

Table 2.7 Calculated velocities and rates values for the Cardenas Field, wells C-109, C-129, and C-308

Discontinuities	Wells	Velocities and volumetric flows			
		u (m/s)	u_r (m/s)	u_θ (m/s)	q (m ³ /s)
Breccia + vugs	C-109	0.0350	0.0129	0.0314	2550.5
Vugs	C-129	0.0146	0.0035	0.0142	2131.1
Sedimentary breccia	C-308	0.0096	0.0068	0.0068	826.9

(59), (60), and (73) with their geometrical parameters. The fluid velocities can help in the interpretation of the type of geological discontinuity; moreover it is necessary to consider static characterization for estimate values of velocities and rates with reduced uncertainty. Kinematics equations validation is developed considering a low fluid velocity in the sedimentary breccia of well Cardenas-308 because clasts are barriers during fluid flow, but porosity and permeability of the sedimentary breccia may store oil. This indicates that path for fluid flow will be slow and tortuous, and then its velocity and flow are low. This premise was corroborated in Table 2.7.

Well Cardenas-129 is studied considering a high oil velocity because vugs are cavities that do not have flow barrier and they are normally connected with limestone matrix.

The porosity in this reservoir layer is a preferential way for fluid flow. When there are connected vugs with oil storage in the rock, production conditions are excellent due to oil free path. In contrast, well Cardenas-129 oil production should be greater than well Cardenas-308 oil production. This claim was demonstrated in Table 2.7.

Well Cardenas-109 presents complex geological events juxtaposition. Sedimentary breccias store fluid and vugs store and transport oil through porous media due to their inter-connection, in this case, porosity (storage) and secondary permeability (transport). Then, the already stated events juxtaposition is applied to the geological events superposition, which is a characteristic of analytical models developed in this paper because our equations are lineal and they are solutions of the Laplace equation. In consequence, the maximum oil production in this well must be obtained, and this is demonstrated in Table 2.7.

Table 2.7 shows the obtained results with input parameters of wells Cardenas-109, Cardenas-129, and Cardenas-308. Chosen wells for models validation have diverse production; in consequence, fluid velocity and flow volumetric are different and they are related to geological event as vugs, sedimentary breccia, and their juxtaposition.

The wells production is associated with phenomenology of complex limestone reservoir. The key point here is that sedimentary breccias contain embedded clasts that are barriers for fluid flow; nevertheless they can store oil. The degree of complexity of clasts interactions with fluid depends on clast diameters and their spacing. In the case of vugs, it depends on their interconnection. When different geological events are juxtaposed and interconnected as in well Cardenas-109, oil production is high.

The Cardenas Field has been chosen because we know, understand, and have geological control of reservoir, which was developed in a doctoral thesis. Data for the field application previously discussed was mainly borrowed from the Ph.D. dissertation of one of the authors of the present paper (Villaseñor-Rojas 2003).






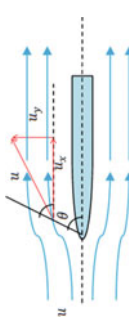

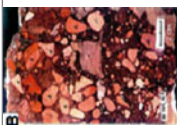
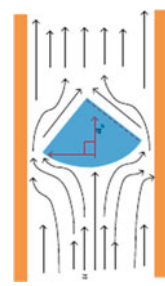
2.19 Mathematical Models Summary

Tables 2.8 and 2.9 present a summary that describe geological events and their developed mathematical models in this doctoral dissertation. In addition, there are different figures about outcrops, cores and streamlines representations. The goal is to compare fluid flow in porous media and the differences between the kinds of discontinuities.

2.20 Nomenclature

x, y, z	Reference axis in Cartesian coordinates
(r, θ)	Radial and angular coordinates
u	Fluid velocity in direction x [m/s]
v	Fluid velocity in direction y [m/s]
w	Fluid velocity in direction z [m/s]
h	Vertical distance [m]
μ	Liquid viscosity [Pa · s]
t	Time [s]
ρ	Density [kg/m ³]
β	Inclination angle [grades]
a	Fracture aperture [m]
a_o	Impact clast radius [m]
p	Pressure [Pa]
γ	Fluid specific gravity [dimensionless]
q	Volumetric flow [m ³ /s]
A	Area [m ²]
U	Terminal velocity of upper plate [m/s]
U_∞	Horizontal flow of uniform velocity [m/s]
\bar{u}	Mean flow velocity [m/s]
u_{max}	Maximum fluid velocity [m/s]
u_r	Radial velocity [m/s]
u_θ	Angular velocity [m/s]
Q	Linear sink or source [m ² /s]
x	Horizontal distance [m]
Φ	Velocity potential [m ² /s]
Ψ	Stream function [m ² /s]



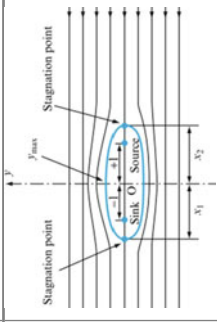


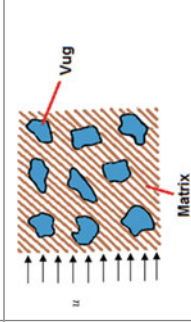
Table 2.8 Mathematical models summary for fractures, impact and fault breccias

Geological events	Cores	Outcrops	Kinematic equations	Kinematics
Tectonic fractures			$\Psi = uy$ $\Phi = ux$ $u = U_\infty$ $v = 0$ $u_r = u \cos \beta$ $u_\theta = u \sin \beta$	
Fault breccia			$\Psi = \frac{1}{2}ur^2 \sin^2 \theta - \frac{Q}{4\pi}$ $u_\theta = -u \sin \theta$ $\Phi = ur \cos \theta - \frac{Q}{4\pi r}$ $u_r = u \cos \theta + \frac{Q}{4\pi r^2}$	
Impact breccia			$\Psi = \frac{r^2}{2}u \left(1 - \frac{3a_0}{2r} + \frac{a_0^3}{2r^3}\right) \sin^2 \theta$ $u_\theta = u \left(-1 + \frac{3a_0}{4r} + \frac{a_0^3}{4r^3}\right) \sin \theta$ $\Phi = u \left(r - \frac{3a_0}{4} - \frac{a_0^3}{4r^3}\right) \cos \theta$ $u_r = u \left(1 - \frac{3a_0}{2r} + \frac{a_0^3}{2r^3}\right) \cos \theta$	

^a After Ortuño (2012)

^b After Grajales (2000)

Table 2.9 Mathematical models summary for sedimentary breccia and vug

Geological events	Cores	Outcrops	Kinematic equations	Kinematics
Sedimentary breccia			$\Psi = \frac{Q}{2\pi} [(\theta_1) - (\theta_2)] + Uy$ $u_x = \frac{Q}{2\pi} \left[\frac{x' - (l/2)}{(x' - (l/2))^2 + y^2} - \frac{x' + (l/2)}{(x' + (l/2))^2 + y^2} \right] + U$ $u_r = -\frac{Q}{2\pi} \left[\frac{y'}{(x' - (l/2))^2 + y^2} - \frac{y'}{(x' + (l/2))^2 + y^2} \right]$ $\Phi = \frac{Q}{2\pi} [\cos(\theta_1) - \cos(\theta_2)] + Uy$ $\theta_1 = \tan^{-1} \left(\frac{y'}{x' - (l/2)} \right)$ $\theta_2 = \tan^{-1} \left(\frac{y'}{x' + (l/2)} \right)$	
Vugs			$\Psi = \frac{ku^*}{2} (AN^2 + BN^4) \sin^2 \theta$ $u_\theta = - \left(\frac{36r^3 + 60\sigma rk}{R^2 + 10\sigma k + 20k} \right) u^* \sin^2 \theta$ $u_r = \left(\frac{9r^3 + 30\sigma rk}{R^2 + 10\sigma k + 20k} \right) u^* \sin \theta \cos \theta$ $\Phi = \left(\frac{\mu \sin \theta \cos \theta}{R^2 + 10\sigma k + 20k} \right) \left(\frac{9r^4}{4} + 15\sigma r^3 k^3 \right)$	

^a After SENER-Conacyt (2013)

r	Clast radius [m]
θ	Clast angle [degrees]
θ_1	Source angle [degrees]
θ_2	Source angle [degrees]
k	Permeability [m^2]
σ	Slip factor [dimensionless]
ϕ	Porosity of porous medium [fraction]
R	Radius of spherical cavity [m]
\aleph	Normalized radial coordinate
X	Normalized radial of spherical cavity
*	Average pertaining to a porous medium

References

- Alhuthali, A., Lyngra, S., Widjaja, D., et al. (2011). A holistic approach to detect and characterize fractures in a mature middle eastern oil field. *Saudi Aramco Journal of Technology*. (Fall).
- Baker, W. (1955). Flow in fissured formation: 5th World Petroleum Cong. Proc., Sec. II/E: 379–393.
- Barton, R., Bird, K., García, J. Grajales-Nishimura, J., et al. (2010). High-impact reservoirs. *Oilfield Review*, 21(4), 14–29 (Winter 2009/2010).
- Bird, R. B., Stewart, W. E., & Lightfoot, E. N. (2002). *Transport phenomena* (2nd ed., pp. 122–125). New York: John Wiley & Sons.
- Bogdanov, I., Mourzenko, V., Thover, J-F., et al. (2003). Pressure drawdown well tests in fractured porous media. *Water Resources Research*, 39(1), 1021. <https://doi.org/10.1029/2000WR000080>, 2003.
- Cervantes, A., & Montes, L. (2014). The stratigraphic-sedimentology model of upper cretaceous to oil exploration field “Campeche Oriente”. Paper SPE 169461-MS Presented at the SPE Latin American and Caribbean Petroleum Engineering Conference, Maracaibo, Venezuela, 21–23 May.
- Choquette, P. W., & Pray, L. C. (1970). Geologic nomenclature and classification of porosity in sedimentary carbonates. *AAPG Bulletin*, 54(2), 207–250.
- Cruz, L., Sheridan, J., Aguirre, E., Celis, E., et al. (2009). Relative contribution to fluid flow from natural fractures in the cantarell field, Mexico. Paper SPE-122182-MS Presented at the Latin American and Caribbean Petroleum Engineering. Cartagena de Indias, Colombia, 31 May–3 June.
- Currie, I. (2003). *Fundamental mechanics of fluids* (3rd ed., pp. 161–195). New York: Marcel Dekker.
- De Swaan, O. A. (1976). Analytical solutions for determining naturally fractured reservoir properties by well testing. *SPE Journal*, 16(3), 117–122. <https://doi.org/10.2118/5346-PA>. (SPE 5346-PA).
- Douglas, J. F., Gasiorek, J. M., Swaffield, J. A., et al. (2005). *Fluid mechanics* (5th ed., pp. 212–254). New York: Pearson Prentice Hall.
- Dressler, B. O., Sharpton, V. L., Morgan, J., Buffler, R., Moran, D., Smit, J., et al. (2003). Investigating a 65-Ma-old smoking gun: Deep drilling of the Chicxulub impact structure. *Eos Transactions AGU*, 84, 125–131.
- Enos, P. (1985). Cretaceous debris reservoir, Poza Rica field, Veracruz, México. In P. O. Roehl, & P. W. Choquette (Eds.), *Carbonate petroleum reservoir*, Chap 28 (455–470). New York: Springer.

- Faber, T. E. (1995). *Fluid dynamics for physicists* (1st ed., pp. 129–131). Cambridge: Cambridge University Press.
- Fossen, H. (2010). *Structural geology* (1st ed., pp. 119–121). Chap. 7. New York: Cambridge University Press.
- Grajales, J. M., Morán, D. J., Padilla, P., et al. (1996). The Lomas Tristes Breccia: A KT impact related breccia from southern México. In *Geological Society of America, Abstract with Programs* (Vol. 28, p. A-183).
- Grajales-Nishimura, J. M., Murillo-Muñeton, G., Rosales-Domínguez, C., et al. (2009). The Cretaceous-Paleogene boundary Chicxulub impact: Its effect on carbonate sedimentation on the western margin of the Yucatan Platform and Nearby Areas. In *Petroleum systems in the southern Gulf of Mexico: The American Association of Petroleum Geologists (AAPG). Memoir*, (Vol. 90, pp. 315–335).
- Grajales-Nishimura, J. M., Cedillo-Pardo, E., Rosales-Domínguez, C. R., et al. (2000). Chicxulub impact: The origin of reservoir and seal facies in the southeastern Mexico oil fields. *Geology*, 28(4), 307–310.
- Gudmundsson, A. (2011). *Rock fractures in geological processes*. Chapters 15 and 16, (pp. 466–520). Cambridge: Cambridge University Press.
- Hildebrand, A. R., Penfield, G. T., Kring, D. A., et al. (1991). Chicxulub crater: A possible Cretaceous/Tertiary boundary impact crater on the Yucatán Peninsula, Mexico. *Geology*, 19(9), 867–871.
- Iverson, R. (1997). The physics of debris flows. *Reviews of Geophysics*, 35(3): 245–296. (Washington: American Geophysical Union).
- Keller, G., Adatte, T., Stinnesbeck, W., Rebolledo-Vierstra, R., Urrutia, J., Kramar, U., et al. (2004a). Chicxulub impact predates the K-T boundary mass extinction. In *The National Academy of Sciences of the USA. PNAS* (Vol. 101, Issue 11, pp. 3753–3758). (March 16).
- Keller, G., Adatte, T., Stinnesbeck, W., Stüben, D., et al. (2004b). More evidence that the Chicxulub impact predates the K/T mass extinction. *Meteoritics & Planetary Science*, 39(7), 1127–1144.
- Kinoshita, M., Tobin, H., Ashi, J., Kimura, G., Lallemand, S., Scream, E., Curewitz, D., Masago, H., & Moe, K. T. (2009). Expedition 316 site C0004. In *Expedition 316 scientists: Proceedings of the Integrated Ocean Drilling Program* (vol. 314/315/316). Washington, DC: Integrated Ocean Drilling Program Management International, Inc.
- Koenraad, J. W., & Bakker, M. (1981). Fracture and vuggy porosity. Paper SPE 10332 Presented at the 56th Annual Fall Technical Conference and Exhibition and Conference, San Antonio, Texas, 5–7 October.
- Kring, D., Hörz, F., Zurcher, L., & Urrutia, J. (2004). Impact lithologies and their emplacement in the Chicxulub impact crater: Initial results from the Chicxulub Scientific Drilling Project, Yaxcopoil, Mexico. *Meteoritics & Planetary Science*, 39(6), 879–897.
- Lee, J., Rollins, J. B., & Spivey, J. P. (2003). *Pressure transient testing*. Chap 1, 9. Richardson, Texas: Series, SPE.
- Levi, E. (1965). *Mecánica de los Fluidos, Introducción Teórica a la Hidráulica Moderna, primera edición* (pp. 87–99). México: Universidad Autónoma de México.
- Levesse, G., Bourdet, J., Tritlla, J., et al. (2006). Evolución de los Fluidos Acuosos e Hidrocarburos en un Campo Petrolero Afectado por Diapiros Salinos. AMGP. Plays y Yacimientos de Aceite y Gas en Rocas Carbonatadas. 15–17 Marzo, Cd Del Carmen Campeche. México.
- Lopez-Ramos, E. (1975). Geological summary of the Yucatán Peninsula in The Ocean Basins and Margins. In A. E. M. Nairn, & F. G. Stehli (Eds.), *The gulf of Mexico and the Caribbean* (Vol. 3, pp. 257–282). New York: Plenum Press.
- Lopez-Ramos, E. (1983). *Geología de México* (3rd ed.). Mexico: Universidad Nacional Autónoma de México. Mexico City.
- Lucia, F. J. (2007). *Carbonate reservoir characterization An integrated approach* (2nd ed., pp. 29–67). Berlin: Springer.
- Manceau, E., Delamaide, E., Sabathier, J. C., Julian, S., Kalaydjian, F., et al. (2001). Implementing convection in a reservoir simulator: A key feature in adequately modeling the exploitation of the

- cantarell complex. *SPE Reservoir Evaluation and Engineering*, 4(2): 128–134. <http://dx.doi.org/10.2118/71303-PA>. (SPE 71303-PA).
- Manrique, E., Gurfinkel, M., & Muci, V. (2004). Enhanced oil recovery field experiences in carbonate reservoirs in the United States. In *Proceedings of the 25th Annual Workshop & Symposium Collaborative Project on Enhanced Oil Recovery*. Stavanger, Norway: International Energy Agency. (September).
- Martínez-Angeles, R., Hernández-Escobedo, L., & Pérez-Rosales, C. (2002). 3D quantification of vugs and fractures networks in limestone cores. Paper SPE 77780 Presented at the SPE Annual Technical Conference, San Antonio, Texas, 29 September–2 October.
- Mayr, S. I., Burkhardt, H., & Popov, Y. (2008). Estimation of hydraulic permeability considering the micro morphology of rocks of the borehole YAXCOPOIL-1 (Impact crater Chicxulub, México). *International Journal of Earth Sciences (Geol Rundsch)*, 97, 385–399. <http://dx.doi.org/10.1007/s00531-007-0227-6>.
- McKeown, C., Haszeldine, R. S., & Couples, G. D. (1999). Mathematical modelling of groundwater flow at Sellafeld, UK. *Engineering Geology*, 52, 231–250.
- McMechan, G. A., Gaynor, G. C., & Szerbiak, R. B. (1997). Use of ground-penetrating radar for 3-D sedimentological characterization of clastic reservoir analogs. *Geophysics*, 62(3), 786–796.
- Mees, F., Swennen, R., Geet, M. V., et al. (2003). *Applications of X-ray computed tomography in the geosciences* (1st ed.). The Geological Society London.
- Moctezuma, A. (2003). Déplacements immiscibles dans des carbonates vacuolaires: expérimentations et modélisation. Thèse de doctorat, Institut du Physique du Globe de Paris, Paris (Juillet, 2003).
- Murillo-Muñetón, G., Grajales-Nishimura, J. M., Cedillo-Pardo, E., et al. (2002). Stratigraphic architecture and sedimentology of the main oil-producing stratigraphic interval at the cantarell oil field: The K/T boundary sedimentary succession. Paper SPE 74431 Presented at the International Petroleum Exhibition and Conference, Villahermosa, México, 10–12 February.
- Muskat, M. (1946). *The flow of homogeneous fluids through porous media* (1st ed., pp. 55–113). United States, Michigan: J.W. Edward Inc. & Ann Arbor.
- Neale, G. H., & Nader, W. K. (1974). The permeability of a uniformly vuggy porous. *SPE Journal*, 13(2): 69–74. <http://dx.doi.org/10.2118/3812-PA>. (SPE 3812-PA).
- Nelson, R. A. (2001). *Geologic analysis of naturally fractured reservoirs* (2nd ed.). Houston, Texas: Gulf Publishing Company.
- Ortuño, E. (2012). Características de la Brecha Híbrida (Estéril, BP0 o Transicional) y su Potencial como Roca Yacimiento en la Sonda de Campeche. Presentación Oral dada en el Congreso Mexicano del Petróleo. Ciudad de México, México, 9–14 Septiembre.
- PEMEX Exploración y Producción: Las Reservas de Hidrocarburos en México. 1 de Enero de 2014. México, D.F. p 107.
- Penfield, G. T., & Camargo, Z. (1981). Definition of a major igneous zone in the central Yucatán a platform with aeromagnetism and gravity. In *Technical program, Abstracts and biographies (Society of exploration geophysicists)* (p. 37). Society of Exploration Geophysicists, Los Angeles, California, USA.
- Pérez-Rosales, C. (1969). Determination of geometrical characteristics of porous media. *Journal of Petroleum Technology*, 8, 413–416.
- Potter, M., Wiggert, D., & Ramadan, B. (2012). *Mechanics of fluids* (4th ed., pp. 281–287). United States: CENGAGE Learning.
- Pringle, J. K., Howell, J. A., Hodgetts, D., et al. (2006). Virtual outcrop models of petroleum reservoir analogues: a review of the current state-of-the-art. *First Break EAGE*, 24, 33–42. (Technical article).
- Rangel-German, E. R., & Kovscek, A. R. (2005). Matrix-fracture shape factors and multiphase-flow properties of fractured porous media. SPE 95105-MS Presented at the SPE Latin American and Caribbean Petroleum Engineering Conference held in Rio de Janeiro, Brazil, 20–23 June. <http://dx.doi.org/10.2118/95105-MS>.

- Rebolledo-Vieyra, M., & Urrutia-Fucugauchi, J. (2004). Magnetostratigraphy of the impact breccias and post-impact carbonates from borehole Yaxcopoil-1, Chicxulub impact crater, Yucatán, Mexico. *Meteoritics & Planetary Science*, 39(6), 821–829.
- Rivas-Gómez, S., Cruz-Hernández, J., González-Guevara, J. A., et al. (2002). Block size and fracture permeability in naturally fractured reservoirs. Paper SPE 78502 Presented at the 10th International Petroleum Exhibition and Conference, Abu Dhabi, 13–16 October.
- SENER-Conacyt. (2013). Proyecto de Investigación 85235.
- Shen, F., Pino, A., Hernandez, J., et al. (2008). Characterization and modeling study of the carbonate-fractured reservoir in the cantarell field Mexico. Paper SPE 115907 Presented at the SPE Annual Technical Conference and Exhibition, Denver, Colorado, USA, 21–24 September.
- Stearns, D. W., & Friedman, M. (1972). *Reservoir in fractured rock: Geologic exploration methods* (pp. 82–106). AAPG Special Volumes. Texas.
- Stearns, D. W. (1992). *Fractured reservoirs schools notes*. Great Falls, Montana: AAPG.
- Stinnesbeck, W., Keller, G., Adatte, T., et al. (2004). Yaxcopoil-1 and the Chicxulub impact. *International Journal of Earth Sciences (Geol Rundsch)*, 93, 1042–1065. <http://dx.doi.org/10.1007/s00531-004-0431-6>.
- Stinnesbeck, W., Keller, G., Adatte, T., Harting, M., Kramar, U., & Stüben, D. (2003). Yucatán subsurface stratigraphy based on the Yaxcopoil-1 drill hole (abstract #10868). *Geophysical Research Abstracts*, 5.
- Stöffler, D., Artemieva, N. A., Ivanov, B. A., et al. (2004). Origin and emplacement of the impact formations at Chicxulub, Mexico as revealed by the ICDP deep drilling at Yaxcopoil-1 and by numerical modeling. *Meteoritics & Planetary Science*, 39(6), 1035–1067.
- Streeter, V. (1961). *Handbook of fluid dynamics* (1st ed.). New York: McGraw-Hill Book Company.
- Tuchscherer, M. G., Reimold, U. W., Koeberl, C., & Gibson, R. L. (2004). Major and trace element characteristics of impactites from the Yaxcopoil-1 borehole, Chicxulub structure, Mexico. *Meteoritics & Planetary Science*, 39(6), 955–978.
- Urrutia-Fucugauchi, J., Camargo-Zanoguera, A., Pérez-Cruz, L., & Perez-Cruz, G. (2011). The Chicxulub multi-ring impact crater, Yucatan carbonate platform, Gulf of Mexico. *Geofísica Internacional*, 50(1), 99–127.
- Urrutia-Fucugauchi, J., Perez-Cruz, L., & Camargo-Zanoguera, A. (2013). Oil exploration in the Southern Gulf of Mexico and the Chicxulub impact. *Geology today*, 29(5). (Blackell Publishing Ltd, The Geologist's Association & The Geological Society of London).
- Villaseñor-Rojas, P. (2003). Structural evolution and sedimentological and diagenetic controls in the lower cretaceous reservoirs of the cardenas field, Mexico. Ph.D. dissertation, Ecole Doctorale Sciences et Ingenierie De l'Université de Cergy-Pontoise (December).
- Voelker, J. (2004). *A reservoir characterization of Arab-D super-K as a discrete fracture network flow system, Ghawar Field, Saudi Arabia*. Ph.D. dissertation, Stanford University, Stanford (December 2004).
- Warsi, Z. U. A. (1999). *Fluid dynamics, theoretical and computational approaches* (2nd ed., pp. 238–243). New York: CRC Press.
- Wenzhi, Z., Suyun, H., Wei, L., Tongshan, W., & Yongxin, L. (2014). Petroleum geological features and exploration prospect of deep marine carbonate rocks in China onshore: A further discussion. *Natural Gas Industry*, 34(4), 1–9.
- Witherspoon, P., Wang, J., Iwai, K., et al. (1980). Validity of cubic law for fluid flow in a deformable rock fracture. *Water Resources Research*, 16, 1016–2024.
- Wittmann, A., Kenkmann, R., Schmitt, T., et al. (2004). Impact-related dike breccia lithologies in the ICDP drill core Yaxcopoil-1, Chicxulub impact structure, Mexico. *Meteoritics & Planetary Science*, 39(6), 931–954.
- Woodcock, N. H., & Mort, K. (2008). Classification of fault breccias and related fault rocks. *Rapid Communication*, 145(03), 435–440. <http://dx.doi.org/10.1017/S0016756808004883>. (Geological Magazine, Cambridge University).

- Wu, Y. S., Di, Y., Kang, Z., et al. (2011). A multiple-continuum model for simulating single-phase and multiphase flow in naturally fractured vuggy reservoirs. *Journal of Petroleum Science and Engineering*, 78, 13–22.
- Zimmerman, R. W., & Yeo, I. (2000). Fluid flow in rock fractures: From the Navier-Stokes equations to the cubic law. In B. Faybishenko, P. A. Witherspoon, & S. M. Benson (Eds.) *Dynamics of Fluids in Fractured Rock* (pp. 213–224). Washington: American Geophysical Union.

Chapter 3

A Ternary, Static, and Dynamic Classification of NFCRs



Naturally Fractured Carbonate Reservoirs (NFCRs) need to be classified based on the detection and evaluation of the dominant discontinuities, integrating dynamic and static parameters. Discontinuities can display flow behaviors and geological features, that may behave according to a variety of reservoir static-dynamic models. An integral classification is essential for optimum reservoir management and hydrocarbon production.

This chapter presents a semi-quantitative methodology to classify naturally fractured reservoirs containing discontinuities, such as tectonic fractures, sedimentary breccias, vugs, impact breccias, caverns, fault breccias or combinations of those, considering their flow models and patterns. The proposed classification was developed using geological parameters, such as compaction and a dominant discontinuity, besides fluid flow parameters as storativity ratio and interporosity flow. A combination of static-dynamic data from various sources allows a reliable classification. Consequently, at least nine types of reservoirs were identified.

To validate this methodology, fractured reservoirs from around the world are classified, such as Cantarell and Ghawar, that are super giant Mexican and Saudi Arabian reservoirs. Comparisons between types of proposed reservoirs in this classification, are provided, defined and described for field case studies, analyzing static-dynamic parameters. The most significant finding is that an understanding and the classification of a reservoir can avoid flow problems; for example, a formation classified and associated to impact breccias, could present no matrix flow due to low permeability, requiring a specific future planning for the application of an enhanced oil recovered method, or a stimulation. Others classifications available in the literature have been incorporated and involved; they are particular cases with respect to our presented proposal, which are geological, petrophysical and fluid flow classifications, that do not consider flow models and patterns.

The novelty of the ternary triangle classification is that provides a means to compare integrated static-dynamic characteristics of real Naturally Fractured Reservoirs

(NFCRs), combining geology and fluid flow. Another aspect that deserves special attention is related to the description of the discontinuities in fractured systems for their recovery factor optimization, contributing to an advanced strategy of field development.

3.1 Classification Proposal

Advances in the understanding of fractured reservoirs are essential for their optimum management. The developed proposal regarding NFCRs classification provides a reasonable explanation for flow behavior (dynamics) and for the analysis of heterogeneous formations, with planar and non planar discontinuities. This new approach extends and modifies the conventional methodology of NFCRs classification; it is quantitative, with interdependent parameters associated to the matrix-discontinuity transfer mechanism, storage relation, and compaction, applied to the different geological discontinuities present in NFCRs. Consequently, this classification is used for an integral exploitation strategy, because of the interrelationship of multiples discontinuities.

There are several NFCRs classifications, such as:

- Static qualitative classifications: (Streltsova-Adams 1978; Saidi 1987 and Aguilera 2003).
- Static quantitative classifications: (Nelson 2001; Bratton et al. 2006) that is the Nelson's proposal modified, and (Soto et al. 2011).
- Qualitative dynamic classification: (Cinco-Ley 1996).
- Semi-dynamic quantitative classification: (Gilman et al. 2011).

Existing reservoirs classifications for fractured carbonate include some genetic, geometrical, fracture-matrix fluid transfer, and petrophysical aspects, but the influence of discontinuities in the fluid flow system and patterns are poorly described. The purpose of this chapter is to develop a ternary classification applied to carbonate reservoirs that encompasses types of discontinuities, flow patterns, matrix-discontinuity fluid transfer.

3.2 Ternary Classification Proposal Considerations

Considerations in this proposal will be given to the criteria which distinguish naturally fractured carbonate hydrocarbon reservoirs from other types. In consequence, the formation must have both sufficient porosity to contain fluids and permeability to permit their extraction. In other words, vugs, channels, fractures, caverns, and breccias may slightly increase porosity, but the permeability can be increased enormously because it depends upon the scale size. For the present doctoral dissertation, a naturally fractured carbonate reservoir will be defined as one from which

hydrocarbons production occurs, if the planar or non planar discontinuity are present. The classification assumptions are as follows:

- NFCRs present planar and non planar discontinuities.
- NFCRs present multi-porosity and multi-permeability behavior.
- Discontinuities must be interconnected for hydrocarbons production.
- Isolated discontinuities are not considered.
- There is a dominant discontinuity for hydrocarbons production.
- There is a matrix-discontinuity transfer mechanism and a storage relation in reservoir.
- It can be applied to real NFCRs.
- NFCRs are considered as composite porous media.
- Fluid flow is controlled by a pressure drop in the porous media.

3.3 Ternary Classification of NFCRs

In this section, a classification will be presented to highlight the importance of interconnected discontinuities, their storativity ratio, fluid transfer (matrix-discontinuity), and compaction. This classification is represented through an equilateral triangular diagram, similar to a two-dimensional ternary diagram, which has a clockwise direction.

Figure 3.1 shows nine types of NFCRs that closely correspond to a combination of the static and dynamic features of a reservoir, related to geological discontinuities through quantitative parameters, such as compaction C , storativity ratio ω , and

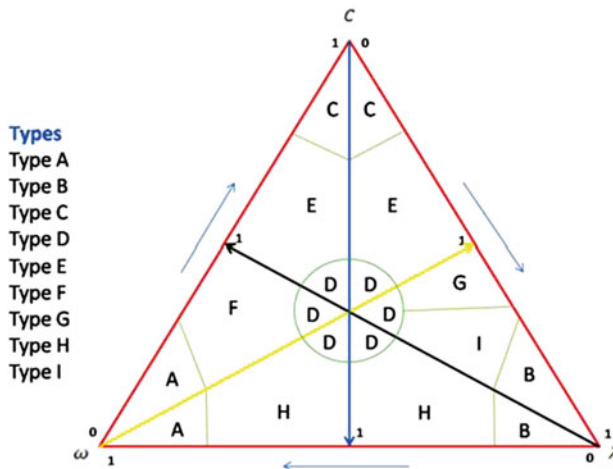


Fig. 3.1 Ternary, static and dynamic classification of NFCRs

interporosity flow λ , normalized between 0 (zero) and 1 (unity). From an engineering perspective, normalized parameters quantify and indicate the type of fractured reservoir; so that, it will be explained in the next section. Also, this Fig. 3.1 displays a red triangle that integrate quantitative parameters, and various inner straight lines or medians, that are geological discontinuities lines. These lines intersect in a single point, called barycenter or interception point of geological discontinuities.

The foundation of the ternary classification, is the concept of discontinuities distribution; that is, the spatial distribution of interconnected heterogeneities within the reservoir. In other words, each discontinuity affects and/or relates to permeability, porosity, fluid flow, fluid flow patterns, discontinuity-matrix fluid transfer, storativity, and productivity within NFCRs.

The diagenesis process and depositional environment associated to discontinuities makes pores systems in carbonates act as porosity and permeability barriers, affecting reservoirs quality. Thus, discontinuities can control oil production and distribution by providing local fluid migration pathways.

Classifications based on porosity types in carbonates were written by Choquette and Pray (1970), and Lucia (2007); these are genetic and petrophysical classifications of pore space, respectively. These classifications present many minor types of porosity that have little or no significance to reservoir exploitation; in consequence, they are pore space classifications. Discontinuities are a pore space, that can be described using the classifications on porosity types; namely, when discontinuities are considered in NFCRs, the types of pore spaces are implicitly included.

The various types of porosity are essential to static characterization; however, they do not explain how fluids flow in NFCRs. From an engineering point of view, the use of dynamic parameters is required. These parameters and types of fractured carbonate reservoirs will be discussed in the next section.

In carbonate formations, oil recovery efficiency depends on the geometry and topology of the conduit system, roughness of pore surfaces, tortuosity, fluid properties, wettability, drive mechanism, and pressure distribution. Consequently, oil recovery efficiency is associated to discontinuities, too.

The difference of the classification proposal based on the ternary plot is its quantitative approach, that integrates the static-dynamic characteristics of real (NFCRs), combining geological discontinuities and fluid flow through well testing. This classification can be applied for advanced development and the exploitation strategy of NFCRs.

3.4 Ternary Classification Parameters

A combination of parameters results in a reliable classification of the carbonates reservoirs. The presence of discontinuities changes the fluid flow patterns in NFCRs. In other words, a network of discontinuities coexists with the matrix, and each system (matrix or discontinuities) has different porosities, permeabilities, compressibilities,

and geometry. The geometrical representation of a planar discontinuity (fracture) in reservoirs, that is most widely used in well testing, is the Warren and Root's model.

The classification proposal is based on the storativity ratio, ω , the interporosity flow coefficient, λ , and compaction, C .

The storativity ratio and the interporosity flow coefficient can be calculated using geological description, and well testing results, such as drawdown and buildup tests for fractured reservoirs. These parameters are defined as

$$\omega = 10^{-\Delta p/m^*} = \frac{(\phi V c_t)_f}{(\phi V c_t)_f + (\phi V c_t)_m}, \quad (3.1)$$

$$\lambda = \frac{(\phi V c_t)_f \mu r_w^2}{\gamma \bar{k} t_1} = ar_w^2 \frac{k_m}{k_f}. \quad (3.2)$$

The storativity ratio defines the contrast between the fracture system and the total system, with different porosity and compressibility for matrix and fracture systems. If matrix compressibility is equal to fracture compressibility implies that there is no hydrodynamical contrast between fracture-matrix system despite porosities are different. Consequently, compressibilities and porosities of fracture-matrix system must be different to create a pressure gradient due to area reduction in the porous media, and fluids flow occurs.

The interporosity flow coefficient is the matrix-fracture fluid flow transfer ability; in the ternary classification. In other words, it is possible to use $\lambda/ar_w^2 = k_m/k_f$, considering that the interporosity flow depends on the shape factor, a , wellbore radius, r_w and matrix and fracture permeabilities. The goal is to develop a dimensionless ratio associated to interporosity flow coefficient.

The compaction is any process by which the pore space is reduced, as overburden load press down on the formation; among the changes we can mention a higher density of the porous media, a decrease of porosity and permeability, and the production of pore-filling fluids. Compaction is related to porosity and depth, through (3.3):

$$\phi = \phi_i e^{-CD}, \quad (3.3)$$

The compaction correction coefficient is determined using sonic logs. Also, rock compaction can be described using the diffusivity equation, assuming that bulk volume reduction equals pore volume reduction (Kohlhass and Miller 1969). If well logs are used, the compaction factor ranges from 0 to 1. When the diffusivity equation or (3.3) is used, a compaction ratio should be determined between calculated compaction at a specific depth and the calculated compaction of the deepest stratigraphic layer, considering the same geologic age of formation. This compaction ratio indicates porosity reduction in the formation. Normally, backstripping procedures are used to study the compaction effect in rocks; initial porosities values in shale, sandstone, and limestone are 0.5, 0.4, and 0.5 respectively.

3.5 Geological Discontinuities Lines

The fundamental reason of the ternary classification of NFCRs is the description and quantification of geological discontinuities, using dynamic and static parameters. Three lines are presented (blue, black and yellow lines) in the ternary diagram, that indicate a geological discontinuity. Frequency of geological event is used to describe the maximum and/or minimum influence of discontinuity in NFCR. In other words, when frequency equals 1, that implies that there is more than one discontinuity per depth feet in NFCR. For example, whether frequency equals 1; namely, several dissolution systems are observed in a measured feet of the formation.

3.5.1 Line of Tectonic-Sedimentary Breccias

Figure 3.2 displays the line of tectonic-sedimentary breccias (blue line), indicating two zones in NFCRs. The first zone (right side) describes reservoirs with tectonic events. Fundamentally, it is associated to tectonic fractures and fault breccias. Second zone (left side) shows sedimentary breccias; specifically, debris flows do not have linear or internal planar structure, resulting from lithification and consolidation of rocks. Thus, these geological events can be observed regardless the formation depth.

3.5.2 Line of Impact Breccias

Figure 3.3 shows the line of impact breccias (black line). NFCRs affected by impact breccias as the Cantarell field, are described by this line. This type of geological

Fig. 3.2 Line of tectonic-sedimentary breccias

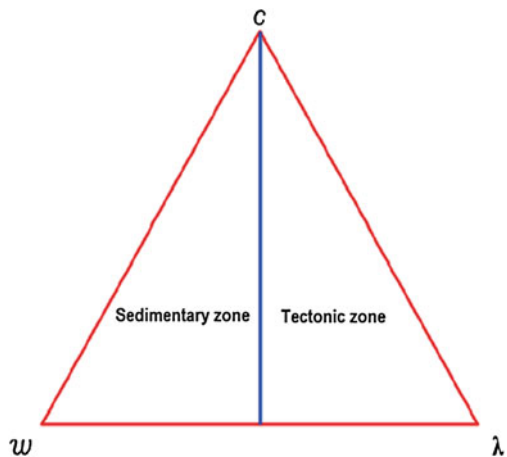
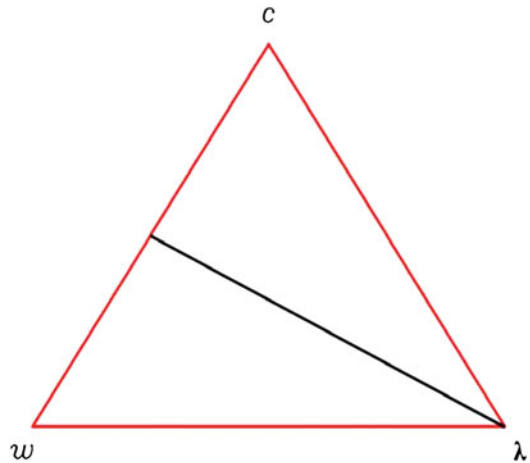


Fig. 3.3 Line of impact breccias



event is related to the ejected material produced by the earth impact of an asteroid. Also, this event can be observed regardless the formation depth.

Impact breccias may act as a seal in the formation. So that, they present high or low porosity, and their high permeability is related to the presence of others geological events because the ejected material acts as a flow barrier. In consequence, the line of impact breccias does not depend on depth; moreover, this geological event can associate to high or low porosity and moderate permeability, that indicates different values of the interporosity flow coefficient and the storativity ratio.

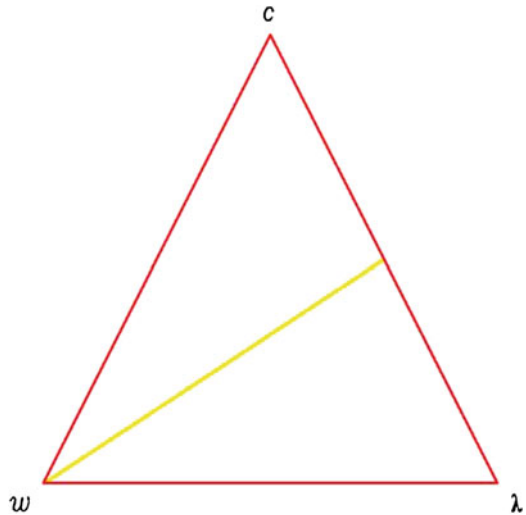
3.5.3 *Dissolution Line*

Figure 3.4 presents the dissolution line (yellow line). The goal is to describe vugs, caverns and dissolution processes associated to chemical diagenesis. This geological event can locally be observed regardless the formation depth, and it is important during hydrocarbon production due to the resulting its high permeability.

Carbonates dissolve easily due to chemical dissolution, meteoric water interaction, or under pressure. Moreover, dissolution may facilitate permeability increase, and can enhance tectonic fractures apertures.

3.5.4 *Interception of Geological Discontinuities Lines*

A NFCR is affected in some way by tectonic fractures, impact breccias, vugs, sedimentary breccias, caverns, and fault breccias, that help create secondary porosity. The interception zone of geological discontinuities lines implies the impact of natural

Fig. 3.4 Dissolution line

geological discontinuities at different zones of the reservoir; namely, the presence of distinct types of discontinuities in a reservoir, where a discontinuity can be dominant. This point called barycenter, which several geological events can be observed in NFCRs.

In consequence, a particular NFCR can fall into different classifications in accordance to several local geological events. Figure 3.1 shows the interceptions of geological discontinuities lines.

3.5.5 *Classifying Fractured Carbonate Reservoirs*

The ternary classification is genetic and petrophysical, based on static and dynamic parameters, that can be obtained using cores information, petrophysical data, outcrops, and well testing. Figure 3.1 showed this ternary classification.

This proposal presents nine types of NFCRs, depending on the geological discontinuities. So that, if discontinuities are dominant dissolution and impact breccias lines, and sedimentary and tectonic zones are considered. A dominant discontinuity or geological event is related to production and storage ability, that impacts fluid flow in NFCRs; consequently, there is a high discontinuity frequency. For example, a reservoir can be located near a fault, but the dominant event could present sedimentary features.

Type A: Single medium

This type of NFCRs is observed in intensively fractured porous media, that can be associated to a fault. Moreover, fractures or planar discontinuities are embedded in the matrix, and they represent physically the limits of narrow discontinuities which

the pressure is continuous at the matrix-fracture interface. So that, fluids in these porous media are in dynamic equilibrium, and a single medium can be considered.

Type A reservoirs are equivalent to homogeneous reservoirs. In other words, the system behavior is dominated by high matrix porosity and permeability, and discontinuities can enhance permeability. Although, hydrocarbon production is the direct result of the whole porous system, matrix-fractures transfer through rock-fluid expansion occurs instantaneously.

The patterns of fluid flow and their geometries estimated by use of the specialized graphs of pressure, p , versus time, t (e.g., p vs. $\log t$, p vs. $t^{1/2}$, p vs. $t^{1/4}$, p vs. $t^{-1/2}$, p vs. $1/t$, and p vs. t) corresponding to radial, linear, bilinear, spherical, constant pressure boundary, and pseudosteady state flow, are present in Type A reservoirs. They present high interporosity flow, low storativity ratio, and high or moderate compaction. In addition, discontinuities can create flow barriers.

Type B: Single discontinuity

Single discontinuities reservoirs are associated to tectonic fracture systems or vugs, connected with poor matrix; provide both storage and permeability to achieve hydrocarbon flow. Moreover, there is no significant matrix to fractures fluid flow and its porosity and permeability are low. Thus, matrix-discontinuity fluid transfer does not occur, and fluid is in dynamic equilibrium with discontinuity only. These reservoirs can be observed in conjugate fractures system.

The interporosity flow coefficient is low. The contrast of permeabilities and porosities, and the storativity ratio are high. Additionally, compaction is moderate to high. Thus, this single discontinuity can observe in layers buried, and fractured later. In consequence, hydrocarbons are produced through fractures.

The fluid flow patterns and their geometries estimated by the use of the specialized pressure graphs, p , versus time, t , corresponding to radial, constant pressure boundary, and pseudosteady state flow, are present in NFCR Type A, too.

Type C: Weakly compacted composite media

Type C reservoirs consider two different media. Each medium is located in distinct zones, that are defined by a flow capacity, porosity and permeability. The system can be characterized by the porosity, and the flow capacity $(k_f h)_1$ and $(k_m h)_2$ of both zones, fractures (f) and matrix (m). These reservoirs are affected locally by tectonic and sedimentary (debris flow) discontinuities, which are composed of two zones: a high-transmissibility and a low-transmissibility zone. Also, composite media can be compared as integrated porous system, changing radially, by which, fractures provide the permeability for the productivity of the wells, with low permeability and porosity in the matrix.

Compaction is low due to low reservoirs depths. The interporosity flow coefficient and storativity ratio are high, depending zone transmissibility. Normally, well is at the center of a circular high-transmissibility zone, with higher productivity than in the outer reservoir structure with respect to well, that corresponds to the homogeneous zone. The objective of this radial geometry is to describe formation

properties changes. These composite media show weakly compaction are related to fault breccias, and reservoirs localized on the fold crest.

Initially, the dynamic behavior is controlled by the fractured zone; after, the pressure behavior is dominated by the homogeneous zone, showing a contrast between the two zones; this behavior is observed in the pressure derivative function (PDF) curve. On the other hand, the specialized graph of pressure, p , versus $\log t$, may suggest the presence of a pseudosteady state matrix-fracture flow (Cinco-Ley 1996).

Type D: Multiple porosities and permeabilities

Type D reservoirs present the highest productivity because they are associated to different geological discontinuities, creating multiples porosities and permeabilities. In other words, discontinuities could be present in NFCRs; so that, this type of reservoir is located near the barycenter, which implies juxtaposition of geological events.

The double-porosity and double-permeability models essentially can describe these reservoirs, considering moderate or high interporosity flow coefficient and storativity ratio. These reservoirs provide added porosity and permeability. Additionally, deep formations exhibit a moderate to high compaction, too.

The pressure behavior is observed in semilog graph, showing two parallel straight lines; namely, a fracture-dominated flow period and a total system (fracture/matrix) dominated flow period (Cinco-Ley 1996), with radial and bilinear flow.

Type E: Composite media compacted moderately

Type E reservoirs are similar to type C, and consider two different media, too. These reservoirs are affected locally by fracturing, impact breccias, dissolution, and debris flow, and are composed of two zones: a high-transmissibility and a low-transmissibility zone. The system is characterized by the porosity, and the flow capacity $(k_f h)_1$ and $(k_m h)_2$ of both zones.

These composite media with moderate compaction are related to fault breccias, local diagenesis zones, and reservoirs localized in the fold.

The pressure behavior shows a contrast between two zones, suggesting the presence of pseudosteady state matrix-fractures flow.

Type F: Fluid flow barriers

Type F reservoirs have low to moderate storativity ratio, and moderate to high interporosity flow coefficient. They can be associated to ejected clasts of impact breccias, and debris flow with little fracturing. Normally, wells productivity depends on fractures or vugs.

The pressure behavior is pseudosteady state flow, and sedimentary and ejected clasts often complicate fluid flow developing barriers. Compaction depends on reservoir depth.

Type G: Dominant discontinuity

Some NFCRs exhibit a dominant discontinuity (planar or nonplanar), that represent a cavern, permeable fault, or fault breccias, that act as a huge channel to drain the reservoir zones. The flow system is dominated by the discontinuity transmissibility.

Both matrix and dominant discontinuity contain hydrocarbons, showing different values ranges for interporosity flow coefficient; however, storativity ratio contribute to hydrocarbons storage. The dominant discontinuities can have complex directional permeability relationships with respect to dissolutions or fractures because they are juxtaposed.

A radial flow period is present when the wellbore is not intercepted by the dominant discontinuity. After a transition period, the well behaves as if it was located near a constant pressure boundary, reaching a final bilinear flow period (Cinco-Ley 1996).

Type H: Fluid transfer mechanism

Type H deep reservoirs have high compaction, so that their storativity ratio values are limited due to the presence of discontinuities. The interporosity flow coefficient can have different values, that implies an effective or poor matrix-discontinuity fluid transfer mechanism. The matrix-discontinuity fluid transfer is a controlling parameter in the long-term behavior of a radial, closed system. The distinct compressibilities, permeabilities, and porosities of porous media change because of hydrocarbon production, and the matrix-discontinuity system depletion.

These NFCRs can be associated to tectonic and sedimentary systems by which should exist two porous media; so that, doble-porosity and doble-permeability models could be used to describe dynamic behavior reservoirs.

Type I: Impact breccias, with others discontinuities

In the absence of others discontinuities (fault breccias, fractures, vugs, sedimentary breccias, and caverns), impact breccias in NFCRs present low volumetric flow because of the ejected clasts act as flow barriers. The presence of fractures or fault breccias is a fluids production way, and impact breccias are fluid storage.

Some NFCRs contain impact breccias, with huge hydrocarbons volume due to high matrix porosity. Moreover, the poor matrix permeability does not permit fluids flow freely. So that, it is necessary the presence of other discontinuities.

The pressure behavior of type I reservoirs is radial. A bilinear flow is observed in fault breccias and fractures. Also, elliptical flow can be found because of the ejected clasts rip-up geometry.

3.6 Generalized Ternary Classification

The ternary classification can incorporate the others classifications available in the literature because this new proposal considers a quantitative, genetic, geological, petrophysical, and dynamic classification. In addition, the present classification does not contrast with others, because all of them are included.

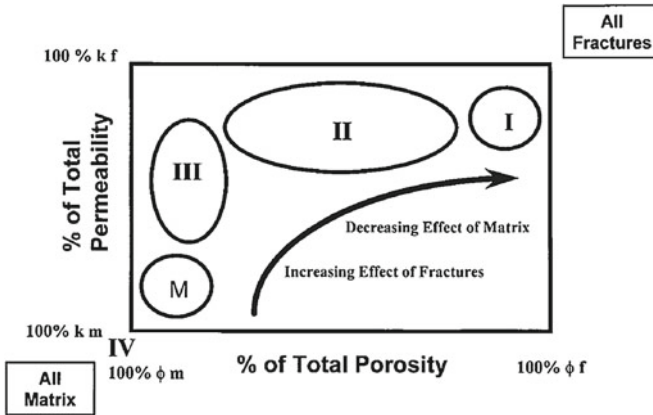


Fig. 3.5 A schematic cross plot of percent reservoir porosity versus percent reservoir permeability (percent due to matrix versus percent due to fractures) for the fractured reservoir classifications used by author (After Nelson 2001, Fig. 2-1, p. 102)

3.6.1 Classification of Naturally Fractured Reservoirs.
Author: Ronald Nelson

Figure 3.5 displays a quantitative and static classification. This plot classification is based on porous media permeabilities and porosities, showing four types of reservoirs. This classification was presented as follows:

3.6.2 Classification for Naturally Fractured Reservoir, by Gilman et al.

In this semiquantitative plot classification, the concepts of interporosity flow coefficient and storativity ratio were redefined. Although, this proposal is based on an interporosity flow term defined as $\lambda_A = \sigma k_m A / k_{fe}$, that indicates the relative contribution of fracture-matrix flow compared to flow through the fractures within the well drainage area, A (Gilman et al. 2011); on the other hand, Gilman’s storativity ratio is defined as $\omega_\phi = \phi_f / (\phi_f + \phi_m)$, and a third ratio called the ratio of effective fracture permeability to matrix permeability defined as $k_{exr} = k_{fe} / k_m$ is also used.

The storativity ratio conceptualized in the Gilman plot does not included porous media compressibilities. Also, it might mean that matrix compressibility is similar to fractures compressibility. Consequently, a hydrodynamical contrast between fracture-matrix system might not occur, and the whole matrix-fracture system is assumed with a homogeneous compaction and deformation. Moreover, this type of fractured reservoirs may be possible (equivalent compressibilities), and it might be a particular type of ternary classification (Type H). Seven cases of naturally fractured reservoir were presented in Gilman’s plot. Figure 3.6 shows two of his seven cases.

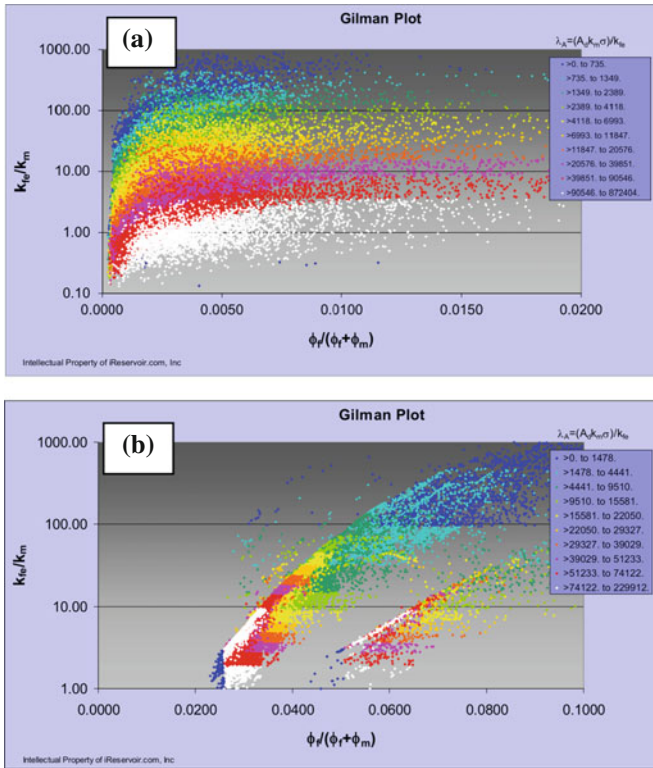


Fig. 3.6 Gilman Plot for conventional reservoirs, Cases 1 and 3. **a** Carbonate, light oil, pressure depletion via horizontal and vertical wells, moderate aquifer influx, **b** Sandstone, heavy oil, water-flood via vertical wells (After Gilman et al. 2011, Fig. 3, p. 16.)

3.6.3 Types of Naturally Fractured Reservoirs. Author: Héber Cinco-Ley

Figure 3.7 and Table 3.1 show a qualitative and dynamic classification based on well testing. The types of naturally fractured reservoirs were presented as follows:

3.6.4 Reservoirs Classification, by Soto et al.

Figure 3.8 displays a petrophysical classification based on pore types and cementation factor, $m_{variable}$, using the fuzzy logic principles (Soto et al. 2011).

This classification is approached to vugs and fractures, including matrix-fracture and matrix-vugs fluid transfers. In addition, a homogeneous reservoir is related to intergranular porosity reservoirs.

Fig. 3.7 Types of NFRs.
a Homogeneous model.
b Fluids contained in the fractures system.
c Multiple region or composite.
d Anisotropic model.
e Single fracture model.
f Double porosity model.
 (After Cinco-Ley 1996, Fig. 2, p. 52)

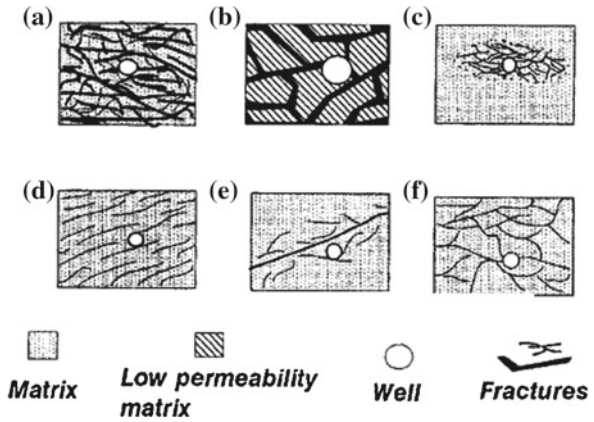


Table 3.1 Parameters and applications of flow models for NFRs (After Cinco-Ley 1996, Table 1, p. 52)

Model	Parameters	Application
Homogeneous	kh and s	Highly fractured reservoir or low-permeability matrix
Multiple region or composite	$(kh)_1, (kh)_2,$ and s	Regionally fractured reservoir
Anisotropic	k_{max} and k_{min}	Oriented fractures
Single fracture	F_{cD}, s_f, d_f, k_f and s	Reservoir with a dominant fracture, or a well near a conductive fault
Double porosity	$(kh)_f, s, \lambda,$ and ω	Heavily fractured reservoir with intermediate matrix permeability

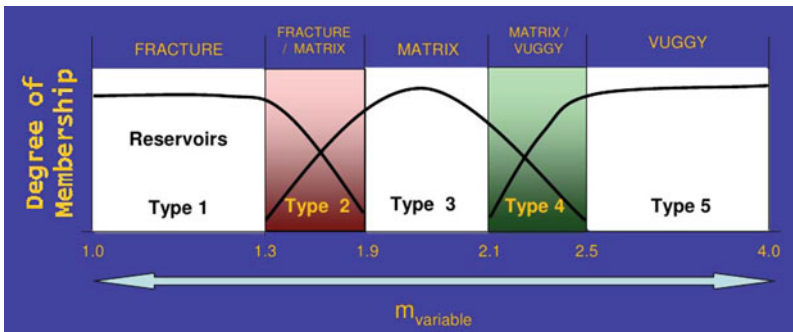


Fig. 3.8 The five types of reservoirs based on the cementation factor variable, related to different kind of reservoirs (After Soto et al. 2011, Fig. 6, p. 8)

Table 3.2 Similarities between the literature available classifications and the ternary classification

Classifications available in the literature	Ternary classification
R. Nelson’s classification	
Type 1	Type B
Type 2	Type G and Type I
Type 3	Type D and Type G
Type 4	Type A and Type F
Cinco-Ley’s types of NFRs	
Homogeneous	Type A and Type B
Multiple region or composite	Type C and Type E
Anisotropic	Type G and Type I
Single fracture	Type G
Double porosity	Type D, Type E, Type H, and Type G
Gilman plot	
Case 1	Type H
Case 2	Type H
Case 3	Type H
Case 4	Type H
Case 5	Type H
Case 6	Type H
Case 7	Type H
Soto et al.’s classification	
Type 1	Type B
Type 2	Type E, Type D, and Type I
Type 3	Type C and Type E
Type 4	Type D and Type G
Type 5	Type G and Type I

3.6.5 *Similarities Between Classifications Available in Literature and Ternary Classification*

Table 3.2 presents similarities between several published classifications with respect to the ternary classification.

The ternary classification defines the quantitative static and dynamic parameters of planar and nonplanar discontinuities, which are necessary in reservoirs evaluation and modeling, and it allows the fluid flow behavior prediction. This is its advantage.

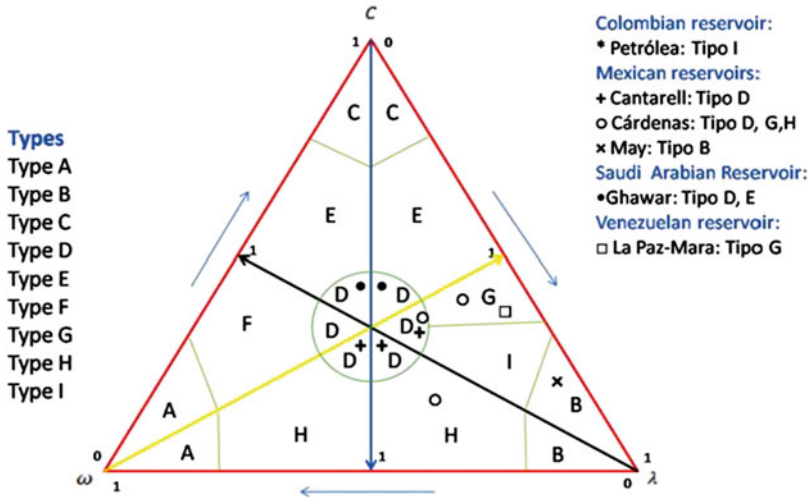


Fig. 3.9 A depiction of the NFCRs ternary classification of the investigated reservoirs

3.7 Examples of NFCRs

The ternary classification scheme subdivides fractured reservoirs, considering similar static and dynamic parameters that describe the flow interaction between the matrix-discontinuities. The examples of NFCRs presented have been investigated on the basis of the porous media connectivity. A depiction of classified NFCRs is shown in Fig. 3.9, considering the literature available for carbonate reservoirs (Villaseñor-Rojas 2003; Voelker 2004 and Nelson 2001).

Different pore types or discontinuities are observed in a reservoir. The juxtaposition of geological planar and nonplanar discontinuities can locally classify a reservoir in different types. In other words, each discontinuity can create a particular fluid flow behavior in NFCRs.

3.8 Nomenclature

Δp	pressure difference, [Pa]
ϕ_i	initial porosity, [fraction]
ϕ	porosity, [fraction]
a, σ	shape factor, [m^{-2}]
h	formation thickness, [m]
ω	storativity ratio, [dimensionless]
ω_ϕ	storativity ratio of Gilman's plot, [dimensionless]
λ	interporosity flow coefficient, [dimensionless]

λ_A	interporosity flow coefficient used in Gilman's plot, [dimensionless]
\bar{k}	average fracture permeability, [m ²]
k_m	matrix permeability, [m ²]
k_f	fracture permeability, [m ²]
k_{fe}	effective fracture permeability, [m ²]
k_{exr}	permeability excess ratio, [dimensionless]
γ	exponential of Euler's constant, ($\gamma = 1.781$)
t_1	time of intersection with respect to midpoint of the transition data (early straight line), [s]
r_w	wellbore radius, [m]
C	compaction factor at the specified depth, [dimensionless]
m	drawdown slope, [Pa ⁻¹]
D	depth, [m]
c_t	total compressibility, [Pa ⁻¹]
V	volume, [m ³]

Subscripts

f	fracture
m	matrix
i	initial
1	first zone
2	second zone

References

- Aguilera, R. (2003). Geologic and engineering aspects of naturally fractured reservoirs. CSEG RECORDER, (pp. 44–49). (February).
- Barros-Galvis, N., Villaseñor, P., & Samaniego, F. (2015). Analytical modeling and contradictions in limestone reservoirs: Breccias, vugs, and fractures. *Journal of Petroleum Engineering*. Article ID 895786. (Hindawi Publishing Corporation).
- Bratton, T., Canh, D. V., Duc, N. V. et al. (2006). The nature of naturally fractured reservoirs. *Oilfield Review*.
- Choquette, P. W., & Pray, L. C. (1970). Geologic nomenclature and classification of porosity in sedimentary carbonates. *AAPG Bulletin*, 54(2), 207–250.
- Cinco-Ley, H. (1996). Well-test analysis for naturally fractured reservoirs. *Journal of Petroleum Technology*, 51–54. (SPE 31162, January).
- Gilman, J. R., Wang, H., Fadaei, S. et al. (2011). A New Classification Plot for Naturally Fractured Reservoirs, paper CSUG/SPE 146580, presented at the Canadian Unconventional Resources Conferences, Calgary, Alberta, Canada, November 15–17.
- Kohlhass, C. A. & Miller, F. G. (1969). Rock-compaction and pressure-transient analysis with pressure-dependent rock properties. Paper SPE 2563, Presented at 44th Annual Fall Meeting of the Society of Petroleum Engineers of AIME, Denver, Colorado, September 28–October 1.
- Lucia, F. J. (2007). *Carbonate reservoir characterization An integrated approach* (2nd ed., pp. 26–67). Berlin: Springer.
- Nelson, R. (2001). *Geologic analysis of naturally fractured reservoirs* (2nd ed.). New York: Gulf professional publishing/BP-Amoco.

- Saidi, A. M. (1987). *Reservoir engineering of fractured reservoirs (fundamental and practical aspects)*. Singapore: TOTAL Edition Presse.
- Soto, R., Martin, C., Perez, O. et al. (2011). A new reservoir classification based on pore types improves characterization. Paper ACIPET TEC-86, Presented at the Congreso Colombiano del Petróleo, Bogotá, Colombia, November 22–25.
- Streltsova-Adams, T. D. (1978). Well hydraulics in heterogeneous aquifer formations. *Advances in Hydroscience*, 11, 357–423.
- Villaseñor-Rojas, P. (2003). Structural evolution and sedimentological and diagenetic controls in the lower cretaceous reservoirs of the cardenas field, Mexico. Ph.D. dissertation, Ecole Doctorale Sciences et Ingenierie De l'Université de Cergy-Pontoise (December).
- Voelker, J. (2004). A reservoir characterization of Arab-D Super-K as a discrete fracture network flow system, Ghawar Field, Saudi Arabia. Ph.D. dissertation, Stanford University, Stanford (December 2004).

Chapter 4

Analytical Model for Non Stress Sensitive Naturally Fractured Carbonate Reservoirs (NFCRs)



4.1 Overview

This chapter compares the obtained solutions in a fractured medium and a fractured porous medium. Both media are slightly deformable without stress-sensitive. The analysis has been developed chiefly with the aim of obtaining exact analytical expressions for the solution of the mathematical model of carbonate reservoirs.

A fractured medium is formed by stresses producing the rock breaking, that contains tectonic fractures between blocks of rock, and there is not interchange fluid between rock and fractures. Some examples as fractured igneous rock, or fractured reservoirs classified as type I by Nelson (2001). A fractured porous medium is generated by stresses producing rock breaking, that contains tectonic fractures and there exist interchange fluid between rock and fractures, such as fractured limestone, or fractured reservoir classified as type II and III by Nelson (2001).

An analytical model for non stress sensitive Naturally Fractured Reservoirs is developed. Their model is solved analytically for flow equation including quadratic gradient term using Cole-Hopf transform for a infinite reservoir case.

Proposed analytical techniques assume constant properties of rock, which yield a constant diffusivity. For use this case, we use a Navier-Stokes solution called the Couette's flow for fractures, which it is similar to Darcy's law.

The theory of fluid flow in fractured media was developed by Barenblatt et al. (1960), and is based on the assumption of constant rock properties. Barenblatt's model consisted of two media: matrix and fractures, which would generate a pressure gradient during hydrocarbon production (Barenblatt et al. 1960).

4.2 Analytical Considerations for Model

In order to develop this mathematical model, let us establish some physical considerations as result of physic phenomenon that would help to obtain the solution:

1. Carbonate reservoirs are usually naturally fractured. So, there are two media that interchange fluid due to pressure gradient between matrix and fractures (Barenblatt et al. 1960).
2. Single phase. Undersaturated oil reservoir (Craft and Hawkins 1991), so that fluid is a liquid.
3. Porosity, permeability, and density are constants. So, they do not depend neither stresses nor fluid pressure.
4. Permeability is isotropic.
5. Liquid of constant compressibility, in consequence fluid density changes exponentially with respect to pressure (Muskat 1945).
6. Isothermal fluid flow of small and constant compressibility.

4.3 Couette and Darcy’s Equation

Darcy’s law is frequently used and sometimes unknowing its basic assumptions. The most restrictive application condition is related to Reynolds number; namely, that fluid flow is dominated by viscous forces, considering laminar flow for Reynolds number, Re smaller than unity Fig. 4.1.

Various authors give different limiting values for Darcy’s laminar flow, between a range of Re from 3 to 10 (Polubarinova-Kochina 1962). However, (Muskat 1945) discussed that Darcy’s Law can be applied to reservoirs flow problems whose conditions yield Reynolds number smaller than unity.

The Reynolds number and the basic Darcy equation may be stated as:

$$Re = \frac{v \bar{D}_p \rho}{\mu} \tag{4.1}$$

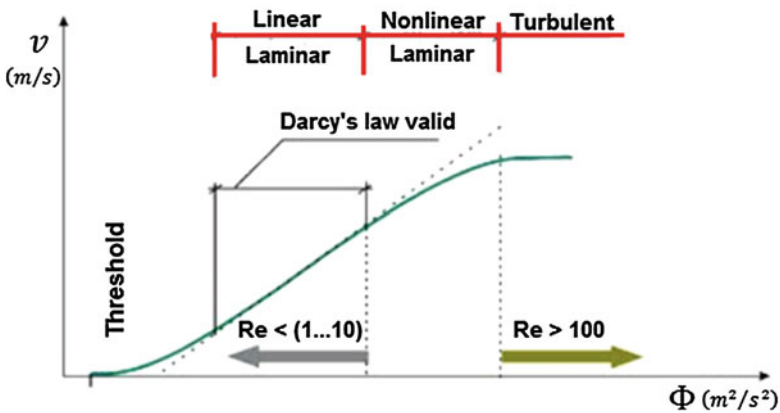


Fig. 4.1 Applicability of Darcy’s law (VICAIRE 2014)

For natural fractures can be expressed as:

$$Re = \frac{qa\rho}{\mu A\phi} \quad (4.2)$$

where

$$v = -\frac{k\rho}{\mu}\nabla\Phi \quad (4.3)$$

where

$\Phi = p/\rho + gz$, flow potential

p = formation pressure

ρ = density

g = gravity

z = elevation

μ = oil dynamic viscosity

$A = 2\pi rh$, area

h = thickness formation

k = total permeability

Re = Reynolds number

\bar{D}_p = average pore diameter

a = fracture aperture

v = specific discharge

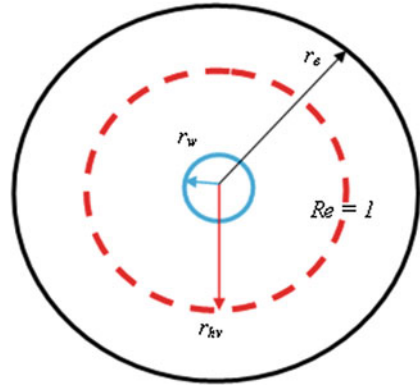
Darcy's law is valid for the median of the flow probability distribution, and is based on the assumption that fluid flow is inertialess (Scheidegger 1960).

It can be stated that for a heterogeneous, anisotropic and fractured porous medium, the upper limit critical Reynolds number for laminar flow ranges from 0.1 to 10. The transition to quadratic flow (without reaching turbulent), see the nonlinear laminar section of Fig. 4.1 was demonstrated by Schneebeli (1955). The nonlinear seepage flow law will be parabolic at with deviation from linearity (Barenblatt et al. 1990; Couland et al. 1986), and nonlinear corrections to Darcy's law at low Reynolds numbers for periodic porous media are applied (Firdaouss et al. 1997). Also, values of Reynolds number between 5 and 13 was calculated with numerical experiments for equations Navier-Stokes (Couland et al. 1986; Stark 1972).

The nonlinear flow law is present in fractured porous media. Consequently, the Couette equation can be used for the analytical modeling because has a quadratic flow profile that is an exact solution for the Navier-Stokes equation; this equation can obtain cubic law and/or Boussinesq's formula. Cubic law estimates the fluid flow rate for flow through fractures systems; usually, this equation is used Naturally Fractured Tectonic Reservoirs (NFTRs) considering the laminar flow of a viscous fluid between parallel flat plates (Barros-Galvis et al. 2015; Potter and Wiggert 2007).

The application of Couette or Darcy equations is associated with the Reynolds number. For Naturally Fractured Tectonic Reservoirs high velocity fluid flow is related to the Reynolds number, too. Figure 4.2 displays two zones in the

Fig. 4.2 Stabilized zone of non Darcy flow (high velocity)



reservoir, a high velocity zone and other low velocity zone. These zones, with high and low fluid velocity radius, are limited with the Reynolds number equals to unity. Where:

r_{hv} = outer (maximum) high velocity radius

r_e = outer radius

r_w = wellbore radius.

For radial flow, it has been described that for a flowing well the high velocity flow stabilizes at a radius r_{hv} where the Reynolds number is one.

The red circle represents the inner (minimum) radius for Darcy's flow; for $r < r_{hv}$ flow is under high velocity conditions, and Couette equation is used.

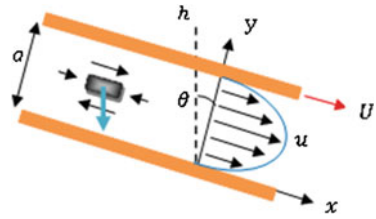
On the other hand, using the Navier-Stokes equations can derive the seepage law by means of integration (Barenblatt et al. 1990) and Couette equation. An extension on the three dimensional Couette flow has been utilized to study the channel flow and the effect of the permeability of the porous medium with heat transfer (Singh and Sharma 2001). In this paper, we use Couette equation to describe fluid flow in natural fractures.

4.4 Analytical Model

The analytical model is based on a partial differential equation that describe the flow of fluids in fractures and matrix. In developing this equation, we combine: continuity equation or law of conservation of mass, a flow law such as the Couette's equation, and an equation of state. Moreover, we obtained linear diffusivity equation depicting the flow of incompressible liquid in a fractured medium.

The fracture is represented as two parallel surfaces. The flow between these plates is taken to be in the x direction, and since there is no flow in the y direction, pressure will only be a function in the x direction. In addition, there are no inertia, viscous, or external forces in the y direction. See Fig. 4.3.

Fig. 4.3 Flow in two parallel surfaces (a tectonic fracture)



Now, we use an exact solution to the Navier-Stokes equations referred to The General Couette Flow. See Eq.4.4. The goal of this equation is describe fluid flow through tectonic fractures or discontinuities (Currie 2003):

$$u(y) = -\frac{1}{2\mu} \frac{d(p_f + \gamma h)}{dx} y (a - y) + \frac{U}{a} y \tag{4.4}$$

where:

- $\frac{dp_f}{dx}$ = fracture pressure gradient
- $u(y)$ = velocity profile
- U = upper surface velocity
- a = aperture
- y = vertical direction
- x = horizontal direction
- γ = specific gravity
- h = vertical distance
- p_f = fracture pressure
- μ = viscosity.

Equation 4.4 shows that the fluid flow is in the direction of the negative pressure gradient and that the velocity profile across the flow field is parabolic. There are two ways of inducing a flow between two parallel surfaces: (1) applying a pressure gradient, and (2) the upper surface is moved in the x direction with constant velocity U . In our case, we induce a flow applying a pressure gradient; the maximum velocity occurs in $y = a/2$. Giving special attention to pressure gradient presupposes that upper surface will be fixed and it will describe Poiseuille Flow. In consequence, Poiseuille Flow is a specific case The General Couette Flow.

The use of the maximum velocity in Couette’s equation indicates the maximum fluid flow into a discontinuity as a consequence pressure gradient. In the solution that follows, gravity is neglected, and Eq. 4.4 can be written as:

$$u(y) = -\frac{1}{2\mu} \frac{dp_f}{dx} y (a - y) \tag{4.5}$$

Equation 4.5 is analogue Darcy’s equation; considering $y = a/2$ this equation can be rewritten:

$$u(y) = -\frac{a^2}{8\mu} \frac{dp_f}{dx} = -\frac{a^2}{8\mu} \nabla p_f \quad (4.6)$$

Remembering that the fracture permeability (k_f) can be expressed as follows:

$$k_f = 54 \times 10^6 (a^2) \text{ darcys} \quad (4.7)$$

and

$$k_f = 8.35 \times 10^6 (a^2) \text{ darcys} \quad (4.8)$$

In Eq. 4.7, the aperture (a) is expressed in inches and in Eq. 4.8 this aperture (a) is used in centimeters (Aguilera 1995). Substituting Eq. 4.8 into Eq. 4.6:

$$u(y) = -\frac{k_f}{8 \times 8.45 \times 10^6 \mu} \nabla p_f = -\frac{k_f}{66.8 \times 10^6 \mu} \nabla p_f \quad (4.9)$$

Field cases have been reported with tectonic and nontectonic fractures conductivity calibrated using well testing (Singha et al. 2012). Conductivity calibrated using the Poiseuille's Law is given by:

$$C_f = k_f h = \frac{a^3}{12 \times 0.98 \times 10^{-6}} \quad (4.10)$$

Considering one meter of formation thickness, the average fracture aperture is given by:

$$a = \sqrt[3]{k_f \times 11.76 \times 10^{-6}} \quad (4.11)$$

where C_f is tectonic fracture conductivity in md.m, a is fracture aperture in mm, k_f is fracture permeability in md, and h is formation thickness in one meter.

Equation 4.10 was determined for rough limestone fractures in a tight carbonate reservoir in the Middle East with tectonic fractures, which its porosity was 0.2%.

Applying Eq. 4.10 was calculated for conductivity values of 20md.m that represents 6.24×10^{-6} mm average aperture in one meter of formation thickness.

Equation 4.10 can be substitute into Eq. 4.6:

$$u(y) = -\frac{(k_f \times 11.76 \times 10^{-6})^{2/3}}{8\mu} \nabla p_f = -\frac{(k_f)^{2/3}}{32.26 \times 10^8 \mu} \nabla p_f \quad (4.12)$$

It can be observed that considering a constant, $C = 66.8 \times 10^6$ for Eq. 4.9, and $C = 32.26 \times 10^8$ for Eq. 4.12. Equations 4.9 and 4.12 are an expression similar to Darcy's Law, which $u(y) = v$:

$$\mathbf{v} = -\frac{k_f}{C\mu} \nabla p_f \quad (4.13)$$

To derive a partial differential equation for fluid flow in a fractured medium, we should combine a flow law with the continuity equation (Mattews and Russell 1967; Lee et al. 2003). The continuity equation can be expressed using a derivative or integrative equation, which they are equivalent, given by

$$\frac{\partial}{\partial t} (\rho\phi_f) = -\nabla \cdot (\rho\mathbf{v}) \quad (4.14)$$

where:

\mathbf{v} = velocity profile using Couette's equation

ϕ_f = fractured medium porosity

ρ = fluid density

t = time

Substituting Eq. 4.10 into Eq. 4.14 gives:

$$\frac{\partial}{\partial t} (\rho\phi_f) = -\nabla \cdot \left[\rho \left(-\frac{k_f}{C\mu} \nabla p_f \right) \right] \quad (4.15)$$

Applying the derivative of a product, and making $\mu^* = C\mu$

$$\frac{\partial}{\partial t} (\rho\phi_f) = \nabla \cdot \left(\frac{\rho k_f}{\mu^*} \right) \nabla p_f + \frac{\rho k_f}{\mu^*} \nabla^2 p_f \quad (4.16)$$

Equation 4.16 contains various two terms right side. Each term involves the permeability, viscosity, and porosity, which are constants. However, fluid density depends incompressibility liquids. Restricting our analysis to single-phase liquids and slightly compressible liquids with constant compressibility, c , where c is defined by the equation

$$c = -\frac{1}{V} \frac{dV}{dp_f} = \frac{1}{\rho} \frac{d\rho}{dp_f} \quad (4.17)$$

For constant compressibility c , integration of Eq. 4.17 gives

$$\rho = \rho_o \exp [c (p_f - p_i)] \quad (4.18)$$

The derivative of Eq. 4.18 with respect to pressure yields Eq. 4.19:

$$\frac{\partial \rho}{\partial p_f} = [\rho_o \exp [c (p_f - p_i)]] c = \rho c \quad (4.19)$$

Applying the chain rule and substituting Eq. 4.19:

$$\frac{\partial \rho}{\partial t} = \frac{\partial \rho}{\partial t} \frac{\partial p_f}{\partial p_f} = \frac{\partial \rho}{\partial p_f} \frac{\partial p_f}{\partial t} = \rho c \frac{\partial p_f}{\partial t} \quad (4.20)$$

For one dimension flow, the gradient in the right side first term of Eq. 4.16 can be written as:

$$\nabla \left(\frac{\rho k_f}{\mu^*} \right) = \frac{\partial}{\partial x} \left(\frac{\rho k_f}{\mu^*} \right) \frac{\partial p_f}{\partial p_f} = \frac{\partial \rho}{\partial p_f} \left(\frac{k_f}{\mu^*} \right) \frac{\partial p_f}{\partial x} \quad (4.21)$$

$$\nabla \left(\frac{\rho k_f}{\mu^*} \right) = \rho c \left(\frac{k_f}{\mu^*} \right) \frac{\partial p_f}{\partial x} = \rho c \left(\frac{k_f}{\mu^*} \right) \nabla p_f \quad (4.22)$$

Substituting Eqs. 4.20 and 4.22 into Eq. 4.16;

$$\rho \phi_f c \frac{\partial p_f}{\partial t} = \rho c \left(\frac{k_f}{\mu^*} \right) (\nabla p_f)^2 + \frac{\rho k_f}{\mu^*} \nabla^2 p_f \quad (4.23)$$

$$D = \frac{k_f}{\phi_f c \mu^*} \quad (4.24)$$

After transposing terms, Eq. 4.22 may be expressed:

$$\frac{\partial p_f}{\partial t} = D \left[c (\nabla p_f)^2 + \nabla^2 p_f \right] \quad (4.25)$$

where D is diffusivity constant.

The tectonic reservoirs with extension fractures present low porosity and permeability of matrix. Permeability and effective porosity of fractures are dominant variables in fluid flow; consequently, formation porosity and permeability may be approximate to fractures properties. In this paper, matrix properties are considered and included in total permeability and porosity of reservoir.

Initial and boundary conditions in radial coordinate are:

- $p_f = p_i$ at $t = 0$ for all r .
- $(r \partial p_f / \partial r)_{r_w} = -6qu/\pi kh$ for $t > 0$.

To develop the solution, this boundary condition is replaced by the condition:

$$\lim_{r \rightarrow 0} (r \partial p_f / \partial r)_{r_w} = -6qu/\pi kh \text{ for } t > 0.$$

- $p_f(r, t) = p_i$ as $r \rightarrow \infty$ for all t .

Equation 4.25 is a nonlinear partial differential equation, and can be referred as a nonlinear diffusivity equation (see Eqs. 4.24 and 4.25). This equation represents an analytical model for non stress-sensitive Naturally Fractured Reservoir, that describes fluid flow in the fracture system for an oil fractured reservoir, considering a nonlinear term of quadratic gradient $(\nabla p_f)^2$, and without transfer between fracture-matrix.

Many papers have been published for the single phase flow in homogeneous reservoirs, that do not include the nonlinear pressure gradient term in the diffusivity equation considered as small negligible pressure gradient, constant rock properties, and a fluid of small and constant compressibility; in effect, the nonlinear quadratic term is usually neglected (see the first right hand side term of Eq. 4.25) for liquid flow (the fluid compressibility c has a small value) (Samaniego et al. 1979; Dake 1998; Matthews and Russell 1967). In addition, for a infinite reservoir and with closed outer boundary, the wellbore pressure predicted by this linear Darcy solution may be significantly smaller than that predicted by the Couette solution at large times. On the other hand, (Jelmert and Vik 1996; Odeh and Babu 1988) concluded that the consideration of the nonlinear quadratic term gives results significantly smaller in pressure prediction and recommended its use as the use pressure solution; although this result was also demonstrated by Chakrabarty et al. (1993) for wellbore pressure prediction for a closed outer boundary, the authors stated that the linear pressure solution is unsatisfactory and should be applied with caution, and the use of the linear solution for infinite reservoirs has a 5% error for large dimensionless times.

Others papers have showed solutions for nonlinear transient flow model including a quadratic gradient term by using transformations, and; however, they assumed a homogeneous porous medium (Chakrabarty et al. 1993; Friedel and Voigt 2009; Cao et al. 2004; Aadnoy and Finjord 1996).

4.5 Mathematical Model and Solution for Constant Rate Radial Flow in an Infinite Reservoir

Our aim is to apply a mathematical transformation to reduce a nonlinear equation to linear equation diffusivity for a naturally fractured system, without matrix-fracture transfer.

The differences between Darcy and Couette equations that applied to the linear diffusivity equation have been described. Previous authors have not included the nonlinear pressure gradient term in the nonlinear diffusivity equation for fractures or homogeneous systems. In both of cases, fluid flow equations (Darcy and Couette equations) are used in this solution, considering parallel (slab), and cubic fractures geometry.

The diffusivity equation models mass and momentum transfer in the reservoir. The phenomenological description for fluid flow in fractured reservoir is given by: (1) complex diffusion in tectonic fractures and (2) hydrodynamics as a result of a pressure gradient in well. Complex diffusion contains various types of diffusion: molecular diffusion, surface diffusion, Knudsen diffusion, and convection due to gradient pressure. The fractured system is heterogeneous and anisotropic, and their diffusion processes depend on fractures aperture or porous diameter (Cunningham and Williams 1980; Treybal 1980). In consequence, fast complex diffusion is reached in a

nonlinear laminar flow that may be modeled by Couette equation. Finally, momentum transfer is modeled using Couette equation.

Hydrodynamics in wellbore is governed by gradient pressure and fluid flow. The fluid velocity is related to oil production rate, and Couette or Darcy equation application depends on the value of the Reynolds number. When Reynolds number is greater than unity Couette equation is applied. This application impacts the boundary condition of the diffusivity equation. For bulk, and slab fractures properties and should be considered the expressions following:

$$\phi = \phi_m + \phi_f \quad (4.26)$$

$$c = \frac{c_o + c_w\phi_m + c_m\phi_m + c_f\phi_f}{\phi_f} \quad (4.27)$$

$$k = \frac{k_f \left[N\pi \left(\frac{a}{2} \right)^2 \right] + k_m \left[A - N\pi \left(\frac{a}{2} \right)^2 \right]}{A} \quad (4.28)$$

$$k_{slab} = \frac{k_f a}{d} \quad (4.29)$$

where

- ϕ = total porosity
- ϕ_f = fracture porosity
- ϕ_m = matrix porosity
- k = total permeability
- k_m = matrix permeability
- k_f = fracture permeability
- c = compressibility
- a = fracture aperture
- c_o = oil compressibility
- c_m = matrix compressibility
- c_w = water compressibility
- c_f = fracture compressibility
- d = distance between fractures
- N = number of fractures per section
- k_{slab} = parallel fractures permeability.

Equations 4.26, 4.27, 4.28, and 4.29 are used by Reiss (1980) and Aguilera (1995).

4.6 Solution of the Nonlinear Partial Differential Equation Without Stress-Sensitive

The Cole-Hopf transformation was used to obtain a solution to the Burger equation, that is a nonlinear partial differential equation (Burgers 1974; Ames 1972). Also, it has been employed to solve a nonlinear diffusion problem for the flow of compressible liquids through homogeneous porous media (Marshall 2009). Transformation is a mathematical technique, which a nonlinear equation may be reduced to a linear equation.

Equation 4.25 models fractured reservoirs as: type I, single-fracture model according (Nelson 2001; Cinco 1996) classification respectively, but without stress-sensitive. The nonlinear diffusivity equation requires to be transformed to obtain an analytical solution. So that, this case will be developed without matrix-fracture transfer function.

4.6.1 Case Without Transfer Function

It was observed that the following transformation $y = F(p_f)$ applied in Burgers Equation generated a linear partial equation of this type: $\partial y/\partial t = D\nabla^2 y$, and this concept was utilized to solve the Nonlinear Diffusivity Equation (Ames 1972; Burgers 1974; Marshall 2009):

$$\frac{\partial p_f}{\partial t} = D\nabla^2 p_f + D \left(\frac{F''(p_f)}{F'(p_f)} \right) (\nabla p_f)^2 \quad (4.30)$$

with a quadratic gradient term. It can be observed that Eq. 4.25 is similar or equivalent to Eq. 4.30. If we wish to solve Eq. 4.25, we would solve for F . Then

$$y = F(p_f) = \frac{1}{c} (\exp(cp_f + a)) + b \quad (4.31)$$

$$F'(p_f) = \exp(cp_f + a) \quad (4.32)$$

$$F''(p_f) = c \exp(cp_f + a) \quad (4.33)$$

where a , and b are arbitrary integration constants generated due to $F''(p_f)$ and $F'(p_f)$. Equation 4.31 is named the Cole-Hopf Transformation. If $a = b = 0$ (Tong et al. 2005), then

$$y = \frac{1}{c} \exp(cp_f) \iff p_f = \frac{1}{c} \ln(cy)$$

$$\frac{\partial p_f}{\partial y} = \frac{1}{cy} \quad (4.34)$$

$$\frac{\partial^2 p_f}{\partial y^2} = -\frac{1}{cy^2} \quad (4.35)$$

Our goal is to eliminate $(\nabla p_f)^2$; to accomplish this goal, we follow the next procedure: $\partial p_f / \partial t$, $\nabla^2 p_f$, and $(\nabla p_f)^2$:

$$\frac{\partial p_f}{\partial t} = \frac{\partial p_f}{\partial y} \frac{\partial y}{\partial t} = \frac{1}{cy} \frac{\partial y}{\partial t} \quad (4.36)$$

For express $(\nabla p_f)^2$ we should consider $\nabla p_f = \partial p_f / \partial x$. Applying the chain rule for one dimension:

$$\frac{\partial p_f}{\partial x} = \frac{\partial p_f}{\partial y} \frac{\partial y}{\partial x} \quad (4.37)$$

$$\frac{\partial p_f}{\partial x} = \frac{\partial p_f}{\partial y} \nabla y \quad (4.38)$$

substituting in Eq. 4.34

$$(\nabla p_f)^2 = \frac{1}{(cy)^2} (\nabla y)^2 \quad (4.39)$$

For the term $\nabla^2 p_f$:

$$\nabla^2 p_f = \frac{\partial^2 p_f}{\partial x^2} = \frac{\partial}{\partial x} \left(\frac{\partial p_f}{\partial x} \right) \quad (4.40)$$

Substituting Eq. 4.37 into Eq. 4.40 gives:

$$\nabla^2 p_f = \frac{\partial}{\partial x} \left(\frac{\partial p_f}{\partial y} \right) \left(\frac{\partial y}{\partial x} \right) \quad (4.41)$$

Applying the product derivative and transposing terms give:

$$\nabla^2 p_f = \frac{\partial}{\partial x} \left(\frac{\partial p_f}{\partial y} \right) \frac{\partial y}{\partial x} + \frac{\partial}{\partial x} \frac{\partial y}{\partial x} \left(\frac{\partial p_f}{\partial y} \right) = \frac{\partial}{\partial y} \left(\frac{\partial p_f}{\partial x} \right) \frac{\partial y}{\partial x} + \frac{\partial^2 y}{\partial x^2} \left(\frac{\partial p_f}{\partial y} \right) \quad (4.42)$$

Substituting Eq. 4.37 into Eq. 4.42, gives:

$$\nabla^2 p_f = \frac{\partial}{\partial y} \left(\frac{\partial p_f}{\partial y} \right) \left(\frac{\partial y}{\partial x} \right) \left(\frac{\partial y}{\partial x} \right) + \frac{\partial^2 y}{\partial x^2} \left(\frac{\partial p_f}{\partial y} \right) = \left(\frac{\partial^2 p_f}{\partial y^2} \right) \left(\frac{\partial y}{\partial x} \right)^2 + \frac{\partial^2 y}{\partial x^2} \left(\frac{\partial p_f}{\partial y} \right) \quad (4.43)$$

Substituting Eqs. 4.34 and 4.35 into Eq. 4.43

$$\nabla^2 p_f = \frac{1}{c(y)} \nabla^2 y - \frac{1}{c(y)^2} (\nabla y)^2 \quad (4.44)$$

Substituting Eqs. 4.36, 4.39, 4.43 into Eq. 4.25 gives:

$$\frac{1}{Dcy} \frac{\partial y}{\partial t} = \frac{1}{c(y)^2} (\nabla y)^2 + \frac{1}{c(y)} \nabla^2 y - \frac{1}{cy^2} (\nabla y)^2$$

Making simplifications, we obtained the Linear Diffusivity Equation, Eq. 4.45. This equation is solved in (Mattews and Russell 1967) with different conditions or cases: (1) Constant rate, infinite reservoir, (2) Constant rate, and (3) Constant rate, constant pressure outer boundary case. Moreover, this type of equation is solved and compared in papers (Chakrabarty et al. 1993; Odeh and Babu 1988).

$$\frac{1}{D} \frac{\partial y}{\partial t} = \nabla^2 y \quad (4.45)$$

References

- Aadnoy, B., & Finjord, J. (1996, August). Analytical solution of the Boltzmann transient line sink for an oil reservoir with pressure-depend formation properties. *Journal of Petroleum Science and Engineering*, 15, 343–360.
- Aguilera, R. (1995). *Naturally fractured reservoirs* (2nd ed.). Tulsa, OK: Penn Well Books.
- Ames, W. F. (1972). *Nonlinear partial differential equations in engineering* (Vol. II). New York: Academic Press.
- Barenblatt, G. I., Zheltov, Iu. P., & Kochina, I. N. (1960). *Basic concepts in the theory of seepage of homogeneous liquids in fissured rocks* (OB OSNOVNYKH PBEDSTAVLENIYAKH TEORII FIL'TRATSII ODNORODNYKH ZHIDKOSTEI V TRESHCHINOVATYKH PORODAKH) (G. H. PMM, Trans.) (Vol. 24 (5), pp. 852–864).
- Barenblatt, G. I., Entov, V. M., & Ryzhik, V. M. (1990). *Theory of fluid flows through natural rocks*. Dordrecht: Klumer.
- Barros-Galvis, N., Villaseñor, P., & Samaniego, V. F. (2015). Phenomenology and contradictions in carbonate reservoirs. *Journal of Petroleum Engineering*.
- Burgers, J. M. (1974). *The nonlinear diffusion equation, asymptotic solutions and statistical problems* (2nd ed.). Dordrecht, Holland: D. Reidel Publishing Company.
- Chakrabarty, C., Farouq Ali, S. M., & Tortike, W. S. (1993). Effect of the nonlinear gradient term on the transient pressure solution for a radial flow system. *Journal of Petroleum Science and Engineering*, 8, 241–256.
- Cinco-Ley, H. (1996, January). Well-test analysis for naturally fractured reservoirs. *Journal of Petroleum Technology*, 51–54. SPE 31162.

- Couland, O., Morel, P., & Caltagirone, J. P. (1986). Effets non lineaires dans les ecoulements en milieu poreux. *Comptes Rendus de l'Académie des Sciences—Series II*, 302, 263–266.
- Craft, E. C., & Hawkins, M. (1991). *Applied petroleum reservoir engineering*. New York, NJ: Prentice Hall.
- Cunningham, R. E., & Williams, R. J. J. (1980). *Diffusion gases and porous media*. New York: Plenum Press.
- Currie, I. G. (2003). *Fundamental mechanics of fluids* (2nd ed.). New York: McGraw-Hill Book Company.
- Dake, L. P. (1998). *Fundamentals of reservoir engineering* (1 ed., Seventeenth impression). The Netherlands: Elsevier Science.
- Firdaouss, M., Guermont, J.-L., & Le Quére, P. (1997). Nonlinear corrections to Darcy's law at low reynolds numbers. *Journal of Fluid Mechanics*, 343, 331–350.
- Friedel, T., & Voigt, H.-D. (2009). Analytical Solutions for the Radial Flow Equation with Constant-Rate and Constant-Pressure Boundary Conditions in Reservoirs with Pressure-Sensitive Permeability. Paper SPE 122768 presented at the SPE Rocky Mountain Petroleum Technology, Denver, Colorado, USA, April 14–16.
- Jelmert, T. A., & Vik, S. A. (1996). Analytic solution to the non-linear diffusion equation for fluids of constant compressibility. *Petroleum Science & Engineering*, 14, 231–233. <http://dx.doi.org/0920-4105/96>.
- Lee, J., Rollins, J. B., & Spivey, J. P. (2003). *Pressure transient testing in wells* (Vol. 9, pp. 1–9). Richardson, TX: Monograph Series, SPE.
- Marshall, S. L. (2009). Nonlinear pressure diffusion in flow of compressible liquids through porous media. *Transport in Porous Media*, 77, 431–446. <https://doi.org/10.1007/s11242-008-9275-z>.
- Matthews, C. S., & Russell, D. G. (1967). *Pressure buildup and flow tests in wells* (Vol. 1, pp. 4–9). Richardson, TX: Monograph Series, SPE.
- Muskat, M. (1946). *Flow of homogeneous fluids through porous media* (2nd ed., p. 145). Ann Arbor, MI: J.W. Edwards.
- Nelson, R. (2001). *Geologic analysis of naturally fractured reservoirs* (2nd ed.). New York: Gulf Professional Publishing, BP-Amoco.
- Odeh, A. S., & Babu, D. K. (1988). *Comparison of solutions of the nonlinear and linearized diffusion equations* (pp. 1202–1206). SPE Reservoir Engineering, SPE 17270.
- Polubarinova-Kochina, P. (1962). *Theory of ground water movement* (1st ed.) (J.M. Roger De Wiest, Trans.). Princeton, New Jersey: Princeton University Press.
- Potter, M., & Wigert, D. (2007). *Mechanics of fluids* (3rd ed.). México: Prentice Hall.
- Reiss, L. H. (1980). *The reservoir engineering aspects of fractured formations*. Paris: Editions Technip.
- Samaniego, F. V., Brigham, W. E., & Miller, F. G. (1979, June). Performance-prediction procedure for transient flow of fluids through pressure-sensitive formations. *Journal of Petroleum Technology*, 779–786.
- Scheidegger, A. E. (1960). *The physics of flow through porous media* (2nd ed.). New York: The MacMillan Company.
- Schneebeli, G. (1955). Experiences sur la limite de validité de la loi de Darcy et l'apparition de la turbulence dans un écoulement de filtration. *Houille Blanche No. 2*, 141–149.
- Singh, K. D., & Sharma, R. (2001). Three dimensional couette flow through a porous medium with heat transfer. *Indian Journal of Pure & Applied Mathematics*, 32(12), 1819–1829.
- Singha, D., Al-Shammeli, A., Verma, N. K., et al. (2012, December). Characterizing and modeling natural fracture networks in a tight carbonate reservoir in the middle east: A methodology. *Bulletin of the Geological Society of Malaysia*, 58, 29–35.
- Stark, K. P. (1972). *A numerical study of the nonlinear laminar regime of flow in an idealized porous medium* (pp. 86–102). Fundamentals of Transport Phenomena in Porous Media, Amsterdam: Elsevier.
- Tong, D.-K., & Wang, R.-H. (2005). Exact solution of pressure transient model or fluid flow in fractal reservoir including a quadratic gradient term. *Energy Sources*, 27, 1205–1215.

- Treybal, R. E. (1980). *Mass-transfer operations* (3rd ed.). New York: McGraw Hill.
- Virtual Campus in Hydrology and Water Resource Management (VICAIRE). (2014). Retrieved October 8, 2014, from http://echo2.epfl.ch/VICAIRE/mod_3/chapt_5/mainhtm.
- Xu-long, C., Tong, D.-K., & Wang, R.-H. (2004, January). Exact solutions for nonlinear transient flow model including a quadratic gradient term. *Applied Mathematics and Mechanics. English Edition*, 25(1), 102–109.

Chapter 5

Analytical Model for Stress Sensitive Naturally Fractured Carbonate Reservoirs (NFCRs)



The goal of this chapter is to develop and to study an analytical and mathematical model for Naturally Fractured Reservoir when there is stress-sensitive in formation. The model is solved analytically to be used and proved with well testing. Solutions obtained with this model will describe the pressure behavior with respect at time considering the change of permeability, porosity and fluid density. In conclusion, this phenomenon is dynamic.

This mathematical solution is used in two aspects: (1) study the transient pressure response of a Stress Sensitive Naturally Fractured Reservoir, and (2) could be applied as a coupled model when is combined with an additional expression that consider mechanic or thermodynamic phenomenon. In this case, analytical solution is associated with other mathematical expression that describe the collapse of fractures.

The theory of fluid flow in fractured media was developed by (Barenblatt 1960), and is based on the assumption of constant rock properties. Barenblatt's model consisted of two media: matrix and fractures, which would generate a pressure gradient during hydrocarbon production.

5.1 Analytical Considerations for Model

In order to develop this analytical and mathematical model, let me establish some simple considerations as result of physic phenomenon that would help to obtain a solution:

1. Carbonate reservoir is naturally fractured. So, there are two media and can exist a flow, and pressure gradient between matrix and fractures (Barenblatt 1960).
2. Single phase. Undersaturated Oil Reservoir, so that fluid is a liquid (Craft and Hawkins 1991).

3. Porosity and permeability change with burial, but these changes are expressed as a function of effective stress or pressure.
4. Porosity depends exponentially with respect to overburden (Enrenberg et al. 2009) and pressure (Pedrosa 1986).
5. Permeability changes exponentially with respect to pressure. In spite of the fact that in carbonates there is no direct relationship between porosity and permeability, only between pore-size distribution, porosity and permeability. In consequence, a geologic and diagenetic model is required to show the distribution associated to the pore space interparticle porosity, separate-vug porosity or touching vugs (tectonic fractures, karst, etc.). In addition to the distribution pore space; grain-dominated packstones, mud-dominated fabrics or dolomitized mud-dominated fabrics should be regarded.¹ So that, variability in how permeability changes with depth is complicated. However, the permeability of matrix-fracture is assumed to be dependent on pressure, expressing said dependency exponentially (Pedrosa 1986).
6. Fluid density changes exponentially with respect to pressure (Muskat 1945).
7. Fluid is incompressible and isothermal.

5.2 Analytical Model

Analytical model is based on develop a partial differential equation that describe the flow of fluids in fractures and matrix. In developing these equation, we combine: continuity equation or law of conservation of mass, flow law such as the Couette's Flow, and an equation of state. Moreover, we obtained nonlinear diffusivity equation depicting the flow of incompressible liquid in a fractured medium.

Let me to represent a fracture as two parallel surfaces. The flow between these plates is taken to be in the x direction, and since there is no flow in the y direction, so pressure will be a function in the x direction only. In addition, there are no inertia, viscous, or external forces in the y direction (Fig. 5.1).

Now, we use an exact solutions to the Navier-Stokes equations referred to The General Couette Flow (see Eq. 5.1). The goal of this equation is describe fluid flow through fractures or discontinuities (Currie 2003).

$$u(y) = -\frac{1}{2\mu} \frac{d(p_f + \gamma h)}{dx} y(a - y) + \frac{U}{a} y \quad (5.1)$$

where:

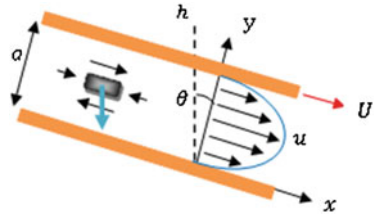
$u(y) = v$ velocity profile

U = upper surface velocity

a = aperture

¹Personal communications with Lucia, J. Doe. 2013. Texas: Bureau of Economic Geology. The University of Texas at Austin.

Fig. 5.1 Parallel surfaces



- y = vertical direction
- x = horizontal direction
- γ = specific gravity
- h = vertical distance
- p_f = fracture pressure
- μ = viscosity
- $\frac{dp_f}{dx}$ = fracture pressure gradient.

Equation 5.1 shows that the fluid flow is in the direction of the negative pressure gradient and that the velocity profile across the flow field is parabolic. There are two ways of inducing a flow between two parallel surfaces: (1) applying a pressure gradient, and (2) the upper surface is moved in the x direction with constant velocity U . In our case, we induce a flow applying a pressure gradient, which the maximum velocity occurs in $y = a/2$. The use of the maximum velocity in Couette’s equation indicates the maximum fluid flow into discontinuity as a consequence pressure gradient. So, gravity may be neglected, and Eq. 5.1 can be written as:

$$u(y) = -\frac{1}{2\mu} \frac{dp_f}{dx} y (a - y) \tag{5.2}$$

Equation 5.2 is analogue Darcy’s equation, and using $y = a/2$ could be rewritten:

$$u(y) = -\frac{a^2}{8\mu} \frac{dp_f}{dx} = -\frac{a^2}{8\mu} \nabla p_f \tag{5.3}$$

Remembering that for fracture permeability (k_f) as follows:

$$k_f = 54 \times 10^6 (a^2) \text{ darcys} \tag{5.4}$$

$$k_f = 8.45 \times 10^6 (a^2) \text{ darcys} \tag{5.5}$$

where aperture(a) is in inches and centimeters respectively (Aguilera 1995). Substituting Eq. 5.5 into Eq. 5.3:

$$u(y) = -\frac{k_f}{8 \times 8.45 \times 10^6 \mu} \nabla p_f = -\frac{k_f}{67.6 \times 10^6 \mu} \nabla p_f \tag{5.6}$$

Assigning a conversion constant, $C = 67.6 \times 10^6$. We have an expression similar to Darcy's Law, which $u(y) = v$:

$$\mathbf{v} = -\frac{k_f}{C\mu} \nabla p_f \quad (5.7)$$

To derive partial differential equation for fluid flow in a fractured medium, we should combine flow law with the continuity equation (Matthews and Russell 1967; Lee 2003). The continuity equation can be expressed using derivative or integrative equation, which they are equivalent (Marshall 2009).

$$\frac{\partial}{\partial t} (\rho\phi_f) = -\nabla \cdot (\rho\mathbf{v}) \quad (5.8)$$

where:

\mathbf{v} = velocity profile using Couette's equation

ϕ_f = fractured medium porosity

ρ = fluid density

t = time

Substituting Eq. 5.7 into Eq. 5.8 gives:

$$\frac{\partial}{\partial t} (\rho\phi_f) = -\nabla \cdot \left[\rho \left(-\frac{k_f}{C\mu} \nabla p_f \right) \right] \quad (5.9)$$

Applying the derivative of a product

$$\frac{\partial}{\partial t} (\rho\phi_f) = \nabla \cdot \left(\frac{\rho k_f}{C\mu} \right) \nabla p_f + \frac{\rho k_f}{C\mu} \nabla^2 p_f \quad (5.10)$$

Equation 5.10 contains various terms, which each term involves the rate of density, permeability, or porosity. Then, we define these expressions using state equation, and considering exponential variation on pressure. For first term $\frac{\partial}{\partial t} (\rho\phi_f)$:

$$\frac{\partial}{\partial t} (\rho\phi_f) = \phi_f \frac{\partial \rho}{\partial t} + \rho \frac{\partial \phi_f}{\partial t} \quad (5.11)$$

Then, we apply the chain rule and Eq. 5.11 becomes:

$$\frac{\partial}{\partial t} (\rho\phi_f) = \phi_f \frac{\partial \rho}{\partial t} + \rho \frac{\partial \phi_f}{\partial t} = \phi_f \frac{\partial \rho}{\partial p_f} \frac{\partial p_f}{\partial t} + \rho \frac{\partial \phi_f}{\partial p_f} \frac{\partial p_f}{\partial t} \quad (5.12)$$

We define the rate of density using the equation state:

$$\rho = \rho_i \exp [c (p_f - p_i)] \quad (5.13)$$

where the subscripts “ i ” refer to an initial condition, and c is the constant compressibility of liquid. Differencing with respect to p_f Eq. 5.13 gives:

$$\frac{\partial \rho}{\partial p_f} = \rho_i \exp [c (p_f - p_i)] (c) = \rho c \quad (5.14)$$

For rate of porosity, we have

$$\phi_f = \phi_{if} \exp [c_f (p_f - p_i)] \quad (5.15)$$

where c_f is the constant compressibility of formation. Differencing with respect to p_f Eq. 5.15 gives:

$$\frac{\partial \phi_f}{\partial p_f} = \phi_{if} \exp [c_f (p_f - p_i)] (c_f) = \phi_f c_f \quad (5.16)$$

Substituting Eqs. 5.14 and 5.16 into Eq. 5.12

$$\frac{\partial}{\partial t} (\rho \phi_f) = \phi_f \rho c \frac{\partial p_f}{\partial t} + \phi_f \rho c_f \frac{\partial p_f}{\partial t} = \phi_f \rho \frac{\partial p_f}{\partial t} (c + c_f) \quad (5.17)$$

For second term $\nabla \left(\frac{\rho k_f}{C\mu} \right)$:

$$\nabla \left(\frac{\rho k_f}{C\mu} \right) = \frac{\partial}{\partial x} \left(\frac{\rho k_f}{C\mu} \right) \frac{\partial p_f}{\partial p_f} = \frac{\partial}{\partial p_f} \left(\frac{\rho k_f}{C\mu} \right) \frac{\partial p_f}{\partial x} = \frac{k_f}{C\mu} \frac{\partial \rho}{\partial p_f} \nabla p_f + \frac{\rho}{C\mu} \frac{\partial k_f}{\partial p_f} \nabla p_f \quad (5.18)$$

considering that

$$k_f = k_{if} \exp [\gamma (p_f - p_i)] \quad (5.19)$$

where γ is the permeability modulus, and differencing with respect to p_f Eq. 5.19 gives:

$$\frac{\partial k_f}{\partial p_f} = k_{if} \exp [\gamma (p_f - p_i)] (\gamma) = k_{if} \gamma \quad (5.20)$$

substituting Eqs. 5.20 and 5.14 into Eq. 5.18 gives:

$$\nabla \left(\frac{\rho k_f}{C\mu} \right) = \left(\frac{\rho k_f}{C\mu} \right) (\gamma + c) \nabla p_f \quad (5.21)$$

Finally, substituting Eqs. 5.17 and 5.21 into Eq. 5.10:

$$(c + c_f) \phi_f \frac{\partial p_f}{\partial t} = \left(\frac{k_f}{C\mu} \right) (\gamma + c) \nabla p_f \nabla p_f + \frac{k_f}{C\mu} \nabla^2 p_f \quad (5.22)$$

$$(c + c_f) \phi_f \frac{\partial p_f}{\partial t} = \left(\frac{k_f}{C\mu} \right) [\nabla^2 p_f + (\gamma + c) \nabla p_f \nabla p_f]$$

$$\frac{\partial p_f}{\partial t} = \left(\frac{k_f}{(c + c_f) \phi_f C\mu} \right) [\nabla^2 p_f + (\gamma + c) \nabla p_f \nabla p_f]$$

$$\frac{\partial p_f}{\partial t} = \left(\frac{k_{if} \exp[\gamma (p_f - p_i)]}{(c + c_f) \phi_{if} \exp[c_f (p_f - p_i)] C\mu} \right) [\nabla^2 p_f + (\gamma + c) \nabla p_f \nabla p_f]$$

$$\frac{\partial p_f}{\partial t} = \left(\frac{k_{if} \exp[(\gamma - c_f) (p_f - p_i)]}{(c + c_f) \phi_{if} C\mu} \right) [\nabla^2 p_f + (\gamma + c) \nabla p_f \nabla p_f]$$

After transposing terms, we have:

$$\frac{\partial p_f}{\partial t} = \left(\frac{k_{if} \exp[(\gamma - c_f) (p_f - p_i)]}{\phi_{if} c_i \mu^*} \right) [\nabla^2 p_f + (\gamma + c) (\nabla p_f)^2] \quad (5.23)$$

$$D_i = \frac{k_{if}}{\phi_{if} c_i \mu^*} \quad (5.24)$$

where D_i Eq. 5.24 is diffusion constant expressed in initial condition. So that, we obtained an analytical model Eq. 5.24 for Stress Sensitive Naturally Fractured Reservoir.

Substituting Eq. 5.24 into Eq. 5.23 become

$$\frac{\partial p_f}{\partial t} = D_i \exp[(\gamma - c_f) (p_f - p_i)] [\nabla^2 p_f + (\gamma + c) (\nabla p_f)^2] \quad (5.25)$$

$$\frac{\partial p_f}{\partial t} = D_i \exp[(\gamma - c_f) (p_f - p_i)] [\nabla^2 p_f + (\gamma + c) (\nabla p_f)^2] \quad (\gamma \geq c_f)$$

Equation 5.25 is a nonlinear partial differential equation, and specifically is the quasi-linear parabolic diffusion equation. This model describes fluid flow in the fracture system for an oil fractured reservoir considering a nonlinear term of quadratic gradient $(\nabla p_f)^2$, and without transfer function between fracture-matrix. Normally, published papers have been developed for homogeneous reservoir, and they does not include or eliminate nonlinear term (Samaniego 1979; Odeh and Babu 1988; Jelmert and Vik 1996).

In Eq. 5.25, we can analyze two cases: (1) when $\gamma = c_f$, and when $\gamma > c_f$

$$\begin{cases} \frac{\partial p_f}{\partial t} = D_i \left[\nabla^2 p_f + (\gamma + c) (\nabla p_f)^2 \right] & \gamma = c_f \\ \frac{\partial p_f}{\partial t} = D_i \exp[(\gamma - c_f)(p_f - p_i)] \left[\nabla^2 p_f + (\gamma + c) (\nabla p_f)^2 \right] & \gamma > c_f \end{cases} \quad (5.26)$$

In radial coordinates:

$$\begin{cases} \frac{\partial p_f}{\partial t} = D_i \left[\frac{\partial^2 p_f}{\partial r^2} + \frac{1}{r} \frac{\partial p_f}{\partial r} + (\gamma + c) \left(\frac{\partial p_f}{\partial r} \right)^2 \right] & \gamma = c_f \\ \frac{\partial p_f}{\partial t} = D_i \exp[(\gamma - c_f)(p_f - p_i)] \left[\frac{\partial^2 p_f}{\partial r^2} + \frac{1}{r} \frac{\partial p_f}{\partial r} + (\gamma + c) \left(\frac{\partial p_f}{\partial r} \right)^2 \right] & \gamma > c_f \end{cases} \quad (5.27)$$

Equation 5.27 is found in Celis (1994), but they not show its deduction. In addition, this proposed zero orden solution using perturbation analysis corresponds to the solution of a naturally fractured reservoir that is not stress sensitive.

5.3 Solution Nonlinear Partial Differential Equation

Equation 5.26 showed two cases. Additionally we will develop another case for NFRs with transfer function or double porosity.

Our motivation to solve these cases obeys modeling of fractured reservoirs called type I, single-fracture, homogeneous reservoir model according to (Nelson 2001) and (Cinco-Ley 1996) respectively.

5.3.1 Case 1: $\gamma = c_f$

$$\frac{\partial p_f}{\partial t} = D_i \left[\nabla^2 p_f + (\gamma + c) (\nabla p_f)^2 \right]$$

considering $\beta = (\gamma + c)$ then

$$\frac{\partial p_f}{\partial t} = D_i \left[\nabla^2 p_f + \beta (\nabla p_f)^2 \right] \quad (5.28)$$

It was observed that the dependent variable transformation $y = F(p_f)$ of the linear parabolic equation (Heat Equation) $\frac{\partial y}{\partial t} = D \nabla^2 y$ generated a equation of this type (Ames 1972; Burger 1974; Marshall 2009):

$$\frac{\partial p_f}{\partial t} = D_i \nabla^2 p_f + D_i \left(\frac{F''(p_f)}{F'(p_f)} \right) (\nabla p_f)^2 \quad (5.29)$$

with quadratic nonlinearities. If we wish to solve the Eq. 5.28, we would set

$$D_i F''(p_f) = \beta F'(p_f) \quad (5.30)$$

and solve for F . Then

$$y = F(p_f) = \frac{1}{\beta} (\exp(\beta p_f + a)) + b \quad (5.31)$$

$$F'(p_f) = \exp(\beta p_f + a) \quad (5.32)$$

$$F''(p_f) = \beta \exp(\beta p_f) \quad (5.33)$$

where a, b are arbitrary constants generated due to integration $F''(p_f)$ and $F'(p_f)$. Equation 5.31 is named the Cole-Hopt Transformation. If $a = b = 0$ (Tong and Wang 2005) then

$$y = \frac{1}{\beta} \exp(\beta p_f) \iff p_f = \frac{1}{\beta} \ln(\beta y)$$

Our goal is eliminated $(\nabla p_f)^2$, so that, we define $\frac{\partial p_f}{\partial t}$, $\nabla^2 p_f$, and $(\nabla p_f)^2$.

$$\frac{\partial p_f}{\partial t} = \frac{\partial p_f}{\partial y} \frac{\partial y}{\partial t} = \frac{1}{\beta y} \frac{\partial y}{\partial t} \quad (5.34)$$

If $\nabla p_f = \frac{1}{\beta y} \nabla y$ then

$$(\nabla p_f)^2 = \frac{1}{(\beta y)^2} (\nabla y)^2 \quad (5.35)$$

$$\nabla^2 p_f = \frac{1}{\beta y} \nabla^2 y - \frac{1}{\beta (y)^2} (\nabla y)^2 \quad (5.36)$$

Substituting into Eq. 5.28:

$$\frac{1}{D_i \beta y} \frac{\partial y}{\partial t} = \frac{1}{\beta (y)^2} (\nabla y)^2 + \frac{1}{\beta y} \nabla^2 y - \frac{1}{\beta (y)^2} (\nabla y)^2$$

Making simplifications, we obtained the Linear Heat Equation. This equation is solved in (Matthews and Russell 1967) with different conditions or cases: (1) Constant rate, infinite reservoir, (2) Constant rate, and (3) Constant rate, constant pressure outer boundary case.

$$\frac{1}{D_i} \frac{\partial y}{\partial t} = \nabla^2 y \quad (5.37)$$

5.3.1.1 Diffusivity Constant and Rock Bulk Compressibility

The change in volume of reservoir rock occurs when overburden or pressure confining acts on rock. Changes in rock properties take place due to compaction and decreasing of pore pressure.

In Eq. 5.24, we can see that diffusivity constant contains oil compressibility c and formation compressibility c_f . Oil compressibility is constant because of subsaturated oil reservoir. On considering formation compressibility is bulk rock compressibility, two types of stress variations have to be analyzed. These types of stress are: pore stress or internal stress, and external stress related to overburden. Moreover, porosity change depends only difference between internal and external stresses.

Normally, in petroleum engineering is used definition of pore volume compressibility as follows:

$$c_f = -\frac{1}{V_b} \left(\frac{\partial V_b}{\partial p} \right) = -\frac{1}{\phi} \left(\frac{\partial \phi}{\partial p} \right) \quad (5.38)$$

Equation 5.38 is employed for constant stress and deformation, respectively. Where V_b is bulk volume.

Although, the reciprocal theorem of Betti and Rayleigh applies to internal and external stresses, which leads to:

$$\left(\frac{\partial V_b}{\partial p} \right)_{\sigma} = - \left(\frac{\partial V_b}{\partial \sigma} \right)_p \quad (5.39)$$

One may define the bulk formation compressibility considering constant pore pressure as:

$$c_f = \frac{1}{V_b} \left(\frac{\partial V_b}{\partial \sigma} \right)_p \quad (5.40)$$

Equation 5.40 expresses change of bulk volume with respect to external stress or overburden. It is shown that transformed Eq. 5.37 contains formation compressibility in diffusivity constant, but transformation provides a diffusivity equation in y , and compressibility depends in pressure p .

References

- Aguilera, R. (1995). *Naturally fractured reservoirs* (2nd ed.). Tulsa, OK: Penn Well Books.
 Ames, W. F. (1972). *Nonlinear partial differential equations in engineering* (Vol. II). New York: Academic Press.

- Barenblatt, G. I., Zheltov, Iu. P., & Kochina, I. N. (1960). *Basic concepts in the theory of seepage of homogeneous liquids in fissured rocks* (OB OSNOVNYKH PBEDSTAVLENIYAKH TEORII FIL'TRATSII ODNORODNYKH ZHIDKOSTEI V TRESHCHINOVATYKH PORODAKH) (G.H. PMM, Trans.) (Vol. 24(5), 852–864).
- Burger, J. M. (1974). *The nonlinear diffusion equation, asymptotic solutions and statistical problems* (2nd ed.). Dordrecht, Holland: D. Reidel Publishing Company.
- Celis, V., Silva, R., Ramones, M. et al. (1994). A New Model for Pressure Transient Analysis in Stress Sensitive Naturally Fractured Reservoir.
- Cinco-Ley, H. (1996, January). Well-test analysis for naturally fractured reservoirs. *Journal of Petroleum Technology*, 51–54. SPE 31162.
- Craft, E. C., & Hawkins, M. (1991). *Applied petroleum reservoir engineering*. NJ: Prentice Hall.
- Currie, I. G. (2003). *Fundamental mechanics of fluids* (2nd ed.). New York: McGraw-Hill Book Company.
- Enrenberg, S. N., Nadeau, P. H., & Steen, O. (2009). Petroleum reservoir porosity versus depth: Influence of geological age. *AAPG Bulletin*, 93(10), 1281–2196.
- Jelmert, T. A., & Vik, S. A. (1996). Analytic solution to the non-linear diffusion equation for fluids of constant compressibility. *Petroleum Science & Engineering*, 14, 231–233. <http://dx.doi.org/0920-4105/96>.
- Lee, J., Rollins, J. B., & Spivey, J. P. (2003). *Pressure transient testing in wells* (Vol. 9, pp. 1–9). Richardson, TX: Monograph Series, SPE.
- Marshall, S. L. (2009). Nonlinear pressure diffusion in flow of compressible liquids through porous media. *Transport in Porous Media*, 77, 431–446. <https://doi.org/10.1007/s11242-008-9275-z>.
- Matthews, C. S., & Russell, D. G. (1967). *Pressure buildup and flow tests in wells* (Vol. 1, pp. 4–9). Richardson, TX: Monograph Series, SPE.
- Muskat, M. (1945). *Flow of homogeneous fluids through porous media* (2nd ed., p. 145). Ann Arbor, MI: J.W. Edwards.
- Nelson, R. (2001). *Geologic analysis of naturally fractured reservoirs* (2nd ed.). New York: Gulf Professional Publishing, BP-Amoco.
- Odeh, A. S., & Babu, D. K. (1988). *Comparasion of solutions of the nonlinear and linearized diffusion equations* (pp. 1202–1206). SPE Reservoir Engineering, SPE 17270.
- Pedrosa, O. A., Jr. (1986). Pressure Transient Response in Stress-Sensitive Formations, paper SPE 15115, presented at the SPE Regional Meeting, Oakland, April 2–4.
- Samaniego, F. V., Brigham, W. E., & Miller, F. G. (1979, June). Performance-prediction procedure for transient flow of fluids through pressure-sensitive formations. *Journal of Petroleum Technology*, 779–786.
- Tong, D.-K., & Wang, R.-H. (2005). Exact solution of pressure transient model or fluid flow in fractal reservoir including a quadratic gradient term. *Energy Sources*, 27, 1205–1215.

Chapter 6

Westergaard's Solution Applied to Carbonate Reservoirs



A tectonic fracture is associated to stresses concentration. Carbonate rocks usually have a history involving mechanical, thermal and chemical actions during millions of years. Fracture mechanics have been used successfully to predict fracture initiation that have regarding structures design using metallic materials. Nevertheless, fracture mechanics, with certain modifications, is a important tool for solving rock mechanics engineering problem.

The limestone rocks include discontinuities such as fault and tectonic fractures, that can be reactivated by tectonism, and/or by man-induced activities during oil production in carbonate reservoirs.

Geometrically, a tectonic fracture can be considered as an elongated elliptical discontinuity; namely, a deformed ellipse. Westergaard's solution is developed in this chapter for uniform biaxial stress σ , with a central fracture of length $2a$. See Fig. 6.1.

A proposed rectangular geometry for natural fractures could derive in a mathematical problem due to rectangle vertex. Namely, derivative function no exist in vertical direction.

6.1 Westergaard's Solution

Westergaard proposed that

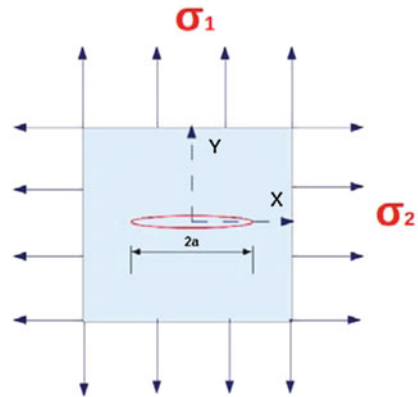
$$\Phi(z) = Re\bar{\phi}(z) + yIm\bar{\phi}(z) \quad (6.1)$$

is a solution to the fracture or the crack problem,

where

$\Phi(z)$: is a harmonic and analytical function in complex variable,

Fig. 6.1 Westergaard's model



$\phi(z)$: another analytical function containing in harmonic function $\Phi(z)$.

So, $Re\bar{\phi}(z)$ and $yIm\bar{\phi}$ are harmonics function. $\Phi(z)$ must satisfy the biharmonic equation or Laplace's equation $\nabla^2\Phi(z) = 0$.

Denoting by $\phi'(z)$ and $\phi''(z)$ the first and second derivatives of $\phi(z)$, and the first and second integrals with respect to z by $\bar{\phi}(z)$ and $\bar{\bar{\phi}}(z)$ respectively; and considering $\partial f(z)/\partial x = f'(z)$ and $\partial f(z)/\partial y = if'(z)$, it is convenient to use the Cauchy-Riemann equations to demonstrate that $\Phi(z)$, is a harmonic function. Analytical function, $\phi(z)$, satisfies harmonic function in complex plane because it is related to real and imaginary plane. Cauchy-Riemann equations are as follows:

$$\frac{\partial(Im)}{\partial x} = -\frac{\partial(Re)}{\partial y};$$

$$\frac{\partial(Re)}{\partial x} = \left(\frac{\partial(Im)}{\partial y}\right).$$

6.1.1 Airy Stress Function

In an elasticity problem we seek a function which can satisfy both the equilibrium and the compatibility equations. Airy (Timoshenko 1951) has shown that we can define such a function $\Phi(z)$ as:

$$\sigma_{yy} = \frac{\partial^2\Phi}{\partial x^2}; \tag{6.2}$$

$$\sigma_{xx} = \frac{\partial^2\Phi}{\partial y^2}; \tag{6.3}$$

$$\sigma_{xy} = \sigma_{yx} = -\frac{\partial^2 \Phi}{\partial x \partial y}. \quad (6.4)$$

If the system is linear and elastic, the compatibility equation further requires that $\Phi(z)$ be reduced to:

$$\nabla^2(\nabla^2 \Phi(z)) \equiv \left(\frac{\partial^2}{\partial x^2} + \frac{\partial^2}{\partial y^2} \right) \left(\frac{\partial^2 \Phi}{\partial x^2} + \frac{\partial^2 \Phi}{\partial y^2} \right) = \frac{\partial^4 \Phi}{\partial x^4} + 2 \frac{\partial^4 \Phi}{\partial x^2 \partial y^2} + \frac{\partial^4 \Phi}{\partial y^4} = 0,$$

to satisfy Laplace equation, where ∇^2 is the Laplace operator. The solution is related to a harmonic function.

$$\sigma_{yy} = \frac{\partial^2 \Phi}{\partial x^2} = \frac{\partial}{\partial x} \left(\frac{\partial \Phi}{\partial x} \right) = \operatorname{Re} \phi(z) + y \operatorname{Im} \phi'(z), \quad (6.5)$$

$$\sigma_{xx} = \frac{\partial^2 \Phi}{\partial y^2} = \frac{\partial}{\partial y} \left(\frac{\partial \Phi}{\partial y} \right) = \operatorname{Re} \phi(z) - y \operatorname{Im} \phi'(z), \quad (6.6)$$

$$\sigma_{xy} = \sigma_{yx} = -\frac{\partial^2 \Phi}{\partial x \partial y} = -\frac{\partial}{\partial x} \left(\frac{\partial \Phi}{\partial y} \right) = -y \operatorname{Re} \phi'(z), \quad (6.7)$$

$$\left(\frac{\partial \Phi}{\partial x} \right) = \operatorname{Re} \bar{\phi}(z) + y \operatorname{Im} \phi(z), \quad (6.8)$$

$$\left(\frac{\partial \Phi}{\partial y} \right) = y \operatorname{Re} \phi(z), \quad (6.9)$$

Note: From a compatibility point of view, the Airy Stress Function generates a biharmonic equation. However, the analysis in Real space \mathbb{R} does not have a similar solution or application. The core of this problem in real space lays on the relationship between Stokes's Theorem, or Gauss's Theorem, and an equilibrium equation. It is necessary to satisfy the equilibrium and compatibility equations.

1. Equilibrium:

$$\frac{\partial \sigma_{xx}}{\partial x} + \frac{\partial \sigma_{xy}}{\partial y} = 0, \quad (6.10)$$

$$\frac{\partial \sigma_{yx}}{\partial x} + \frac{\partial \sigma_{yy}}{\partial y} = 0, \quad (6.11)$$

To satisfy the obtained Eqs. 6.10 and 6.11, a force balance in Cartesian coordinate was developed. The following equations are needed in complex variable;

$$\frac{\partial \sigma_{xx}}{\partial x} = \operatorname{Re} \phi'(z) - y \operatorname{Im} \phi''(z), \quad (6.12)$$

$$\frac{\partial \sigma_{xy}}{\partial x} = \frac{\partial \sigma_{yx}}{\partial x} = -y \operatorname{Re} \phi''(z), \quad (6.13)$$

$$\frac{\partial \sigma_{xy}}{\partial y} = \frac{\partial \sigma_{yx}}{\partial y} = -\operatorname{Re} \phi'(z) + y \operatorname{Im} \phi''(z), \quad (6.14)$$

$$\frac{\partial \sigma_{yy}}{\partial y} = y \operatorname{Re} \phi''(z). \quad (6.15)$$

If we substitute Eqs. 6.12, 6.13, 6.14, and 6.15 in 6.10 and 6.11:

$$\operatorname{Re} \phi'(z) - y \operatorname{Im} \phi''(z) + (-\operatorname{Re} \phi'(z) + y \operatorname{Im} \phi''(z)) = 0, \quad (6.16)$$

$$y \operatorname{Re} \phi''(z) + (-y \operatorname{Re} \phi''(z)) = 0. \quad (6.17)$$

The equilibrium conditions have been satisfied; it is important to keep in mind that these conditions are an expression of the Stokes theorem.

2. Compatibility conditions: these conditions are used to analyze deformations. For this case the surface of interest is a vertical plane stress. In strain plane, displacements are given by

$$2Gu = -\frac{\partial \Phi}{\partial x} + \frac{4}{1+\nu} p, \quad (6.18)$$

$$2Gv = -\frac{\partial \Phi}{\partial y} + \frac{4}{1+\nu} q, \quad (6.19)$$

$$p = \frac{1}{2} \operatorname{Re} \bar{\phi}(z), \quad (6.20)$$

$$q = \frac{1}{2} \operatorname{Im} \bar{\phi}(z). \quad (6.21)$$

where

- v : displacement in the vertical y direction.
- p, q : complex variables obtained after integration.
- u : displacement in the horizontal x direction.
- G : shear modulus, $G = E/2(1 + \nu)$
- E : Young modulus.
- ν : Poisson's ratio.

Equations 6.18, 6.19, 6.20 and 6.21 allow the estimation of u and v when ϕ is known. However, it is necessary to find $P = \nabla^2 \phi$. We require to determinate complex conjugate, Q , using Cauchy-Riemann conditions, and considerer $f(z) = P + iQ$. Integrating, we can obtained p and q in complex space \mathbb{C} .

Substituting Eqs. 6.5 and 6.17 in Eq. 6.15, we obtain:

$$2Gu = \frac{Re\bar{\phi}(z)(1-\nu)}{1+\nu} - yIm\phi(z) \quad (6.22)$$

and defining an average with $\bar{\nu} = \nu/1-\nu$, finally

$$2Gu = (1-2\nu)Re\bar{\phi}(z) - yIm\phi(z) \quad (6.23)$$

Now, substituting Eqs. 6.6 and 6.18 in Eq. 6.16 and doing an analogous way as in Eq. 6.22:

$$2Gv = -yRe\phi(z) + \frac{2}{1+\nu}Im\bar{\phi}(z) \quad (6.24)$$

and doing an average with $\bar{\nu} = \nu/1-\nu$ finally

$$2Gv = -yRe\phi(z) + 2(1-\nu)Im\bar{\phi}(z) \quad (6.25)$$

Note

Our goal is to find an analytical expression that describes the displacements in the vertical and horizontal directions, that should be symmetrical with respect to the x -axis, because as already stated tectonic fractures are horizontal.

6.1.2 Displacement in the Horizontal Direction, u

Substituting $y = 0$ into Eq. 6.23

$$2Gu = (1-2\nu)Re\bar{\phi}(z), \quad (6.26)$$

$$\sigma_{yy} = Re\phi(z), \quad (6.27)$$

$$\sigma_{xx} = Re\phi(z), \quad (6.28)$$

$$\sigma_{xy} = \sigma_{yx} = 0, \quad (6.29)$$

Considering, $G = E/2(1+\nu)$ and substituting into Eq. 6.26:

$$u = \frac{(1-2\nu)(1+\nu)Re\bar{\phi}(z)}{E} \quad (6.30)$$

6.1.3 Displacement in the Vertical Direction, v

Substituting $y = 0$ into Eq. 6.25

$$2Gv = 2(1 - \nu)Im\bar{\phi}(z), \quad (6.31)$$

$$\sigma_{yy} = Re\phi(z), \quad (6.32)$$

$$\sigma_{xx} = Re\phi(z), \quad (6.33)$$

$$\sigma_{xy} = \sigma_{yx} = 0, \quad (6.34)$$

Substituting the expression for G in Eq. 6.31:

$$v = \frac{2(1 - \nu^2)Im\bar{\phi}(z)}{E} \quad (6.35)$$

Equations 6.30 and 6.35 can be followed in Westergaard (1939), De Vedia (1986), Sih (1966), and Saouma (2000).

6.2 Westergaard's Application for Tectonic Fractures

Horizontal natural fractures could close during reservoir depletion due to overburden see Fig. 6.2. Moreover, this specific application has three aspects: $\sigma_{xx} = \sigma_{yy}$, $\sigma_{xy} = 0$, and $y = 0$, which they implicate that there are symmetry with respect to x -axis, stress field in 2D is uniform (hydrostatic test), and normal stresses are considered. The Laplace (bi-harmonic), compatibility and equilibrium equations are considered in the plane state of stress (x, y) and deformation (u, v).

The Anderson's classification scheme for relative stresses magnitudes in normal, strike-slip and reverse faulting Fig. 6.3 based on his faulting theory. This faulting theory limits the magnitudes of the three principal stresses at any depth by the strength of the crust at depth. The Westergaard's application can be used for normal, and reverse or thrust regimes.

Pore fluid pressure and vertical effective stress should support overburden pressure to keep open fractures in a normal regime of stresses. This state is related to the concept of effective stress, which is the difference between overburden pressure and pore pressure (Terzaghi 1923). Compaction disequilibrium; namely, the reduction of pore fluid pressure and overburden weight will result in the closing of horizontal fractures in the reservoir (Fig. 6.2).

The mathematical flow problem is to find and propose an analytical function $f(x)$ that describe would equilibrium stresses through following conditions:

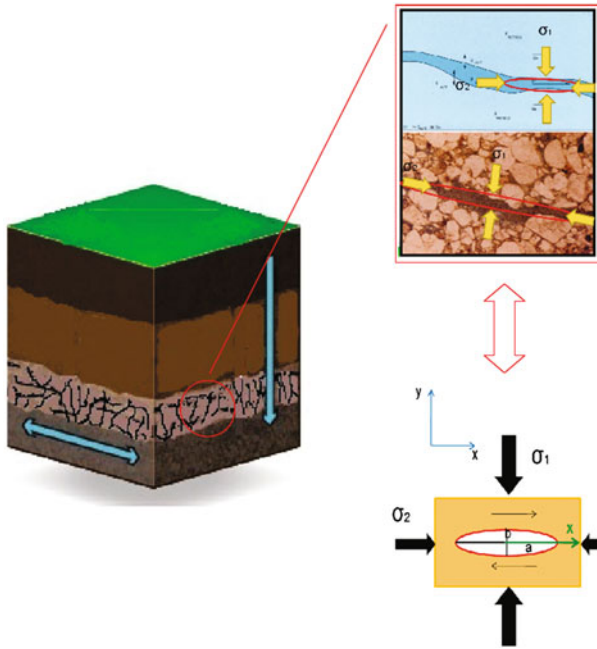


Fig. 6.2 Effect of overburden during reservoir depletion

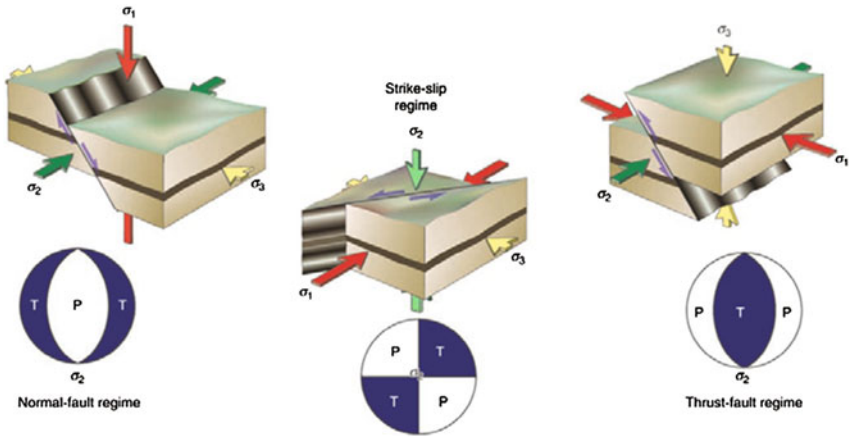


Fig. 6.3 E. M. Anderson's classification. (Fossen 2010)

1. $y = 0 \Rightarrow \sigma_{yy} = 0$ for $-a \leq x \leq a$
2. $\lim_{x \rightarrow \infty} f(x) = \sigma$ for $-a \leq x \leq a$

In consequence, the proposed analytic function $f(x)$ is given by:

$$f(x) = \frac{\sigma}{(1 - a^2/x^2)^{0.5}}, \quad (6.36)$$

Applying conditions.

If $f(x) = 0$ then $\sigma = 0$ and $\sigma_{yy} = \sigma = 0$. This is a initial condition.

Now, if $x \rightarrow \infty$ then $f(x) = \sigma$. Namely, the fracture is elongated and closed, and Eq. 6.36 can be rewritten:

$$\sigma_{yy} = \frac{\sigma}{(1 - a^2/x^2)^{0.5}}, \quad (6.37)$$

if $x = z$, then our expression is given by

$$\phi(z) = \frac{\sigma}{(1 - a^2/z^2)^{0.5}}, \quad (6.38)$$

Displacement v is changing, then the ellipse should be symmetrical with respect to x -axis, and this displacement is given by Eq. 6.35. Additionally, Eq. 6.35 requires to estimate $\bar{\phi}(z)$:

$$\bar{\phi}(z) = \int \frac{\sigma}{(1 - a^2/z^2)^{0.5}} dz = \int \frac{z\sigma}{(z - a^2)^{0.5}} dz$$

Applying integration by trigonometric substitution, and by parts

$$\bar{\phi}(z) = \sigma \left[z \operatorname{acosh} \left(\frac{z}{a} - a \left(\frac{z}{a} \right) \operatorname{acosh} \left(\frac{z}{a} \right) + a \sqrt{\left(\frac{z}{a} \right)^2 - 1} \right) \right] = \sigma \sqrt{z^2 - a^2}, \quad (6.39)$$

substituting Eq. 6.39 in Eq. 6.35, analyzing conditions, and considering a finite fracture of length $2a$:

$$v = \frac{2(1 - \nu^2)\sigma\sqrt{a^2 - x^2}}{E} \quad (6.40)$$

If $x = \pm a$, then $v = 0$. However, $x^2 > a^2$ then v would be a complex number, and this should be a displacement in real space. Moreover, square of Eq. 6.40:

$$v^2 = \left(\frac{2(1 - \nu^2)\sigma}{E} \right)^2 (a^2 - x^2) \quad (6.41)$$

Equation 6.41 represents an ellipse, which E and ν are intrinsic parameters of limestone rock, and σ requires to be uniform to keep the fracture open. Equation 6.41 can be rewritten as

$$\frac{v^2}{cte^2} + \frac{x^2}{l^2} = a^2 \quad (6.42)$$

where $cte = 2(1 - \nu^2)\sigma/E$. Up to this point we have discussed the Westergaard's solution.

6.3 Westergaard's Solution Applied to a Limestone Reservoir with Tectonic Fractures

The objective of this application is to determine fracture collapse conditions, considering mechanical properties and fluid pressure. Different geological and dynamic features of field will be described.

6.3.1 Field Geological Aspects

The Complejo Antonio J. Bermúdez (CAJB) is located in Cunduacán and Centro towns, Estado de Tabasco, México, some 20 km north-east of Villahermosa city. Figure 6.4 shows its location. Antonio J. Bermúdez is conformed by Carrizo, Cunduacán, Íride, Oxiacaque, Platanal, and Samaria fields (CNH 2013).

The CAJB fields are a chain of structures with salt intrusion, and strongly folded. These mature fields are separated by normal, strike-slip, and reverse faults, creating blocks with different lithologic characteristics, but hydraulically interconnected.

Hydrocarbons accumulation is limited by low permeability zone (0.001–0.1 md) in the north, a gas-oil contact in the north-east, a water-oil contact in the south and the west, a in the east for a normal fault with direction north-south, see Figs. 6.5¹ and 6.6. Figure 6.5 shows salt that yielded complex faults system, indicating strong regional and local stresses, which can be observed in the 3D structure presented in Fig. 6.6.

Fields conform a tectonic carbonate reservoir with black oils (20–31° API gravity); initial pressure was 533 kg/cm² (7581.06 psi), and saturation pressure 319 kg/cm² (4537.24 psi) (Fong et al. 2005).

So that, CAJB is a complicated limestone reservoir due to presence of salt domes, faults, and tectonic fractures.

In 1974, Madrigal reported the presence of salt that influenced folding and faulting. In Samaria and Cunduacán fields, salt does not penetrate limestone layers, forming domes structures affected by normal and slike-slip faults; namely, there was a

¹Authorized by field manager for academic objectives.

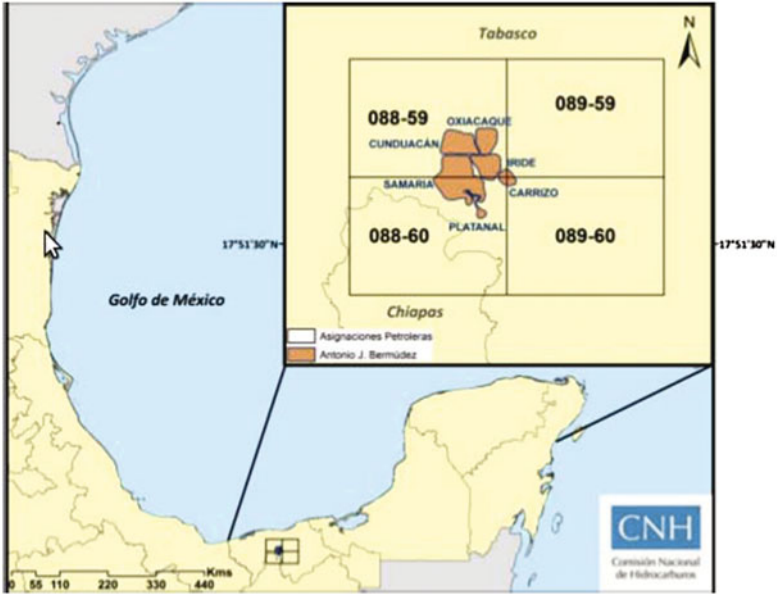


Fig. 6.4 Complejo Antonio J. Bermúdez geographic location (CNH 2013)

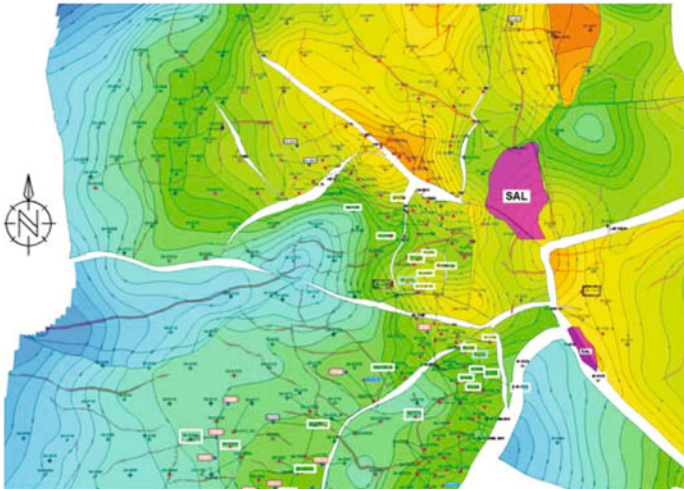


Fig. 6.5 CAJB structural contour map on top of Late Cretaceous

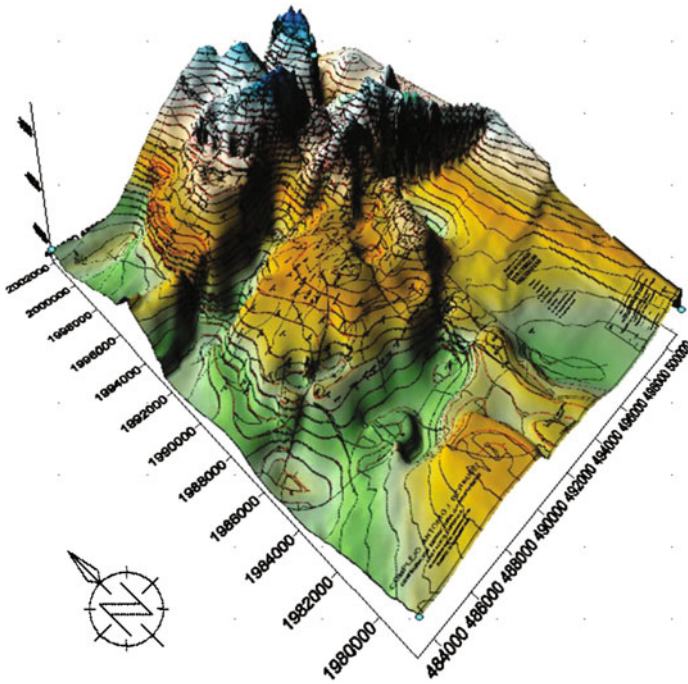


Fig. 6.6 3D structural contour of the Complejo J. Bermúdez on top of Late Cretaceous

limestone layers deformation (Madrigal 1974). In consequence, changes and reduction of thickness can be observed in each well that indicate the presence of salt and its effects Fig. 6.7 shows this reduction of thickness.

Structural properties of an active diapirs are (Yin and Groshong 2007):

- Active diapirs are circular or elliptical in map view.
- Active diapirs rise above the surrounding area.
- Active domes have few faults in the early stage, and many fault in the late stage.
- The overburden strata above active diapirs are ruptured by radial normal faults.

Mentioned properties can be observed in the Fig. 6.8.

When Fig. 6.5 is compared with Fig. 6.8, it observed some similarities due to the presence of salt domes in the Complejo Antonio J. Bermúdez.

An application will be developed for a single fracture model. Also, a fracture network can be considered. A recommendation for the Complejo Antonio J. Bermúdez was the development of a fracture model (CNH 2013).

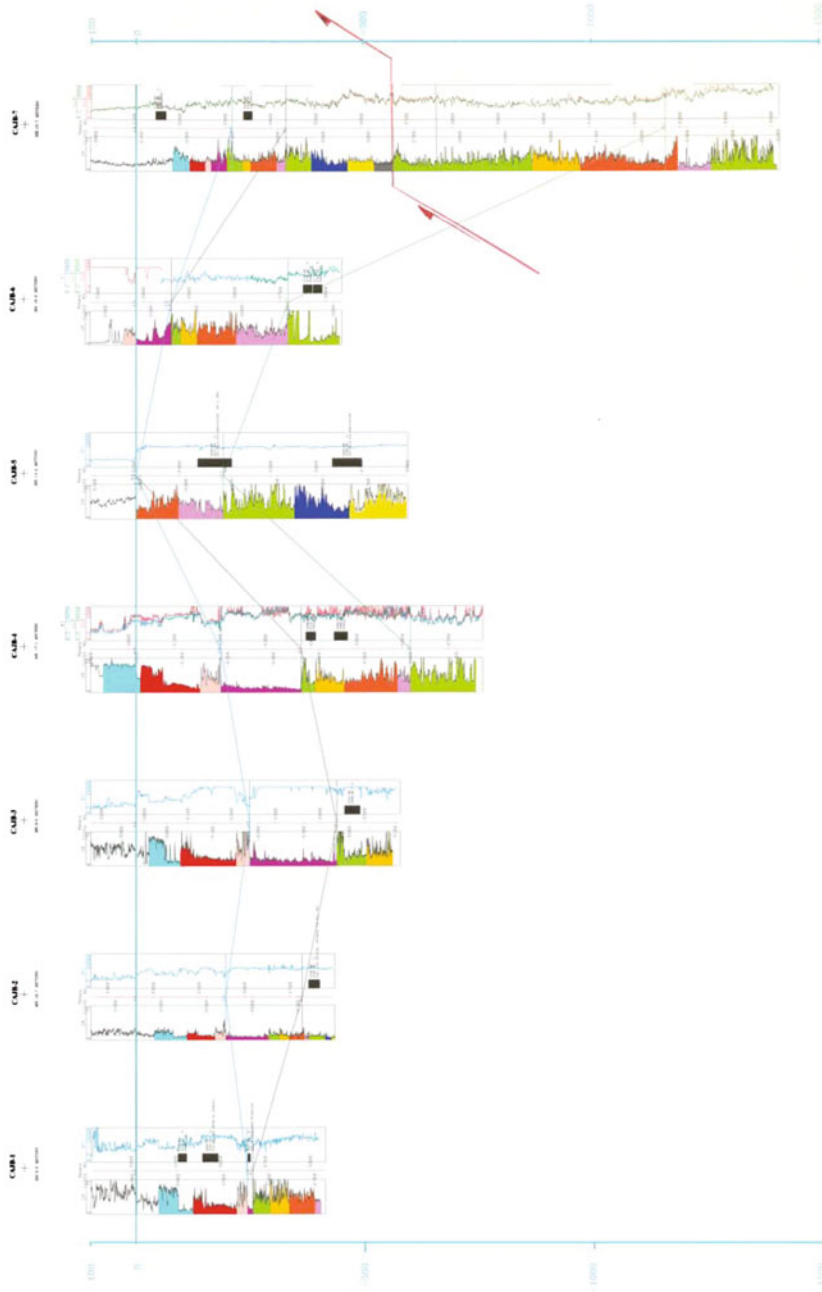


Fig. 6.7 Thickness change in wells of CAJB

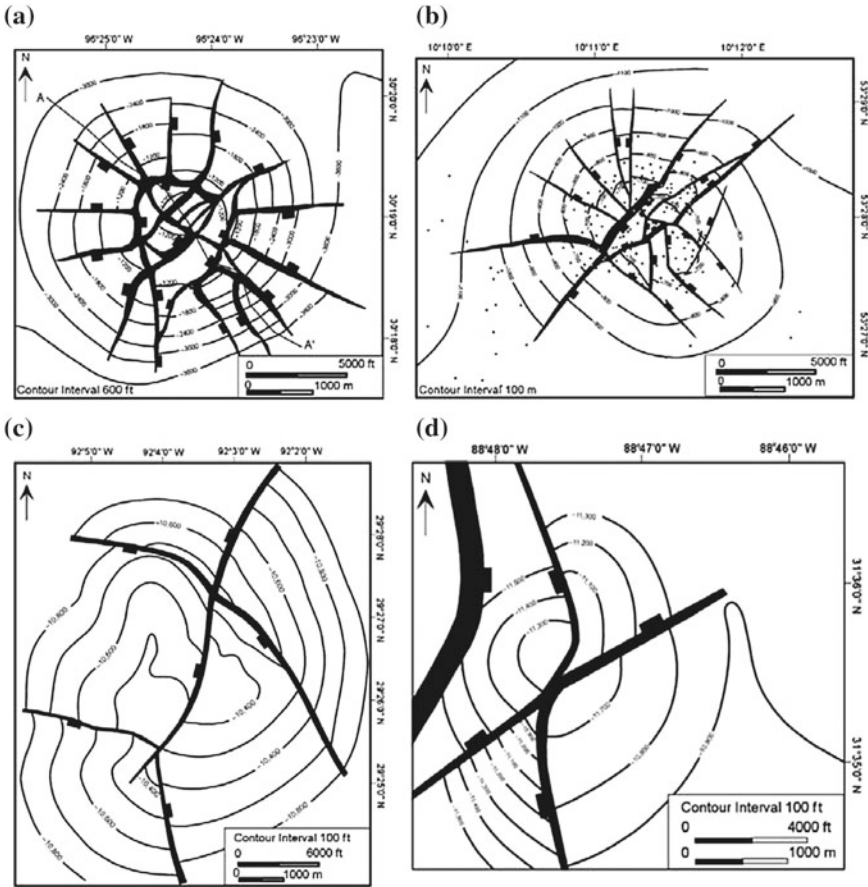


Fig. 6.8 Structure contour maps of representative active salt domes. Latitudes and longitudes of maps in this and the figures, except the Reitbrook dome, are derived from Lat-Long Services (2006). **a** Clay Creek dome, Texas, showing normal faults and contours on top of the Wilcox Formation (from McDowell 1951). **b** Reitbrook dome, Germany, showing normal faults and contours on the base of the Tertiary (from Schmitz and Flixeder 1993, with kind permission of Springer Science and Business Media). **c** Tiger Shoal dome, Louisiana, showing normal faults and contours on the top of T sand (from Smith et al. 1988; reprinted with permission from the New Orleans Geological Society). **d** West Clara dome, Mississippi, showing normal faults and contours on the base of the Ferry Lake anhydrite (from Davis and Lambert 1963; reprinted with permission from the Mississippi Geological Society) (After Yin and Groshong 2007, Fig. 1, p. 346.) This figure is taken from Yin and Groshong. McDowell, Schmitz and Flixeder, and Smith are authors and references than have included and modified. On the other hand, Lat-Long Services (2006) is a program and company

6.3.2 *Paleontological Description*

Paleontological studies on the² north, eastern and southern of the CAJB were done, where profitable hydrocarbon occurrences are discovered in the seventies of the last century.

In the CAJB, planktonic foraminifera, undifferentiated fragments, and microfauna are observed.

Planktonic foraminifera as *Globotruncanita stuartiformis*, *Globotruncana ventricosa*, *Pseudotextularia cf nuttalli*, *Pseudotextularia sp.*, *Cotosotruncana sp.*, *Globigerinelloides sp.*, *Globotruncana sp.*, and *Globotruncanita sp.* are generally common in the Late Cretaceous to Campanian-Maastrichtian age.

On the other hand, the presence of planktonic foraminifera such as *Globotruncanita stuartiformis*, *Globotruncanita cf stuarti*, *Radotruncana calacarata*, *Globotruncana sp.*, *Globotruncanita sp.*, and axial and subaxial cut of *Sulcoperculina sp* (benthonic foraminifera) indicates microfauna late Campanian.

Microfauna such as *Marginotruncana undulata*, *Globotruncana bulloides*, *Marginotruncana sp.*, *Globotruncana sp.*, *Cotosotruncana cf fornicata*, and *Cotosotruncana fornicata* were observed in thin-section, indicating Late Cretaceous to Santonian age.

Undifferentiated Biogenic fragments, abundant radiolarian, and few cuts of benthonic foraminifera without identify could indicate a facies late Cretaceous.

6.3.3 *Petrography*

Petrography was³ used to document the diagenetic processes that affected the CAJB carbonates (pressure-solution seams, burial fractures and mineralization), and general burial history.

Thin-section in horizontal direction of Complejo Bermúdez limestones identified a facies type radiolarian wackstone. This type of limestone is fine-grained (mud-supported), micrit matrix (microcrystalline limestone), with more than 10% allochemes. Allochemes are circular radiolaria molds of calcite, with partially recrystallized material structures of algae. Also, there are microfractures refilled with recrystallized calcite. This is observed in Figs. 6.9 and 6.10.

In additional, a pseudostratification can be observed with calcitized microfractures, and others without calcite dyed in dark blue. In thin-section photomicrographs moderate interparticle porosity, and low intrafossilar porosity with impregnated oil have been observed. Also, micrit matrix contains black organic material Fig. 6.9.

Thin-section in vertical direction identified a microfacies (circular radiolarian mudstone-wackstone). This facies consists predominantly of micrite (grain-supported) with circular radiolaria molds of calcite impregnated oil (light brown).

²Report developed by micropaleontology personal.

³Report developed by specialized personal of petrography.

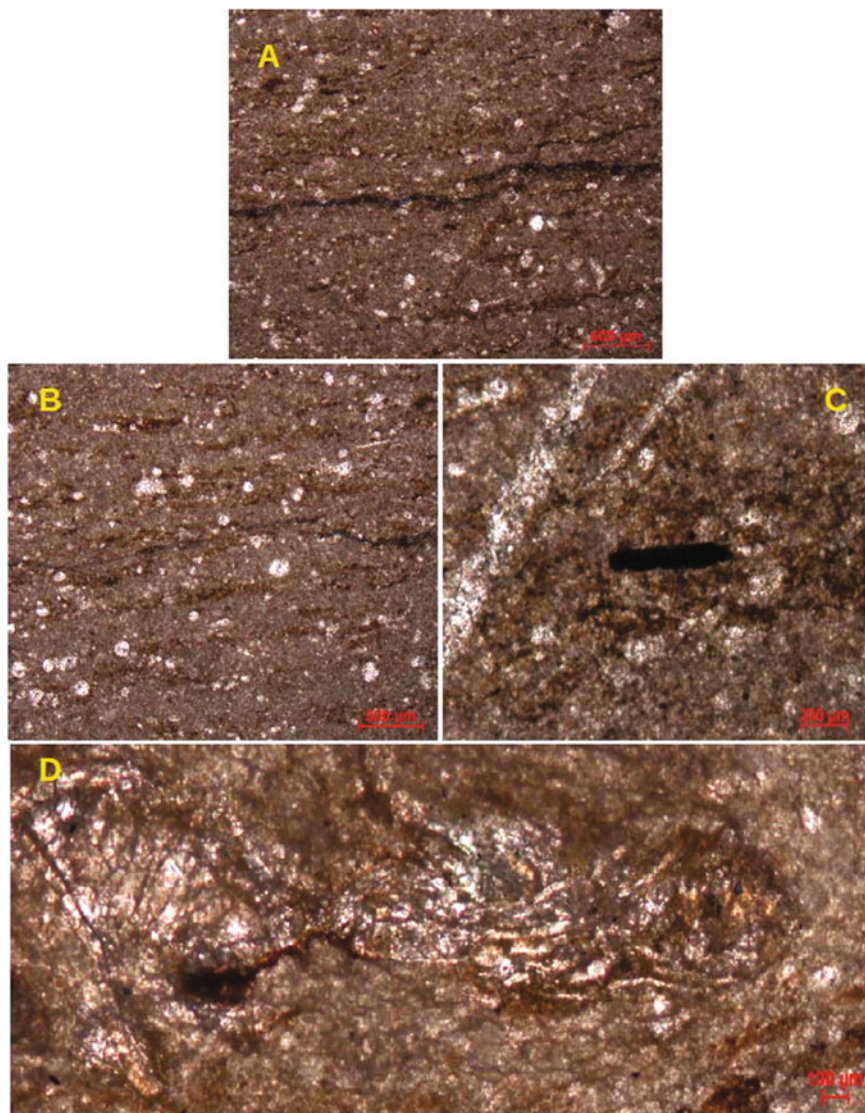


Fig. 6.9 Photomicrographs of radiolarian wackestone. **a** and **b** Discontinuous fractures without cement (dark color). Taken with parallel Nicols (2.5X). **c** Pseudostratification or interlayers of calcareous shale and oil (black color), and crystallized fracture. Taken with parallel Nicols (20X). **d** Photomosaic illustrating Algae recrystallized by calcite. Taken with parallel Nicols (2.5X)



Fig. 6.10 Photomosaic illustrating parallel continued fractures recrystallized by calcite. Taken with crossed Nicols (2.5X)

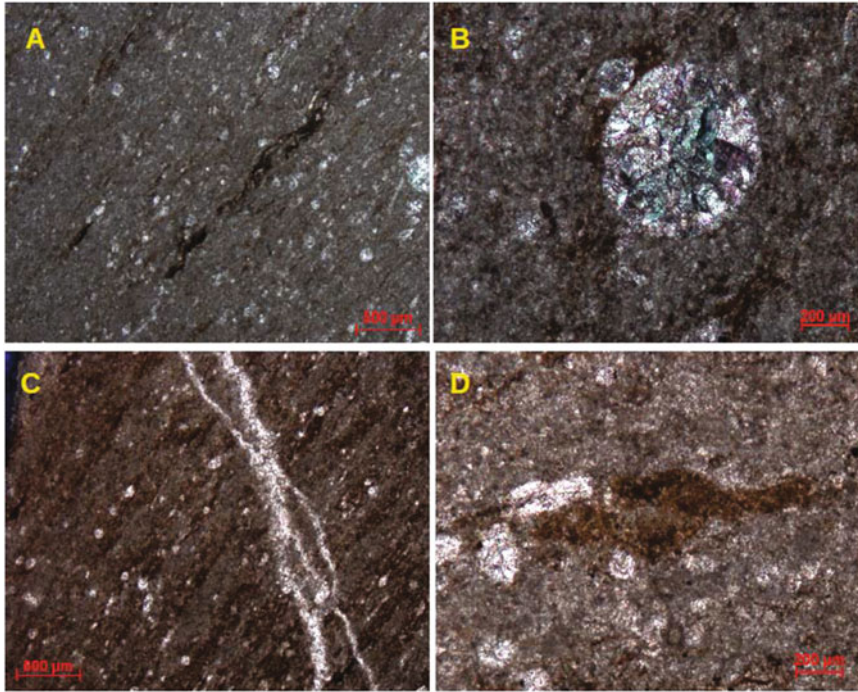


Fig. 6.11 Photomicrographs of radiolarian wackestone. **a** Micrit matrix with circular radiolarian. Taken with crossed Nicols (2.5X). **b** Radiolarian totally recrystallized. Taken with crossed Nicols (20X). **c** Alternation of brown hydrocarbon in micrit matrix and thin fractures partially cemented by calcite. Taken with crossed Nicols (2.5X). **d** Recrystallized radiolarian with impregnation of brown hydrocarbon. Taken with crossed Nicols (20X)

Although, fractures refilled by calcite cut across pseudostratification or interlayers of calcareous shale. Also, in thin-section photomicrograph is observed interparticle porosity and low intrafossilar porosity with oil. See Fig. 6.11.

Figure 6.12 delays interlayers of calcareous shale, which were crossed by thin fractures and are intercepted between them, but they are filled by crystalline calcite.

In thin-sections do not identify dolomitization process because of mineral dolomite crystallizes in the trigonal-rhombohedral system, that was not observed. It does not rapidly dissolve or effervesce (fizz) in dilute hydrochloric acid as calcite did.

There are not presence of mineral alteration and/or vugs caused by dissolution. It is possible to find stylolites, because of overburden pressure, but they can be oblique or even perpendicular to bedding, as a result of a strong tectonic activity that might occur in the CAJB.



Fig. 6.12 Photomosaic. Micrit matrix with radiolarian, and cemented fractures. Taken with crossed Nicols (2.5X)

Table 6.1 Permeabilities and porosities under 800 psi confining pressure results

Cores samples	Diameter (cm)	Length (cm)	Porosity (%)	Permeability (md)
1 (southern)	10	15.9	4.5	4.1
2 (southern)	2.539	5.248	2.9	3.1
3 (north)	2.528	4.575	0.5	0.0148
4 (north)	2.526	3.929	1.3	0.0743
5 (eastern)	2.519	5.742	5.8	2.20
6 (eastern)	2.531	3.234	7.3	0.0921

6.3.4 Permeability and Porosity

Permeabilities and⁴ porosities measures on cores samples localized the north, eastern and southern of the Complejo A. J. Bermúdez were estimated, using a poropermeameter. The values of porosities and permeabilities in samples 3 and 4 (north) are the lowest of all; although, this zone might act as seal. See Table 6.1.

Fractures and/or microfractures are not visible in cores samples, due to sample size; moreover; the absence of discontinuities implies low permeability. It will indicate that samples are matrix.

6.3.5 X-Ray Diffraction for the Identification and Analysis of Carbonates Rocks

The main objective⁵ was rock components identification and quantification. The analyzed material often has to be destructively prepared by cutting, grinding, deformation or polishing to get “homogeneous” samples. In this point, it is used X-ray diffraction (DRX) patterns.

The composition of inhomogeneous material can be possible by a non-destructive analysis; namely, can be estimated by X-ray fluorescence (FDRX). Major elements composition (oxides) were obtained X-ray fluorescence spectrometer.

Six limestone samples were prepared for whole rock mineralogy following standard X-ray diffraction procedures (Hardy and Tucker 1988). The powder samples were scanned from 4–80°, scattering angle (degrees) 2θ , and different values of intensity L in (counts) were obtained.

⁴Report developed by specialized petrophysicists.

⁵Report developed by specialized personal in X-ray diffraction and combinatorial catalysis.

Table 6.2 Oxides quantification in carbonates rocks samples

Samples	CaO (wt.%)	SiO ₂ (wt.%)	SO ₃ (wt.%)	SrO (wt.%)	Fe ₂ O ₃ (wt.%)	Al ₂ O ₃ (wt.%)	MgO (wt.%)
1 (southern)	97.06	2.13	0.42	0.24	0.15	–	–
2 (southern)	95.83	3.74	0.21	0.17	0.05	–	–
3 (north)	93.78	5.37	0.45	0.22	0.18	–	–
4 (north)	93.93	5.21	0.39	0.25	0.22	–	–
5 (eastern)	93.73	5.13	–	–	0.31	0.83	–
6 (eastern)	93.62	5.04	–	–	0.36	0.98	–

Trace and oxides compositions were determined, according to standard analytical procedures suggested in laboratory (Oxides-Helio method), quantifying oxides like silicon dioxide (SiO₂), magnesium oxide (MgO), iron oxide (Fe₂O₃), strontium oxide (SrO), aluminium oxide (Al₂O₃), sulfur trioxide (SO₃), and calcium oxide (CaO). The analytical accuracy error of trace elements was better than $\pm 6\%$.

Table 6.2 presents large variations in CaO (93.62–97.06%), and SiO₂ (2.13–5.04%), whereas small variations in SrO (0.17–0.24%) are observed. Fe₂O₃ content in all samples varies from 0.15 to 0.36%. The contents of SO₃ and Al₂O₃ are very low in carbonate samples. In contrast, MgO was not observed in rock samples. The low concentration of SrO content indicates that, the precursor limestone had undergone considerable diagenesis which resulted in SrO depletion. The available source of Al₂O₃ may be associated fine grained siliciclastic-rich sediments that supply valuable amount of Fe and Al.

The source of magnesium oxide could be observed in calcium magnesium carbonates. The absence of MgO may indicate that all rock samples are limestones. Many dolomites are formed due to the replacement of pre-existing CaCO₃ (calcite and aragonite minerals) or altered during diagenesis. Moreover, Sr depletion indicates diagenesis process. According to X-ray diffractograms presented in Figs. 6.13 and 6.14 this alteration process did not occur in these rocks samples; moreover, the process of dolomitization in the Complex J. A. Bermúdez can not be excluded because dolomite is related to diagenesis.

Figure 6.13 displays quartz crystals SiO₂ (hexagonal quartz syn), and calcite Ca(CO₃). On the other hand, Fig. 6.14 presents two configurations quartz crystals (hexagonal quartz syn and hexagonal quartz), calcite, and iron oxide.

The clastic and carbonate percentages were calculated using the quartz, iron oxide, and calcite peaks in the X-ray diffractograms, and results are shown in Table 6.3.

Note

We compared thin-sections petrography and X-ray diffractions for the quantification and identification of carbonate rocks composition. Results exhibit similar minerals as calcite and quartz. There are not discrepancy between thin-section and X-ray results.

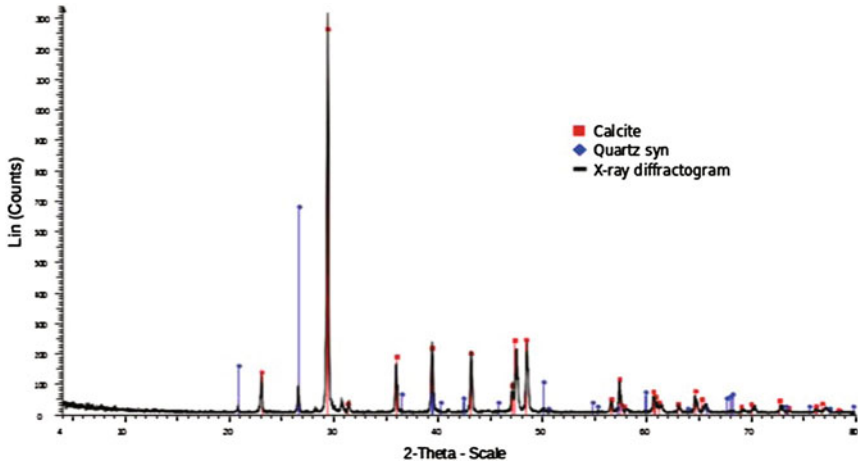


Fig. 6.13 X-ray diffraction 1 southern sample

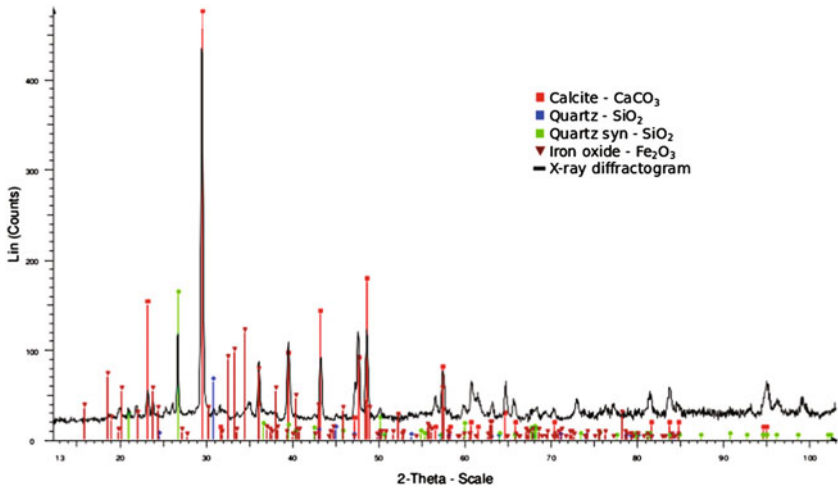


Fig. 6.14 X-ray diffraction 1 north sample

Table 6.3 Content of calcite, quartz and others elements in samples

Samples	Ca(CO ₃) (wt. %)	SiO ₂ (wt. %)	Others (wt. %)
1 (southern)	93.75	5.02	1.23
2 (southern)	96.48	2.12	1.40
3 (north)	95.83	3.37	0.80
4 (north)	94.93	4.19	0.88
5 (eastern)	96.73	3.13	0.14
6 (eastern)	96.62	3.04	0.34

Also, these procedures show that dolomite is not present in these samples; although, will be inappropriate to argue that there is only calcite in the CAJB.

6.3.6 *Computed Tomography, CT*

Tomography was used to show the internal fractures and micro-fractures and to verify their geometry and morphology. Useful, calcareous cores without dissolutions or visible discontinuities, are considered as matrix rock without fractures. Narrow subplanar fractures can be observed, if the density in the core internal structure shows changes.

A sample cored in a carbonate reservoir (15.9 cm in length and 10 cm in diameter) was obtained. Figure 6.15 displays the scan of a limestone core at 3 mm spacing, showing narrow subplanar fractures. They are open, deformed and/or mineral-filled. In images 16 to 21 an open fracture with great aperture can be observed, and in images 30 to 42 there are others fractures with small aperture. Moreover, a visual inspection of the core does not show any fractures that may be connected (see slides 30 to 53 in Fig. 6.15). Approximately, these limited length fractures have 1 to 2 mm apertures and would allow hydrocarbons flow; in effect they also provide effective porosity because fracture connects spaces in this rock. Dissolutions as vugs and caverns are not present in these samples.

There are many factors that dominate the rate-transient and production behavior of NFCR, such as fracture conductivities, dip angles, lengths, and discontinuities distribution, as well as whether or not discontinuities intersect between them. The CT showed that planar discontinuities do not intersect.

6.3.7 *Fluid Pore Pressure*

Figure 6.16 exhibits a pressure depletion pattern not like the harmonic function. Also, it shows a similar trend between distinct fields (Samaria, Íride, Platanal, Cunduacan, and Oxiacaque), with initial pressure of CAJB was 540 kgf/cm^2 (7680.60 psi), and its depletion rate is 6 kgf/cm^2 (85.34 psi) per year, its bubblepoint pressure is 318.50 kgf/cm^2 (4530.13 psi) (Fong et al. 2005).

These fields present gravity segregation gas caps, and a strong natural aquifer support. In consequence, wells produce water along with oil. The CAJB contains more than 8 billion bbl of original oil in place (OOIP). Cumulative production is 2850 MMbbls de aceite, and recovery factor is approximately 35%. Wells with an average measured depth of 4500 m (14763.78 ft). The gross thickness is 800 m (2624.67 ft) of limestone (Guerrero and Mandujano 2014).

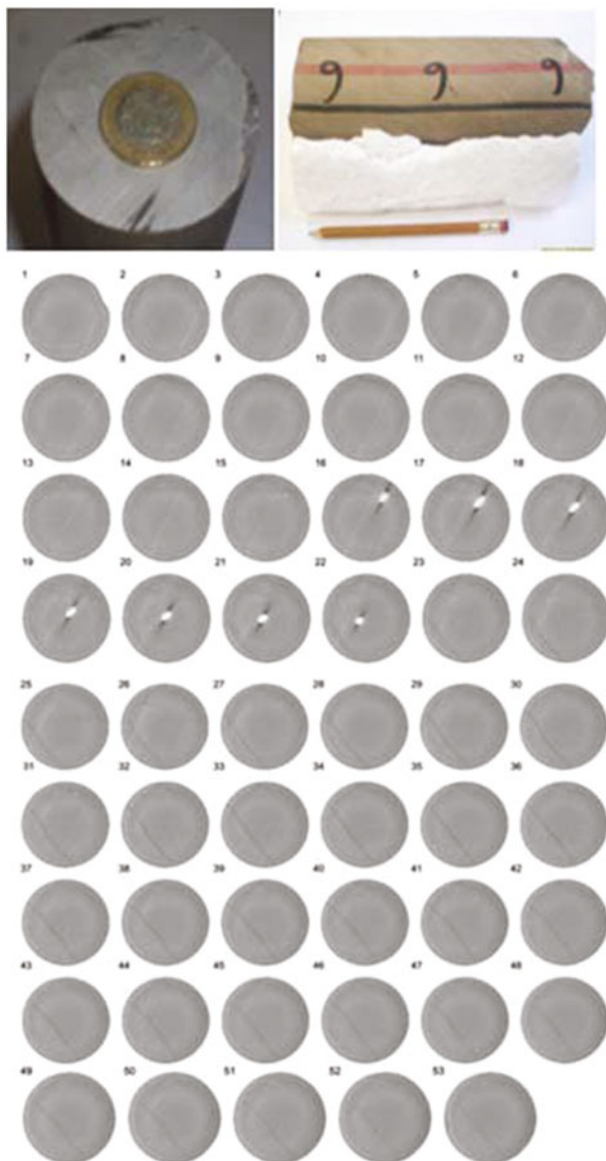


Fig. 6.15 Scan of limestone core, with dark shading associated to low density and white to high density regions with evident macroscopic fractures. Early Cretaceous, Complejo A. J. Bermúdez, Samaria-Luna Region, Tabasco. Mexico

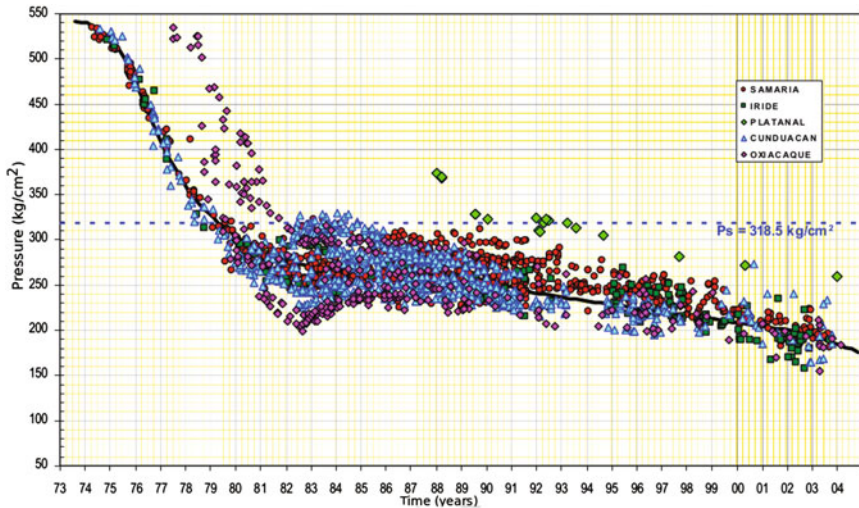


Fig. 6.16 Pressure behavior of CAJB

6.4 Carbonate Rock Mechanical Properties

The carbonate rock mechanical properties depend on its mineral composition, the arrangement of the grains, discontinuities, and geological history. The surfaces of fractures are influenced by the stresses distribution and mechanical properties. Aperture is associated with local displacement, where substantial nonlinearity is confined within a linear-elastic field surrounding the fracture. Consequently, significant mechanical parameters (Young's modulus and Poisson's ratio) of linear-elastic fractures are determined to apply Westergaard's solution.

Fracture collapse can be described insofar as overburden stress (σ_1), and pore pressure may be calculated. A tectonic fracture is both fluid dynamic and mechanical discontinuity. A reduction of the pore pressure will increase the effective stress, and cause the reservoir strain. The fractures permeabilities change due to generated strain field, affecting the balance between the viscous and capillary forces (changed capillary entry pressures) in the fracture.

A saturated porous rock with oil will show poroelastic behavior. Moreover, the formation behaves elastically to the stress level at which it yields and then deforms plastically without limit. In principle, this poroelastic behavior occurs when a strength of materials approach assumes that rock deformation will be elastic until the point of failure.

6.4.1 Overburden Stress, S_v

The magnitude of the overburden stress, S_v , is reliably obtained by integration of rock densities from surface to the depth of interest h (Zoback 2007), using the density log. The reservoir has to carry the weight of the overlying formations. Overburden stress is estimated from Eq. 6.43 as

$$S_v = \int_0^h \rho(h)gdh \approx \bar{\rho}gh \tag{6.43}$$

where $\rho(h)$ is the density as a function of depth, g is gravitational acceleration and $\bar{\rho}$ is the mean overburden density (Jaeger and Cook 1971), with $h = 0$ corresponding to the Earth surface. Figure 6.17 shows density log (RHOB) and calculated overburden stress, using Eq. 6.43. The density log is somewhat noisy and no data are available between the surface (0 ft) and specific depth (2329 ft). So that, it is necessary to extrapolate densities to the surface where the density is approximately 1.8 g/cc (shale density). Figure 6.17 shows density log and overburden stress estimation considering extrapolated densities to the surface. Density log realistic behavior describes a nonlinear increment with respect to depth, which implies a slope change

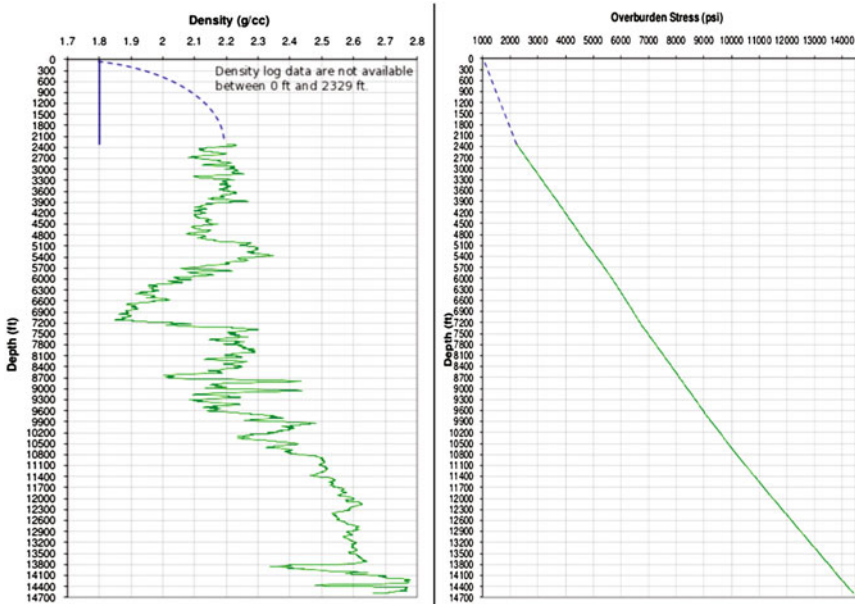


Fig. 6.17 Density log and overburden stress

in overburden stress estimate. An approximated solution consists in to assume that superficial layers are shale.

When the vertical stress dominates in normal faulting regions ($\sigma_1 \geq \sigma_2 \geq \sigma_3$), where $S_v = \sigma_1$, $S_{Hmax} = \sigma_2$, and $S_{hmin} = \sigma_3$. An upper limit for the magnitudes of the principal stresses in situ is the frictional strength of pre-existing fractures and faults.

6.4.2 *Maximum and Minimum Horizontal Stresses Magnitudes*

Reliable estimates of formation stresses are important for coupling geomechanical evaluations with reservoir flow analyses. The formation stress state is characterized by the magnitude and direction of three principal stresses, the overburden, S_v , maximum horizontal, S_{Hmax} , and minimum horizontal, S_{hmin} , stresses. Existing techniques for the estimation of horizontal stresses magnitudes include borehole breakout analysis, leak off test, mini-frac, step-rate test, and hydraulic fracturing.

Leak off test, LOT, and extended leak off test, ELOT, give a measure of the S_{Hmax} and S_{hmin} magnitudes. The S_{Hmax} magnitude is the most difficult parameter to determine, unlike S_{hmin} , which can be measured by the hydraulic fracturing and LOTs. However, there are no methods to measure S_{Hmax} directly. If the formation tensile strength, T_0 , is known it is possible to determinate S_{Hmax} , using LOTs or step-rate tests. The T_0 parameter is estimated from core tests, logs, and mini-frac ELOT; and is also employed to describe tensile failure.

The differences between LOT and ELOT are the following:

- LOT pressure is established to reach the formation breakdown pressure. ELOT pressure passes leak-off pressure and reach the formation breakdown pressure.
- ELOT performs more than one cycle to overcome the effect of T_0 while standard LOT usually performs only cycle.
- Shut-in time for LOT is 10–15 min while ELOT requires 30 min for shut-in time.

It is recommended to calculate the S_{Hmax} direction and magnitude, using mechanic damage constraints based on borehole breakouts.

Figure 6.18 shows the stages of a LOT during mud pumped in borehole. The Leak off point, LOP, is approximately equal to the least principal stress when a break-in slope is observed. If the LOP is not reached, a formation integrity test, FIT, has been developed. The peak pressure reached during a LOT or ELOT is termed the formation breakdown pressure (FBP), by which fracture propagation is unstable. After, the pumping pressure drops at the FPP (Fracture propagation pressure) that may be S_{hmin} for conditions of low tortosity and fluid viscosity. However, the FCP (Fracture closure pressure) and ISIP (Instantaneous shut-in pressure) are a better measure of the least principal stress if it is detected a change in linearity of the pressure decay during the hydraulic fracturing (Nolte and Economides 1989).

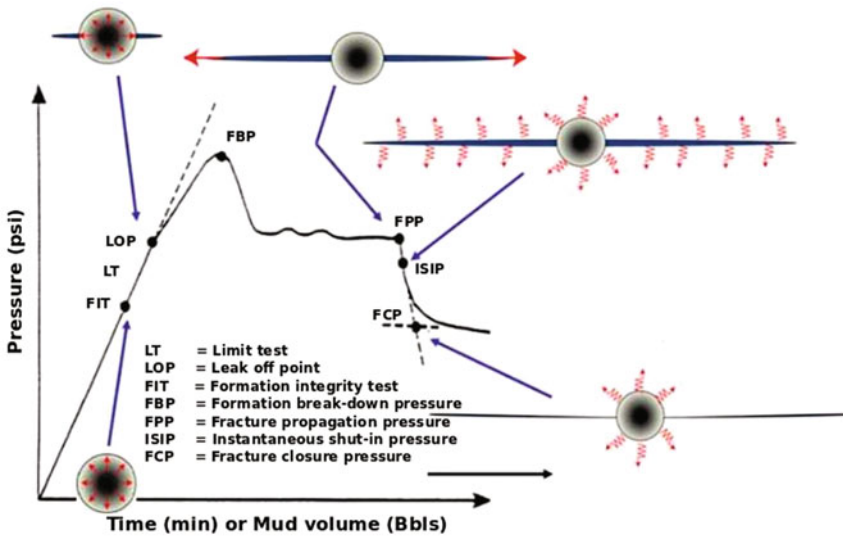


Fig. 6.18 Leak off Test (LOT). Cambridge University Press Zoback, Reservoir Geomechanics (Fig. 7.2, p. 211)

In the absence of the above described test, an approximate estimate of the horizontal stress magnitude is made using dynamic Poisson’s ratio, it may not be a reliable value because of the local stresses change and rocks lateral expansion that occur in stratigraphic layers.

Figure 6.19 shows a LOT⁶ for the CAJB at a depth of 13845 ft (4220 m). A leak off test is taken only to the LOP, which is a typical oil-field practice. Numerical data were represented on the graph to determine the minimum principal stress. Red line describes Formation Integrity Test (FIT), that indicates wellbore pressure was not sufficient to initiate a fracture of the wellbore wall, and did not exceed the minimum horizontal stress. Green line describes Leak-off point (LOP), which the fluid pressure begins its propagation through the wellbore wall, and the peak pressure reached is termed the formation breakdown pressure (FBP) and represents an unstable fracture propagation away from a wellbore. For this well, $S_{hmin} = 10223.35$ psi, with gradient of 0.74 psi/ft, and formation break-down pressure is 10321 psi.

Table 6.4⁷ displays an indirect test of tensile strength in three samples of the CAJB, with similar diameter and length. The core sample of 5 (eastern) had the highest porosity and moderate permeability between samples. Tensile strength of a material is the tension stress at which a material breaks or permanently deforms (changes shape). An average value of tensile strength was 413.06 psi in this static

⁶Numerical data were authorized by field manager for academic objectives.

⁷Data determined by specialized persona in rock mechanical properties. Class notes: Geomechanics for Petroleum Engineers.

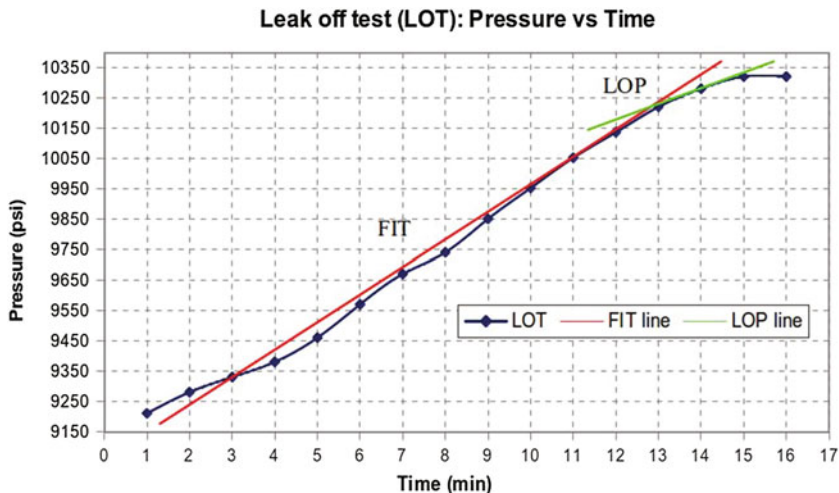


Fig. 6.19 Leak off test of the Complex Antonio J. Bermúdez

Table 6.4 Indirect test of tensile strength

Samples	Diameter (in)	Length (in)	Stress (psi)	Tensile strength (psi)
2 (southern)	1.487	1.170	765.00	280.05
4 (north)	1.486	0.893	741.00	355.58
5 (eastern)	1.486	0.918	1293.00	603.56

test. Also, Table 6.4 shows several values of tensile strength due to the presence of weak bedding planes, cracks and other heterogeneities in three samples.

For determination of S_{Hmax} can be used the following expression:

$$S_{Hmax} = 3S_{hmin} - p_b - p_p + T_0 \tag{6.44}$$

where

p_b = Formation break-down pressure

T_0 = Tensile strength

p_p = Reservoir pore pressure.

Considering that well was drilled in 1998, and substituting $p_b = 10321$ psi, $T_0 = 413.1$ psi, $(S_{hmin}) = 10223.35$ psi, and $p_p = 240 \text{ kgf/cm}^2$ (3413.6 psi), (see Fig. 6.16) in Eq. 6.44, $S_{Hmax} = 17349$ psi, while $(S_v) = 18017$ psi.

Figure 6.20 shows the overburden stress (S_v), the hydrostatic pore pressure (p_p), the minimum horizontal stress (S_{hmin}), and the maximum horizontal stress (S_{Hmax}) at depth (13845 ft), and casing points. The hydrostatic pore pressure is conventionally estimated using $p_h = 0.433 * \rho_w * h$ by which water density $\rho_w = 1.0 \text{ g/cc}$. For the estimation of the overburden stress, a shale density was used between 0 and

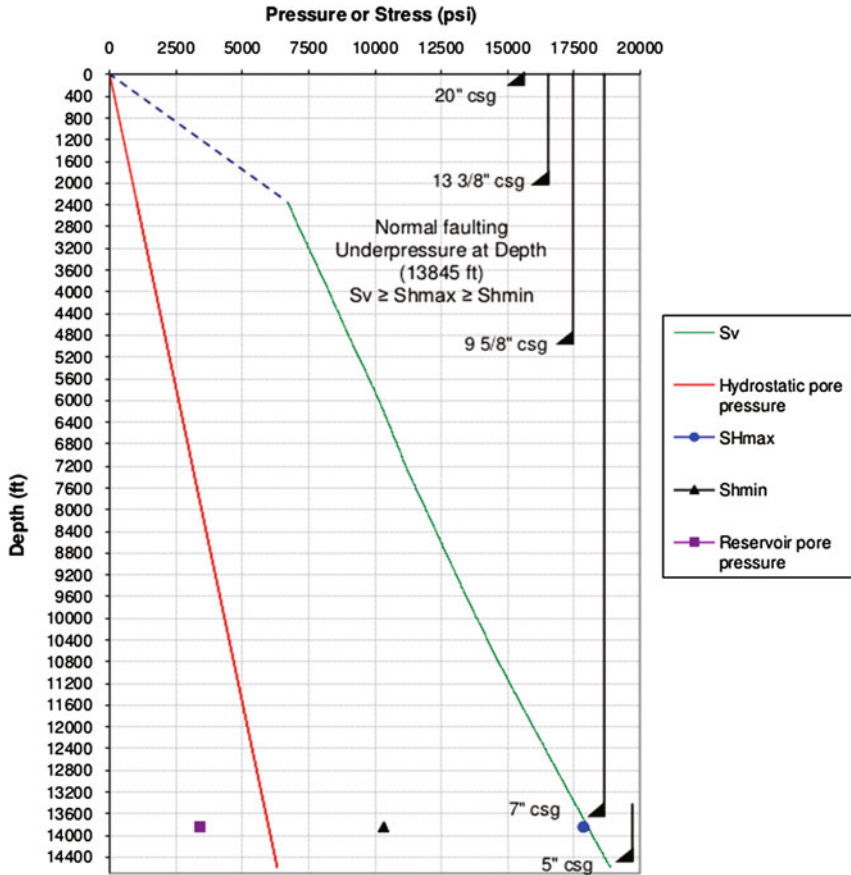


Fig. 6.20 Pressure or Stress versus depth

2329 ft of depth. Figure 6.20 also displays the reservoir average pressure, which is lower (underpressure) than the hydrostatic pressure, and S_{Hmax} is close to S_v . It physically implies that local reservoir stresses are changing, describing a rotation and a new relation between them. In accordance to field experience, the orientation of horizontal stresses can be verified using image logs and studying breakouts orientation. Additionally, a change from normal to strike-slip faulting is considered in Anderson’s classification scheme described in Fig. 6.3, is occurring in the CAJB due to reservoir depleting. The hydrocarbons production during twenty-four years generated a pressure drop between the initial pressure and average pressure, of 4267.20 psi.

There are four important features to note about the horizontal stress values at depth. First, the magnitude of S_{Hmax} is extremely close to S_v such that a strike-slip faulting regime ($\sigma_1 \geq \sigma_2 \geq \sigma_3$) exists in this region where $S_{Hmax} = \sigma_1$, $S_v = \sigma_2$, and $S_{Hmin} = \sigma_3$. Second, the CAJB features are characteristic of the tectonic processes,

data are Quaternary in age, and they represent episode of deformation in area. Third, A strike-slip faulting regime was formed due to pre-existing tectonic processes; namely, those structures evolved during previous tectonic regimes, in some cases, regimes have not been active for tens of million of year. Madrigal (1974) describes strike-slip faulting, lateral faults, and normal fault with lateral component in region. In consequence, it is coherent to find a change from normal to strike-slip faulting of Anderson's classification. Another aspect that deserve especial attention is related to the geological memory; in other words, static behavior associates to all tectonic events from the youngest until the oldest. This behavior also observed in the reservoirs fluid dynamics when NFCRs trend to keep a pre-existing flow pattern during its initial production stage until their depleting, expressing carbonate rocks history.

6.4.3 *Elastic Parameters: Young's Modulus and Poisson's Ratio*

The modulus of elasticity is the ratio of stress to strain. Using the velocity of compressional waves (V_p) and shear waves (V_s) the elastic moduli considering the Biot-Gassmann velocity relationships can be estimated. As already stated, Westergaard's solution uses Young's modulus and Poisson's ratio. Three types of deformation can result, depending upon the mode of the acting force. The three elastic moduli are:

$$\text{Young's modulus, } E = (F/A)/(dL/L)$$

$$\text{Bulk modulus, } K = (F/A)/(dV/V)$$

$$\text{Shear modulus, } G = (F/A)/\tan x$$

Where F/A is the force per unit area and dL/L , dV/V , and $\tan x$ are the fractional strains of length, volume, and shape, respectively.

Another important elastic parameter, called Poisson's ratio, is defined as the ratio of strain in a perpendicular direction to the strain in the direction of extensional force, ($\nu = (dx/x)/(dy/y)$).

Where x and y are the original dimensions, and dx and dy are the changes in x and y directions respectively, as the deforming stress acts in y the direction.

The frequency of seismic waves generates differences in velocity (or elastic moduli). A reflection seismic measurement (~10–50 Hz) are slower (yield lower moduli) than sonic logs (~10 kHz), and sonic logs yield slower velocities than ultrasonic laboratory measurements (typically ~1 MHz).

6.4.3.1 **Elastic Parameters Determination: Logs and Compression Test**

Elastic moduli were measured using a triaxial compression testing system (static tests), where confining stresses were applied hydrostatically. Young's modulus (E) was determined from the tangent to the stress-strain slope, and Poisson's ratio, (ν), was derived from the ratio of radial to axial strain. Table 6.5 shows the results of

Table 6.5 Triaxial test and elastic properties

Sample	Confining pressure (psi)	Temp. °F	Young’s modulus (kpsi)	Poisson’s ratio (dimensionless)
2 (southern)	500	76	6192.40	0.28
	1000	72	5239.92	0.33
	2000	72	5608.80	0.38
	2500	71	5466.62	0.38

Table 6.6 Wave velocities

Sample	Confining pressure (psi)	Axial load (kip) ^d	Frequency (kHz)	v_p^a (ft/s)	v_{s1}^b (ft/s)	v_{s2}^c (ft/s)
2 (southern)	0	0.5	400	10717	6675	6580
	500	0.87	400	11297	6859	6731
	1500	2.64	400	12820	7177	7314
	2500	4.38	400	13673	7587	7677

^a v_p = P-wave velocity (compressional, primary, or longitudinal)

^b v_{s1} = S1-wave velocity (shear-1, secondary-1, or transversal-1)

^c v_{s2} = S2-wave velocity (shear-2, secondary-1, or transversal-1)

^d 1 kip = 4448.22 Newtons (N)

elastic constants determined for samples.⁸ Also, It is possible to express the elastic parameters in terms of the phase velocities, and to find the corresponding expressions for Young’s modulus and Poisson’s ratio given by:

$$E = \rho v_p^2 \frac{3v_p^2 - 4v_s^2}{v_p^2 - v_s^2} \tag{6.45}$$

$$\nu = \frac{v_p^2 - 2v_s^2}{2(v_p^2 - v_s^2)} \tag{6.46}$$

v_p = P-wave velocity (compressional, primary, or longitudinal)

v_s = S-wave velocity (shear, secondary, or transversal)

ρ = bulkdensity.

Tables 6.5 and 6.6 show measured elastic parameters and wave velocities for a limestone sample. Although, static compression tests were developed considering three important conditions that can generate a marked contrast, with dynamic data:

1. Temperature: 72 °F (approximately)
2. Confining pressure: 500–2500 psi (Range)
3. Acoustic frequency: 400 kHz (Tests design)

⁸Data determined by specialized personal in rocks mechanical properties. Class notes: Geomechanics for Petroleum Engineer.

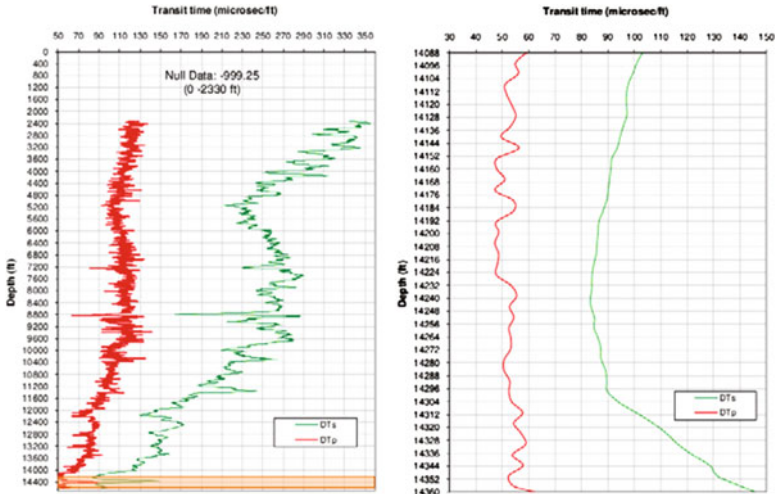


Fig. 6.21 Sonic log transit times, with pay zone respectively

Elastic moduli can be determined from acoustic data (logs or seismic), also called dynamic tests. The main differences between static and dynamic moduli is often explained by the difference in frequency of the measurements and strain amplitude used in tests. In the compressive test, strain is larger and a non-elastic deformation of the sample can occur.

Figure 6.21 displays compressional and shear transit times of sonic log. Interval travel time, Δt , or slowness is used to estimate porosity in formations. A similar pattern emerges in both transit times, which is decreasing. The presence of secondary porosity as vugs and fractures, complicates the quantitative evaluation of sonic logs. In such cases, it is necessary to compare with other logs that reflects total porosity. Figure 6.21 indicates a formation with low porosity and very consolidated. The reservoir pay zone presents planar or nonplanar discontinuities, which are detected due to a significant increase in transit time and density observed in Figs. 6.17 and 6.21. Shear waves are propagated in solid medium, and compressional wave in liquid medium. Null data mean noise data during the process of logs measuring.

Figure 6.22 shows pay zone wave velocities in reservoir, which are reciprocal values to transit times obtained during sonic log. So that, compressional and shear wave velocities behavior will be completely opposite with respect to transit times. The shear and compressional wave velocities increase in the pay zone, that indicates a particular porous medium with low consolidation.

Poisson's ratio was calculated using sonic log wave velocities in Eq. 6.46.

Figure 6.23 shows decreasing data, tend to have low Poisson's ratio values. The deviation can be attributed to little pore pressure, or partially liquid-filled fractures. Pay zone presents a formation containing discontinuities; so that, Poisson's ratio is less than the intrinsic effective Poisson's ratio of a homogeneous rock. In contrast,

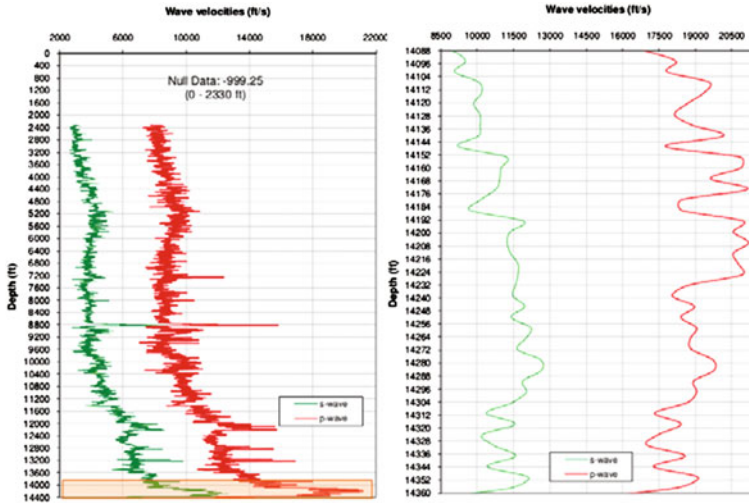


Fig. 6.22 Shear and compressional waves velocities, with pay zone respectively

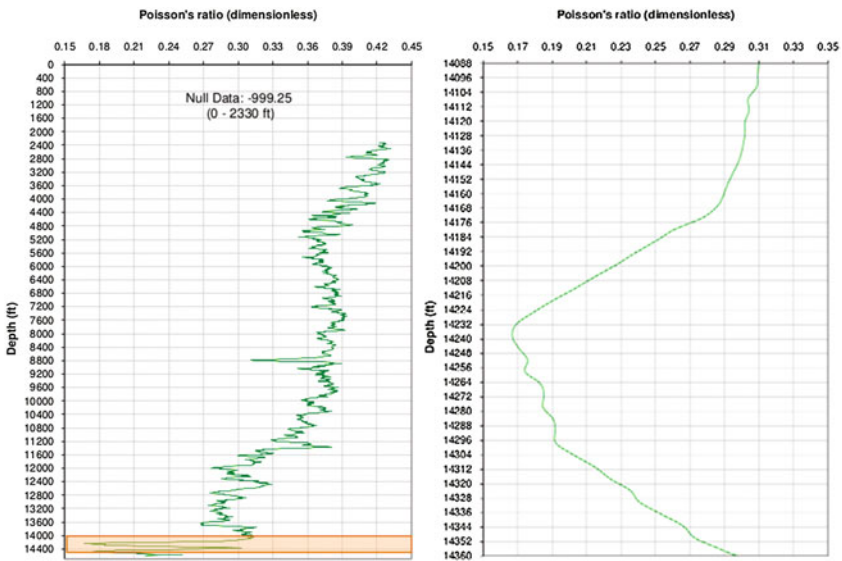


Fig. 6.23 Poisson's ratio determined using sonic log, with pay zone respectively

the effective Poisson's ratio of a formation containing closed fractures is greater than its intrinsic Poisson's ratio, it implies that, fractures is opened, yet.

It is well-known that several factors controlling Poisson's ratio for limestone rock. The rock depends on volume and geometry of pore space, mineral constitution, and saturating-fluid types and distribution (Chopra and Castagna 2014).

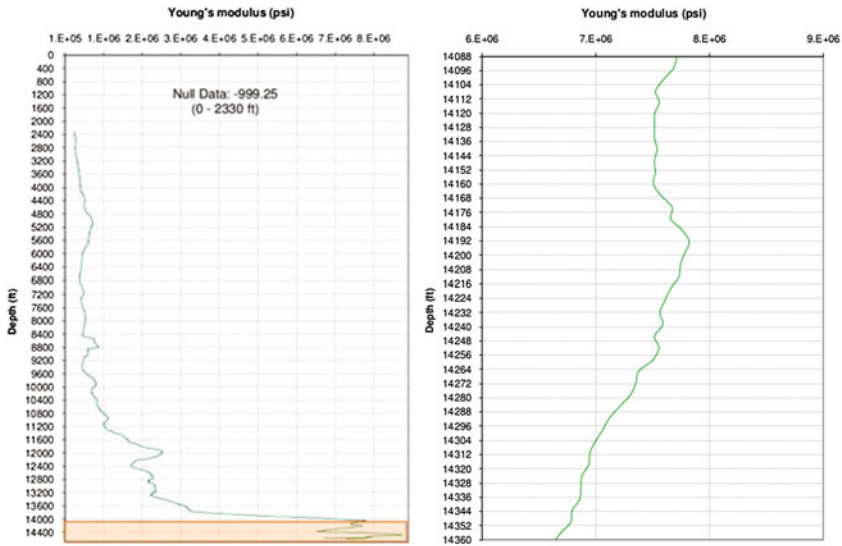


Fig. 6.24 Young’s modulus using sonic log, with pay zone respectively

Figure 6.24 shows dynamically determined values of Young’s modulus, which tend to be high. These values were estimated using Eq. 6.45. It indicates high density and moderate formation compaction level, that reduces porosity limestone.

Values of Young’s modulus decreased in pay zone, and our general analysis is that when cracks, fractures and vugs are present, the yielding of the rock to dynamically-applied stresses is increased by the closing of such cavities. Only part of the force is effective in compressing the solid and liquid material of the formation during oil production. For this reason measured values of elasticity (Young’s modulus) tend to be low, and the compressibility of this limestone layer tends to be high.

On the other hand, closed tectonic fractures containing formation can present a Young’s modulus less than its intrinsic Young’s modulus (without fractures) if the surfaces of the sliding do not slide past one another. This hypothesis can explain the peak of Young’s modulus in pay zone.

The conditions of geophysical problems are closely approximated if the rock sample is set into similar frequency. Moreover, minute cracks in the specimens affects results. So that, the presence of secondary porosity in the formation and rock samples explains the remaining differences between static and dynamic measurements.

Tables 6.7, 6.8, and 6.9 present reservoir properties, pay zone mechanical properties, and its waves velocities estimated using sonic log. These values will use to describe the collapse of tectonic fractures considering Westergaard’s application.

The stiffness of a hydrocarbon saturated rock depends on the rate at which external load is applied. When force is applied quickly, if stress is applied faster than fluid pressure can drain away, the fluid carries some of the applied stress and the rock is

Table 6.7 Reservoir properties

Sample	Initial ^a pressure (psi)	Pressure ^b (psi)	Temperature (°F)	Thickness (ft)	Width (ft)	Length (ft)
Pay zone	7680.60	3413.60	252	269	132	569

^aPressure estimated in 1973^bPressure estimated in 1998**Table 6.8** Mechanical properties

Sample	(S_v) (psi)	(S_{Hmax}) (psi)	(S_{Hmin}) (psi)	Poisson's ratio (dimension- less)	Young's modulus (kpsi)
Pay zone	18017	17349	10223.35	0.26	8598.47

Table 6.9 Wave velocities

Sample	(S_v) (psi)	Frequency (kHz)	DTp (μ s/ft)	V_p (ft/s)	DTs (μ s/ft)	V_s (ft/s)
Pay zone	18017	5	52.69	19051.71	91.77	10983.28

 V_p = compressional wave velocity V_s = shear wave velocity

DTp = transit time of compressional wave

DTs = transit time of shear wave

relatively stiff, and the rock behaves in an undrained manner. This manifestation of poroelasticity is frequently observed in typical laboratory stress-strain data.

The discrepancy between static and dynamic moduli can be explained by the non-elastic strain component invariably present in compression tests and that is absent in dynamic acoustic measurements. Also, this difference is explained by different authors as due to the presence of fractures, cracks, cavities, planes of weakness and foliation that relates to low ultrasonic velocities, and low values of dynamic parameters (Al-Shayea 2004.; Martínez-Martínez et al. 2012).

6.5 Closed or Open Natural Horizontal Fractures

From an engineering perspective, an elastic and infinite reservoir represents the ration of lateral extent to thickness. Reservoirs that are laterally extensive with respect to their thickness, the horizontal stresses will decrease with depletion but the vertical stress remains constant.

Many reservoirs present a change in horizontal stress with depletion in the range 0.5–0.7 (Chan and Zoback 2002). An elliptical inclusion model (Westergaard's application) will describe the effects of reservoir depletion on fractures deformation for CAJB.

Using Eqs. 6.37 and 6.40, and input parameters listed in Tables 6.7, 6.8, and 6.9; fracture width was determined, considering pore pressure and effective stress. Effective stress (S_{eff}) is given by:

$$S_v = S_{eff} + \alpha p \quad (6.47)$$

where

α = Biot coefficient.

Biot (1941) proposed an equation to estimate the coefficient for rock consolidation. Others authors as Bishop (1954), Geertsma (1957), Suklje (1969), Nur and Byerlee (1971) and Lade and De Boer (1997) (Shimin and Satya 2013). The coefficient ranges from near zero to unity, which depends on the property of the porous media, and can determinate using the bulk modulus of dry porous material K_s and grain bulk modulus K , respectively, and C_s and C are compressibilities of the solid material (grains) and skeleton. In this thesis, the value of Biot coefficient was unity because of compressibilities of the solid material and skeleton might be similar, which is an accepted assumption.

Table 6.10 shows calculated pressure for single fracture, its length less than formation length (60% approximately). This value of calculated pressure corresponds to pore pressure and effective stress to keep opened fracture with a width 0.056 ft. If calculated pressure is numerically equal to overburden stress, there is a static equilibrium, and homogeneous material without fractures or fractures totally closed.

Table 6.11 displays fracture width and length determined using initial reservoir pressure. Fracture deformation and its geometrical change is generated because effective stress tends to equilibrate reservoir pressure drop. In consequence, fracture width decrease and its length increase, but also provide a fundamental means to integrate the induced elasto-plastic deformation.

Table 6.12 shows fracture width and length determined using actual reservoir pressure, which the lateral deformation does not exist. Fracture width is strongly reduced.

Normally, reservoirs present fractures networks. Table 6.13 shows a similar effect in fractures width due to pressure drop. In this case, fractures depend on their length; namely, the shortest fracture will close with respect to others fractures.

Table 6.10 Single fracture width and length

Sample	Static equilibrium pressure (psi)	Calculated pressure (psi)	Length (ft)	Width (ft)
Single fracture	18017	14446.74	328.08	0.056

Table 6.11 Single fracture width and length with initial pressure

Sample	Static equilibrium pressure (psi)	Initial pressure (psi)	Length (ft)	Width (ft)
Single fracture	18017	7680.60	514.7	0.018

Table 6.12 Single fracture width and length with initial pressure

Sample	Static equilibrium pressure (psi)	Actual pressure (psi)	Length (ft)	Width (ft)
Single fracture	18017	3413.60	328.08	1.9×10^{-6}

Table 6.13 Fracture network width and length with initial pressure

Sample	Static equilibrium pressure (psi)	Actual pressure (psi)	Length (ft)	Width (ft)
Fracture 1	18017	3413.60	328.08	1.91×10^{-6}
Fracture 2	18017	3413.60	180.45	1.41×10^{-6}
Fracture 3	18017	3413.60	32.80	6×10^{-7}

References

- Al-Shayea, N. A. (2004). Effects of testing methods and conditions on the elastic properties of limestone rock. *Engineering Geology*, 74, 139–156.
- Biot, M. (1941). General theory of three-dimensional consolidation. *Journal of Applied Physics*, 12, 155.
- Bishop, A. W. (1954). The use of pore-pressure coefficients in practice. *Géotechnique*, 148–152.
- Chan, A. W., & Zoback, M. D. (2002). Deformation Analysis in Reservoir Space (DARS): A simple formalism for prediction of reservoir deformation with depletion. Presented at the SPE/ISRM Rock Mechanics Conference, Irving, Texas, 20–23 October.
- Chopra, S., & Castagna, J. P. (2014). In *AVO. Investigations in geophysics N° 16*. Tulsa, Oklahoma: Society of Exploration Geophysicists (pp. 3–5).
- Comisión Nacional de Hidrocarburos (CNH). (2013). Dictamen Técnico del Proyecto de Explotación Antonio J. Bermúdez (Modificación Sustantiva). Mayo (pp. 2, 44).
- De Vedia, L. A. (1986). Mecánica de Fractura. Proyecto Multinacional de Investigación y Desarrollo de Materiales, OEA, Argentina (pp. 25–68).
- Fong, A. J. L., Villavicencio, A. E., Pérez, H. R., et al. (2005). Proyecto Integral Complejo Antonio J. Bermúdez: Retos y Oportunidades. Presentado en el cuarto Exitep, CIPM celebrado en Veracruz, México, 20–23 de febrero.
- Fossen, H. (2010). *Structural geology* (1st ed.). New York: Cambridge University Press.
- García, M. (2010). *Notas de clase: Geomecánica Petrolera*. México: Posgrado en Ingeniería Petrolera. UNAM. D.F.
- Geertsma, J. (1957). The effect of fluid pressure decline on volumetric changes of porous rocks. *Petroleum Trans., AIME*, 210, 331–340. (Original paper presented at AIME Petroleum Branch Fall meeting in Los Angeles, 14–17 October, 1956).
- Guerrero, A. R., & Mandujano, S. H. (2014). Estrategias de Incremento de la Producción de Aceite en el Complejo Antonio J. Bermúdez: próximo reto después de lograr el mantenimiento de la producción. *Ingeniería Petrolera* (Vol. 54. No. 4, pp. 216–232).
- Hardy, R., & Tucker, M. (1988). X-ray powder diffraction of sediments. In M. Tucker (Ed.), *Techniques in sedimentology* (pp. 191–228). Oxford: Blackwell Scientific Publications.
- Jaeger, J. C., & Cook, N. G. W. (1971). *Fundamentals of rock mechanics*. London: Chapman and Hall.
- Lade, P. V., & De Boer, R. (1997, February). The concept of effective stress for soil, concrete and rock. *Géotechnique*, 47(1), 61–78.

- Madrigal, L. R. (1974). Descubrimiento de Yacimientos Petrolíferos en Rocas Carbonatadas del Cretácico, en el Sureste de México. Boletín de la Asociación Mexicana de Geofísicos de Exploración. (Vol. XV, Núm. 3). Julio-Agosto-Septiembre.
- Martínez-Martínez, J., Benavente, D., & García-del-Cura, M. A. (2012). Comparison of the static and dynamic elastic modulus in carbonate rocks. In *Bulletin of engineering geology and the environment* (Vol. 71, pp. 263–268). Springer.
- Nolte, K. G., & Economides, M. J. (1989). Fracturing diagnosis using pressure analysis. In M. J. Economides & K. G. Nolte (Eds.), *Reservoir simulation*. NJ, Englewood Cliffs: Prentice Hall.
- Nur, A., & Byerlee, J. D. (1971). An exact effective stress law for elastic deformation of rock with fluids. *Journal of Geophysical Research*, 32–39.
- Saouma, V. E. (2000, May 17). *Lecture notes in fracture mechanics CVEN-6831*. Department of Civil Environmental and Architectural Engineering, University of Colorado, Boulder. Part III, Chapter 6 (Linear Elastic Fracture Mechanics) (pp. 1–28).
- Schmitz, J., & Flixeder, F. (1993). Structure of a classic chalk oil field and production enhancement by Horizontal Drilling, Reitbrook, NW Germany. In: Spencer A. M. (eds) Generation, Accumulation and Production of Europe's Hydrocarbons III. Special Publication of the European Association of Petroleum Geoscientists, vol 3. Springer, Berlin, Heidelberg.
- Shimin, L., & Satya, H. (2013, October). Determination of the effective stress law for determination in coalbed methane reservoirs. In *Rock mechanics and rock engineering*. Wien: Springer.
- Sih, G. C. (1966, March). On the Westergaard Method of Crack Analysis, Technical Report No. 1. Department of Applied Mechanics, Lehigh University, Bethlehem, Pennsylvania.
- Suklje, L. (1969). *Rheological aspects of soil mechanics*. London: WILEY-INTERSCIENCE.
- Terzaghi, K. (1923). *Theoretical soil mechanics*. New York: Wiley.
- Timoshenko, S. P., & Goodier, J. N. (1951). *Theory of elasticity (International Student Edition* (3rd ed., p. 32). Tokyo: McGraw-Hill.
- Westergaard, H. M. (1939, June). Bearing pressures and cracks. Bearing pressures through a slightly waved surface or through a nearly flat part of a cylinder, and related problems of cracks. *Journal of Applied Mechanics*, A-49–A-53.
- Yin, H., & Groshong, R. H. (2007). A three-dimensional kinematic model for the deformation above an active diapir. In *The American association of petroleum geologist, AAPG Bulletin* (Vol. 91, No. 3, pp. 343–363).
- Zoback, M. (2007). *Reservoir geomechanics*. Cambridge: Cambridge University Press.

Chapter 7

Applicability and Benefits of Doctoral Thesis for Hydrocarbons Industry



Naturally Fractured Carbonate Reservoirs (NFCRs) present a significant challenge because they are complex flow systems, with interdependence variables that need to be fully characterized to describe the heterogeneities that impact fluid flow. In consequence, optimizing production and the recovery factor in carbonate reservoirs result from a combination of geological, geomechanical and dynamic factors that should be included in an integrated reservoir characterization.

Integration of related topics such as fracture mechanics, well testing, compaction potential, type of reservoir, fluid dynamics of geological discontinuities, data production, and analytical coupled model can be simply understood as an operating methodology, wherein the various sources of information are organized and collaborate around the static-dynamic characterization with the common objective of optimizing the production and recovery factor using an advanced strategy of reservoir development.

Figure 7.1 displays a workflow for fractured system, and its principal objective is to propose an advanced development of NFCRs. The workflow presented in the chapters of this doctoral thesis allows achieving integrations of distinct areas, for better mathematical simulations and predictions can be made reducing uncertainty, so that problems can be anticipated and avoided during the life of carbonate reservoirs.

Exploitation planning requires good reservoir anatomy understanding, so that reservoir behavior predictions and quantification of the geological heterogeneities and oil flow would help the better implementation of pressure maintenance and exploitation can be approach optimum conditions. It is well-known that recovery factor in NFCRs is a function of primary porosity development, the degree of matrix-discontinuity (fractures, breccias) connectivity, aquifer strength and matrix wettability (Shulte 2005). Although, workflow and technology integration can make the difference.

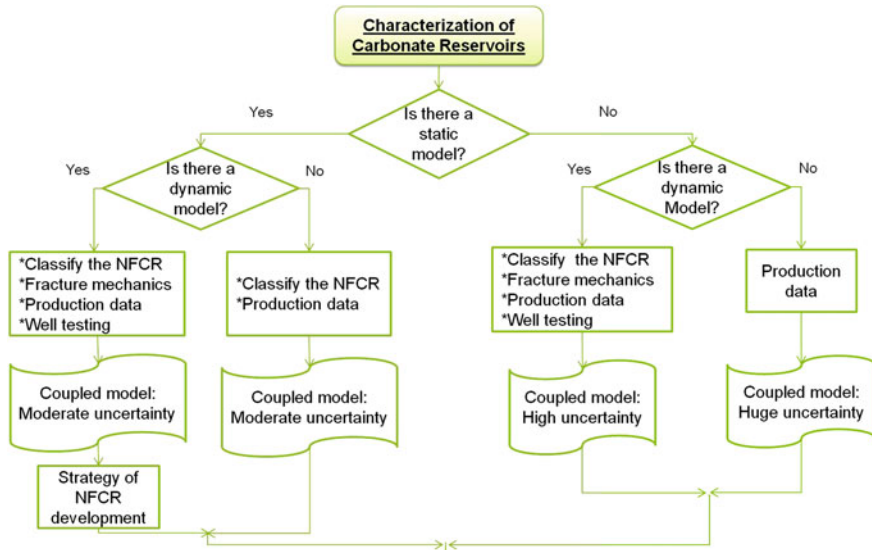


Fig. 7.1 Workflow of NFCR, for an advanced strategy and reservoirs production

Table 7.1 Applicability and benefits of the doctoral thesis

Ideal parameters for evaluation	Conventional	Thesis
Include NFCR static characterization	Yes	Yes
Include the NFCR dynamic characterization	Yes	Yes
Integrate the well testing and production data	Yes	Yes
Increase the reservoir productivity	Yes	Yes
Help in an advanced strategy for NFCR development	Yes	Yes
Include the seismic interpretation	No	No
Develop a stochastic model for NFCR	No	No
Develop a discrete fracture network (DFN) model for NFCR	No	No
Prognosis of the fractures distribution in NFCR	No	No
Prognosis of the stresses distribution in NFCR	No	No
Describe the NFCR connectivity	No	Yes
Describe the oil flow in NFCR	No	Yes
Include the dynamic-static characterization for NFCR	No	Yes
Diagnostic the dominant geological events, such as breccias, fractures, vugs, and caverns	No	Yes
Prognostic the dynamic stresses	No	Yes
Describe the petrophysical sensitivity related to stresses	No	Yes
Integral classification of the reservoir	No	Yes
Determinate the collapse of conductive fractures	No	Yes

This research discusses topics that could complement a technology for the reservoir exploitation, and NFCR workflow. In the present thesis, a discussion has been presented to improve the conventional current development and exploitation method used for NFCRs. In addition, there are some aspects that could be potentially utilized as theoretical fundamentals or direct application, see Table 7.1. This table provides information about the scope of this thesis and its potential applications in the industry, aiming at approaching an optimal production scheme and in the increment of factor recovery.

Reference

Shulte, W. M. (2005). Challenges and strategy for increased oil recovery. Paper IPTC 10146 Presented at the International Petroleum Technology Conference, Doha, Qatar.

Chapter 8

Conclusions and Recommendations



This doctoral dissertation has presented a discussion on the effects of planar and nonplanar discontinuities in fluid flow through porous media, reservoir classification, mechanical behavior of fractures during depletion, dynamic analysis of pressure and fluid flow modeling applied to stress-sensitive and non stress-sensitive carbonate reservoirs. The proposed mathematical models have provided a method to identify the flow characteristics and stresses effects.

From the results of the study the conclusions and recommendations are as follows:

8.1 Conclusions

1. Strict geological control of NFCRs and the description of the stress path during hydrocarbon production, may avoid drilling problems, wells stimulation, and a better manage of water conning.
2. Rotation and magnitude change of stresses is created due to the depletion of NFCRs.
3. Horizontal tectonic fractures can close due to pressure drop, and overburden stress in NFCRs.
4. In a normal faulting regime, overburden can control effective NFCR properties.
5. Mechanical, petrophysical, and flow properties during NFCRs exploitation production are dynamic in the time because data obtained in drained rock (production) are quite different compared to fully saturated rock (initial production).
6. It has been demonstrated through the analytical models of this thesis, tomography, and observations of outcrops and cores, that planar and nonplanar discontinuities in carbonate reservoir show distinctive representative flow characteristics. Fault breccias, tectonics fractures, sedimentary breccias, vugs, and impact

- breccias, have flow and geological patterns that affect oil production, and generate differences in static and dynamic characteristics that affect flow behavior.
7. There is a disparity between measured data from cores compared with logs data, mass-balance calculations, well testing, geomechanical and production tests, because only the worst portion of NFCRs formation is obtained during cores procedures, as a consequence of low tension strength and cohesion.
 8. It was demonstrative that discontinuities (vugs, fault breccias, and tectonic fractures) are superhigh permeability production ways and others (impact and sedimentary breccias) are storage zone. In effect, each discontinuity is different and cannot be called or analyzed as tectonic fractures, unknowing their geological genesis and flow patterns.
 9. A static and dynamic classification applied to NFCRs has been proposed that implies the identification of dominant discontinuities and their dynamic and static properties.
 10. The impact of fractures on reservoir deformation plays a noticeable role in fluid flow behavior; especially, in systems with low compressibility.
 11. The integration of static-dynamic classification and characterization, mechanical models of fractures in NFCRs, reduces uncertainty with respect to modeling, exploitation strategy, and reservoir simulation.
 12. It has been shown that unknowing of the origin of discontinuities causes confusions and contradictions for static-dynamic characterization, simulation, and exploitation strategy of NFCRs. This is one of the most important conclusions of this doctoral dissertation.
 13. Fluid velocity and volumetric flow for fault breccias and vugs (planar and nonplanar discontinuity) present the greatest obtained values between all of discontinuities, because they are cavities that have the fewest flow barriers. In consequence, as field evidence has widely demonstrated, a limestone reservoir well with connected vugs will have a high oil production.
 14. In the absence of fault breccias, vugs, sedimentary breccias, and tectonic fractures; impact breccias in limestone reservoirs present low fluid velocity and volumetric flow because they have flow barriers (ejected clasts), that act as a type of primary porosity depending on their values of porosity and low permeability. In effect, these impact breccias would not have high oil production, and must be superposed with an additional geological event for a high volumetric flow.
 15. Oil production of NFCRs with juxtaposition of geological events (breccias, fractures and vugs) is high, obeying a dominant geological event in fluid production (vugs, fault breccias and tectonic fractures), and other dominant geological events in fluid storage (sedimentary breccias and impact breccia).
 16. The analytic model provided an analysis of the single phase flow equation for incompressible fluid, in non-stress sensitive Naturally Fractured Tectonic Reservoirs. That showed the error in using the linear solution for naturally fractured carbonate tectonic reservoirs (NFCTRs).
 17. An analytical solution to quantify fluid dynamics in non-stress sensitive NFCTRs was proposed.

18. This study explains the phenomenon of high initial production rates, and how production declines after a short period of time in wells completed in fissured formations without fluid transfer matrix-fractures.
19. The nonlinear solution shows that for high flow rates there is a correction for the pressure and fluid flow, suggesting that the nonlinear term in diffusivity equation must be taken into account to correctly describe oil flow through NFCTRs due to non-Darcy laminar flow.
20. Our results suggest that the exact solution of the Navier-Stokes equation, namely Couette's flow, does not underestimate the pressure behavior and fluid flow in NFCTRs.

8.2 Recommendations

1. It is necessary to develop conceptual and numerical models based on each discontinuity to consider the depositional environment and/or tectonic fractures distribution.
2. Many of the examples studied in this work were small scale. Analytical models should be applied to field scale to identify further possible problems.
3. More studies should be performed to estimate mechanical properties and horizontal stresses of NFCTRs.
4. Analytical models for stress-sensitive reservoirs should be applied to reverse, and strike-slip faulting regime, to understand their fractures behavior.
5. The effects of fracture morphology and roughness on permeability and fluid flow, should be accounted for fractures deforming under stresses.